UCLA
UCLA Electronic Theses and Dissertations

Title
Stellar Evolution in Hierarchical Triples: Applications for Supermassive Black Holes and Exoplanets

Permalink
https://escholarship.org/uc/item/2pg804gn

Author
Stephan, Alexander Patrick

Publication Date
2020

Peer reviewed|Thesis/dissertation

eScholarship.org Powered by the California Digital Library
University of California

UNIVERSITY OF CALIFORNIA

Los Angeles

Stellar Evolution in Hierarchical Triples: Applications for Supermassive Black Holes and Exoplanets

A dissertation submitted in partial satisfaction
of the requirements for the degree
Doctor of Philosophy in Astronomy and Astrophysics

by

Alexander Patrick Stephan

2020

© Copyright by
Alexander Patrick Stephan
2020

ABSTRACT OF THE DISSERTATION

Stellar Evolution in Hierarchical Triples:
Applications for Supermassive Black Holes and Exoplanets

by

Alexander Patrick Stephan
Doctor of Philosophy in Astronomy and Astrophysics
University of California, Los Angeles, 2020
Professor Smadar Naoz, Chair

Triple body systems are relevant in a wide variety of astrophysical contexts. Two of the most interesting areas in which triples can play crucial roles are exoplanet systems in binary star systems and binary stars orbiting supermassive black holes. While these two types of systems are on two extreme ends of astrophysical mass scales, their dynamical behaviors are governed by the same gravitational physics. Stability considerations require such systems to be hierarchical, such that two bodies forming an inner binary are accompanied by the third body on a much wider outer orbit. These systems will undergo long-term changes in their orbital parameters on such long timescales that stellar evolution must be included for an accurate understanding of the dynamical evolution. I have developed a secular (long-term, orbit-averaged) code that allows to accurately follow the dynamical evolution of these systems, including Newtonian gravitation, general relativity, tidal forces, and, as a key new feature, stellar evolution effects, namely mass loss, radial expansion and contraction, and stellar spin changes. Using this tool for the studies presented in this dissertation, I found that these stellar evolution processes can significantly alter the dynamical behavior of many astrophysical systems.

In the context of exoplanet systems, my studies have shown that a large fraction of planets is eventually engulfed by their host stars, at many different stellar evolution stages. They

predicted the existence of "Temporary" Hot Jupiters and of giant planets polluting white dwarfs, both of which have been confirmed by recent observations. Furthermore, planet engulfment offers an explanation for many observed phenomena such as the shapes of many non-spherical planetary nebula, stellar spin and chemical abundance anomalies, and periodic gas ejections from red giants. An additional, yet to be confirmed, prediction is the existence of a substantial population of red giants with excess X-ray and UV radiation from ongoing planetary engulfment processes.

Concerning binaries orbiting supermassive black holes, my studies have shown that a large fraction of such binaries will merge or undergo common-envelope stellar evolution. They have explained the existence of the Galactic Center infrared-excess source G2 as a stellar binary merger product and predicted the presence of a whole population of similar sources. The latter prediction was recently confirmed by observations. The high density of X-ray sources in the Galactic Center is also explained by the results of my studies, as they predict the formation of X-ray binaries, cataclysmic variables, and symbiotic binaries. The predicted close interactions and mergers of binary stars can also strip the outer layers of giant stars, explaining the lack of giant star observations. Finally, compact object binaries can also be formed from binaries in galactic nuclei, producing gravitational wave sources observable by the Laser Interferometer Gravitational-Wave Observatory (LIGO) or the Laser Interferometer Space Antenna (LISA). Also predicted is a substantial population of white dwarf binaries that will form the dominant background signal in LISA and that can produce supernovae.

The dissertation of Alexander Patrick Stephan is approved.

Andrea M. Ghez

Hilke E. Schlichting

Bradley M. S. Hansen

Smadar Naoz, Committee Chair

University of California, Los Angeles

2020

To my parents, Petra and Thomas,

for introducing me to the wonders of the universe.

To my wife, Duran,

for exploring them with me.

Table of Contents

List of Figures . . . . . **vii**

Acknowledgments . . . . . **viii**

Curriculum Vitae . . . . . **x**

1 Introduction **1**

1.1 Background 1

1.2 The Dynamics of Hierarchical Triples 2

1.3 Stellar Evolution in Hierarchical Triples 6

1.4 Application to Astrophysical Phenomena 10

1.5 Structure of the Dissertation 11

2 Exoplanets in Evolving Binary Systems **13**

2.1 A-type Stars, the Destroyers of Worlds 15

2.2 Eating Planets for Lunch and Dinner 27

2.3 Throwing Icebergs at White Dwarfs 38

3 Binary Stars in the Galactic Center **46**

3.1 Merging Binaries in the Galactic Center 48

3.2 The Fate of Binaries in the Galactic Center 59

4 Conclusions **66**

List of Figures

1.1 Hierarchical Triple Schematic 3

1.2 Octupole vs. Quadrupole Dynamical Evolution 5

1.3 Enhancing EKL through Mass Loss 9

Acknowledgments

The studies presented in this dissertation have been supported or partially supported by NASA grant 80NSSC19K0321 and NSF grant AST-1739160. I would like to thank Martha Jura and the Jura family, Howard and Astrid Preston, and the Hellman Fellows Program for their generous support.

I would also like to thank my fellow students at UCLA, in particular the other current or former members of our research group, Bao-minh Hoang, Jesus Salas, Yeou Chiou, Sanaea Rose, Chris O'Conner, Cicero Lu, Paul Denham, Shelley Cheng, Ahmed Qureshi, Isabella Goetting, Isabel Angelo, Cheryl Wang, Thea Faridani, and William Lake, for many discussions, their comradeship, and fruitful collaborations during these last few years. I thank the professors of the Division of Astronomy and Astrophysics, as well as the administrative and IT staff of the Physics and Astronomy for their assistance and guidance during my years at UCLA. Additional thanks also to my thesis committee, Andrea Ghez, Hilke Schlichting, and Brad Hansen, for their guidance and mentorship.

I also thank all my research collaborators that I have not mentioned yet, including members of UCLA's Galactic Center Group and of the COSMIC collaboration for their research contributions and for sharing their data, expertise, and codes, as well as their mentorship. They are Scott Gaudi, Mark Morris, Ben Zuckerman, Fred Rasio, Tuan Do, Bence Kocsis, Will Farr, Anna Ciurlo, Breann Sitarski, Katie Breivik, Devin Chu, Gunther Witzel, Tassos Fragos, Aaron Geller, Aurélien Hees, Carl Rodriguez, Scott Coughlin, Kelly Kosmo O'Neil, Randall Campbell, and Greg Martinez.

I am also immensely grateful to my parents, Petra Steinke-Stephan and Thomas Stephan, who introduced me to the sciences and the universe when I was still a little child, and who always supported my curiosity and the studies I wanted to pursue. Special thanks here to my father for his advice and recommendations when writing this dissertation. Likewise, I am extremely grateful to my wife, Duran Stephan, who has supported me greatly during these last few years.

Finally, very special thanks to my PhD advisor, Smadar Naoz, who has tirelessly mentored me and driven me to become a better scientist, and who has build an immensely supportive, stimulating, and productive research group that I am lucky to have been part of for these last six years.

Curriculum Vitae

2010 – 2014	B.A. in Physics, The University of Chicago, Illinois, USA.
2014 – 2016	M.S. in Astronomy, University of California, Los Angeles (UCLA).
2014 – Present	Ph.D. student in Astronomy and Astrophysics, University of California, Los Angeles (UCLA).

Publications

[1] Alexander P. Stephan, Smadar Naoz, B. Scott Gaudi, and Jesus M. Salas, "Eating Planets for Lunch and Dinner: Signatures of Planet Consumption by Evolving Stars," ApJ, **889**, 45 (2020).

[2] Alexander P. Stephan, Smadar Naoz, Andrea M. Ghez, Mark R. Morris, Anna Ciurlo, Tuan Do, Katelyn Breivik, Scott Coughlin, and Carl L. Rodriguez, "The Fate of Binaries in the Galactic Center: The Mundane and the Exotic," ApJ, **878**, 58 (2019).

[3] Alexander P. Stephan, Smadar Naoz, and B. Scott Gaudi, "A-type Stars, the Destroyers of Worlds: The Lives and Deaths of Jupiters in Evolving Stellar Binaries," AJ, **156**, 128 (2018).

[4] Alexander P. Stephan, Smadar Naoz, and B. Zuckerman, "Throwing Icebergs at White Dwarfs," ApJ Letters, **844**, L16 (2017).

[5] Alexander P. Stephan, Smadar Naoz, Andrea M. Ghez, Gunther Witzel, Breann N. Sitarski, Tuan Do, and Bence Kocsis, "Merging binaries in the Galactic Center: the eccentric Kozai-Lidov mechanism with stellar evolution," MNRAS, **460**, 3494–3504 (2016).

CHAPTER 1

Introduction

1.1 Background

The study of planetary and stellar dynamics goes back to the earliest days in the history of physics and astronomy, originating in the desire of ancient civilizations to understand the movements of stars and planets in the night sky and to determine the timing of the seasons. Despite millennia of observations and investigations, the first mathematically successful models to understand these phenomena were described only a few centuries ago, namely through Kepler's laws of planetary motion and Newton's law of universal gravitation. With these laws, the gravitational two-body problem can be solved analytically, allowing us to understand and investigate the dynamics of a large number of astrophysical phenomena.

From a multitude of observational studies, we know that stellar binary systems are common in the universe (e.g., Duquennoy and Mayor 1991; Raghavan et al. 2010) and such systems are the target of a variety of modern astrophysical studies. Topics of interest include, among many others, how stars evolve in the presence of binary star companions (e.g., Pinsonneault and Stanek 2006; Izzard et al. 2007; Kobulnicky and Fryer 2007; Kiel et al. 2008; Sana et al. 2012; Ivanova et al. 2013), stellar binary mergers (e.g., Tylenda et al. 2011; Nicholls et al. 2013), and the mergers of compact stellar remnants such as black holes and neutron stars as studied by the Laser Interferometer Gravitational-Wave Observatory (LIGO) over recent years (e.g., Abramovici et al. 1992; Abbott et al. 2016). The study of many of these phenomena also requires the inclusion of more complex dynamical effects beyond simple two-body dynamics, such as tidal forces, and to go beyond Newtonian gravitation by applying Einstein's theory of general relativity.

While a large number of astrophysical phenomena can be studied through binary dynamics, many of these systems are in general not true binaries, but contain or interact with other bodies. The full behavior of such systems must therefore be explored using multi-body dynamics. Unfortunately, studies by mathematicians like Euler, Laplace, Lagrange, Poincaré, and others over the last centuries have shown that finding analytical solutions for systems with more than two bodies requires specific restrictions or approximations, making each particular solution only valid for a limited subset of systems and phenomena, if an analytical solution exists at all. In many cases, one must use direct N-body integration to numerically calculate the dynamics of multi-body systems. However, some approximations are well motivated by observations, such as, for example, the restricted three-body problem, where a third body of negligible mass moves within the gravitational field of two massive bodies, allowing analytical solutions to be found. The movements of comets or asteroids under the influence of the Sun and Jupiter are generally well described by such an approximation. Another common configuration, which has been the focus of many studies over recent decades, is the so-called "hierarchical triple".

1.2 The Dynamics of Hierarchical Triples

In a hierarchical triple system, two bodies orbit each other as a tight "inner binary", accompanied by a third body on a much wider orbit forming an "outer binary" with the inner binary's center of mass, as shown in Fig. 1.1. The dynamics of such systems has been studied over the last half century, beginning with important publications by Kozai (1962) and Lidov (1962), who independently described the systems' basic evolution. Assuming that the outer orbit is much wider than the inner orbit, these systems can be described by the following Hamiltonian (Harrington 1969):

$$H = \frac{k^2 m_1 m_2}{2a_1} + \frac{k^2 (m_1 + m_2) m_3}{2a_2} + \frac{k^2}{a_2} \sum_{j=2}^{\infty} \left(\frac{a_1}{a_2}\right)^j M_j \left(\frac{r_1}{a_1}\right)^j \left(\frac{a_2}{r_2}\right)^{j+1} P_j(\cos S), \tag{1.1}$$

with

$$M_j = m_1 m_2 m_3 \frac{\left(m_1^{j-1} - (-m_2)^{j-1}\right)}{(m_1 + m_2)^j}, \tag{1.2}$$

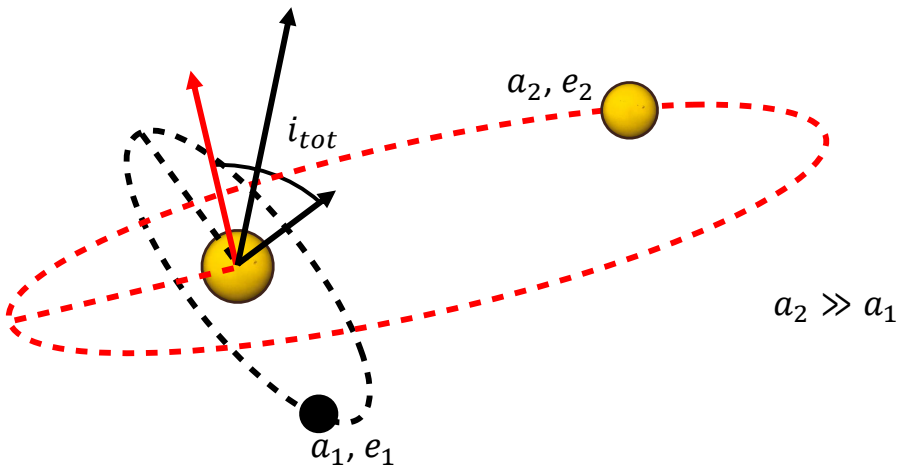

Figure 1.1: **Schematic of a Hierarchical Triple Configuration (not to scale).** The inner two bodies form an "inner binary" (black, dashed orbit), and their center of mass forms an "outer binary" (dashed, red orbit) with the third, distant companion. The straight dashed lines indicate the orbits' arguments of periaps. The short, black and red arrows represent the angular momentum vectors for the inner and outer orbits, respectively, and the long, black arrow represents the total system's angular momentum vector. Each orbit behaves quasi-Keplerian over short timescales. The orbits' eccentricities e_1 and e_2, semi-major axes a_1 and a_2, orientation, and mutual inclination i_{tot} determine the gravitational interactions between the inner and outer orbits. i_{tot} is defined as the angle between the inner and outer orbit angular momentum vectors.

and where k^2 is the gravitational constant, m_1 and m_2 are the masses of the inner bodies, m_3 is the mass of the outer companion, a_1 (a_2) is the semi-major axis of the inner (outer) orbit, $\vec{r_1}$ ($\vec{r_2}$) is the position vector of the inner (outer) binary, S is the angle between $\vec{r_1}$ and $\vec{r_2}$, and P_j is the Legendre polynomial of order j.

In hierarchical triples, the inner and outer orbits essentially behave like two Keplerian two-body orbits over short timescales on the order of the orbital periods, as signified by the first two terms in Eq. (1.1). Over long timescales of many orbital periods, however, the inner and outer orbits will exchange their angular momenta through mutual gravitational perturbations, represented by the third term in Eq. (1.1). This so-called "Kozai-Lidov effect" causes the orbits to precess and can lead to oscillations in orbital eccentricity and inclination, while preserving each orbit's semi-major axis value. As any changes in the orbital parameters occur very slowly compared to the orbital timescales, one can calculate the dynamics "secularly", i.e., orbit-averaged (Kozai 1962; Lidov 1962; Ford et al. 2000), which significantly reduces the required computation time compared to a direct N-body integration. Hierarchical triples are thus an example for long-term stable systems with "semi-analytical" solutions.

In the original studies by Kozai and Lidov, one of the bodies in the inner binary was a massless particle, and the eccentricity of the outer binary was zero, which restricted the expansion of the third term in Eq. (1.1) to the quadrupole order and limited the degree to which angular momenta could be exchanged (Kozai 1962; Lidov 1962), fixing the orientation of the orbits to be either prograde or retrograde. Over recent years, however, a more general approach has been developed that also considers the octupole order term of the Hamiltonian, allows all objects in the systems to have masses, and allows the outer orbit to be eccentric. This more general treatment has been called the "Eccentric Kozai-Lidov" (EKL) mechanism (Naoz et al. 2011, 2013a). Applying the EKL mechanism revealed that in many systems the orientation of the orbits can indeed change from prograde to retrograde and vice versa, and that the inner orbit can reach extreme eccentricity values (e.g., Li et al. 2014a,b; Naoz 2016). The qualitative differences between the previous, quadrupole-restricted treatment

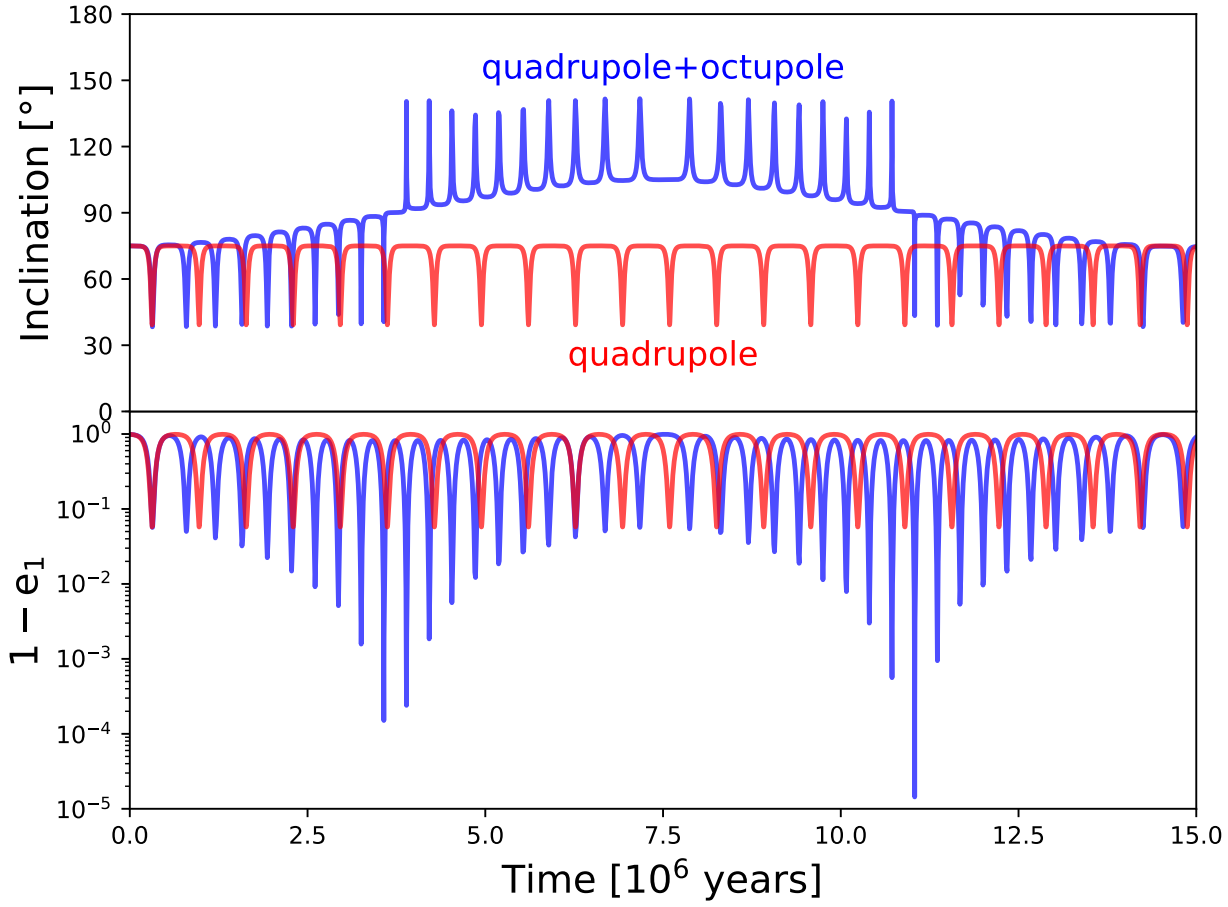

Figure 1.2: **Example: Dynamical Evolution of a Hierarchical Triple.** Shown is the dynamical evolution of a hierarchical triple system's inclination (upper panel) and inner orbit eccentricity (lower panel, shown as $1 - e_1$) over time. The red curve shows the evolution if only the quadrupole level of the expansion is included in the calculation, the blue curve additionally includes the octupole level for the same initial system parameters ($m_1 = 4$ M$_\odot$, $m_2 = 0.001$ M$_\odot$, $m_3 = 2$ M$_\odot$, $e_1 = 0.001$, $e_2 = 0.5$, $a_1 = 10$ AU, $a_2 = 250$ AU, $i_{tot} = 75°$). Including the octupole term allows the system to undergo inclination flips between prograde and retrograde and leads to extreme eccentricity spikes.

and the expanded, octupole-including treatment can be see in Fig. 1.2, where the dynamical evolution of a hierarchical triple is shown for both cases.

The extreme eccentricities caused by the EKL mechanism can lead to very short distances for the inner orbit periapsis, $a_{1,per} = a_1(1 - e_1)$, so much that the sizes and physical characteristics of the inner bodies become relevant for a full understanding of the orbital evolution. In some cases, the bodies would actually collide at these periapsis distances (e.g., Naoz et al. 2012; Naoz and Fabrycky 2014; Stephan et al. 2016, 2017, 2018). Tidal effects (Hut 1980; Eggleton et al. 1998; Kiseleva et al. 1998) and general relativity (Einstein 1916) have to be considered together with the EKL mechanism to properly investigate many astrophysical phenomena, such as the formation of Hot Jupiters (e.g., Naoz et al. 2011, 2012; Anderson et al. 2016) or the evolution of triple stars (e.g., Thompson 2011; Naoz and Fabrycky 2014). However, another crucial component that has to be added for a full understanding of hierarchical triple dynamics is stellar evolution, as stars change and evolve over timescales of millions and billions of years. Investigating the effects of combining stellar evolution and the EKL mechanism has been the main focus of the studies presented in this dissertation.

1.3 Stellar Evolution in Hierarchical Triples

As stars age, they lose mass through stellar winds, and they change their internal structure, spin period, overall sizes, and energy output depending on the nuclear fusion processes occurring inside of them. When stars exhaust their hydrogen fuel towards the end of their main-sequence lifetime, their cores contract and heat up, eventually fusing helium or heavier elements, if the stars had enough mass to begin with. This process leads to an expansion of the stellar envelope, often to extreme sizes of several astronomical units (AU). Massive stars eventually end this evolution once their cores are made of iron and nickel, preventing energy gains from further fusion, and collapse in on themselves, exploding in supernovae and sometimes leaving behind compact remnants such as black holes or neutron stars. Less massive stars do not produce iron or nickel in their cores and eventually simply cease fusion, upon which the stellar envelope is ejected and the stellar core forms a white dwarf, which

slowly radiates away its energy as it contracts.

The changes in stellar mass, size, and internal structure have profound effects on the dynamics of a binary or triple system, for one, by changing the strength of tidal effects, since the tidal energy dissipation timescale t_{tide} in a body of size R generally behaves as $t_{tide} \sim R^{-5}$. Furthermore, the reduction in mass will expand the semi-major axes of inner and outer orbits, potentially changing the strength of the third term in Eq. (1.1), which depends on the semi-major axis ratio a_1/a_2. This is particularly important if one of the bodies in the inner binary has a much lower mass than both the other inner body and the outer companion, such as for a star–planet pair with a stellar third body. The strength of the EKL mechanism depends on the factor ϵ, defined as

$$\epsilon = \frac{a_1}{a_2}\frac{e_2}{1-e_2^2}, \tag{1.3}$$

which has to be < 0.1 to ensure system hierarchicalness and stability (Lithwick and Naoz 2011). When deriving the secular equations for the Hamiltonian described in Eq. (1.1), by averaging over both the inner and outer orbits, ϵ becomes the prefactor for the octupole term (e.g., Katz et al. 2011; Lithwick and Naoz 2011; Naoz et al. 2012; Naoz 2016), with octupole-level EKL effects being stronger for higher values of ϵ. The semi-major axes in the system, a_1 and a_2, will change if the central star loses mass. If this mass loss is adiabatic, i.e., on a much slower timescale than the orbital timescales, the new semi-major axis a_f can be determined from the initial semi-major axis a_i and the initial (m_i) and final (m_f) masses of the objects in the system, such that $a_f = \frac{m_i}{m_f}a_i$. Assuming that the mass of the planet, m_2, is negligible compared to the masses of the stars, m_1 and m_3, one can determine the value of the new factor ϵ_f after mass loss has occurred, such that

$$\epsilon_f = \frac{m_{1,i}}{m_{1,f}}\frac{m_{1,f}+m_3}{m_{1,i}+m_3}\epsilon. \tag{1.4}$$

In star–planet–star systems $\epsilon_f > \epsilon$, meaning that EKL effects will increase in strength as stellar evolution progresses and mass loss continues. This can even change the qualitative behavior of a given system, by enhancing the strength of the octupole term and triggering orbital inclination flips, as shown in Fig. 1.3. The extreme eccentricity spikes associated

with these flips can lead to stellar and planetary collisions and other close-encounter events. This effect can also apply to systems with three stars of similar masses, albeit with slightly different equations (Shappee and Thompson 2013).

In the case of supernovae, the explosions will most likely impart a "kick" onto the star, changing the orbital trajectories instantaneously (Lu and Naoz 2019). Over recent years, I have developed a secular code that combines these stellar evolution effects with the EKL mechanism, considering also tidal effects and general relativistic precession. The basis of the code consists of the secular hierarchical triple equations as presented by Naoz et al. (2013a), with general relativistic effects from Naoz et al. (2013b), and the equilibrium tide model as described by Hut (1980) and Eggleton et al. (1998). The equations for these effects are also fully described by Naoz (2016). I have combined these effects with the stellar evolution code `SSE` by Hurley et al. (2000), with some adjustments to the magnetic braking coefficients following Dobbs-Dixon et al. (2004). `SSE` is a 1D stellar evolution code that produces a grid of information about a star's mass, size, spin, and luminosity as a function of its age and initial mass, which my code uses to calculate changes in the orbital semi-major axes, stellar tidal forces, and sizes of the stellar Roche limits. This, in turn, allows the code to calculate the dynamical evolution of a given hierarchical triple system over the whole lifetime of the stars.

In cases where two stars actually collide or form very tight binaries, the EKL mechanism becomes suppressed, and it becomes necessary to investigate the stars' common-envelope evolution. For this purpose, I have been using `BSE` by Hurley et al. (2002), which is a 1D binary stellar evolution code related to `SSE` that calculates the binaries' stellar parameters as the stars evolve or merge. An improved version of this code has been produced by the COSMIC group for their population synthesis studies (Breivik et al. 2019), and was also used for some parts of these studies.

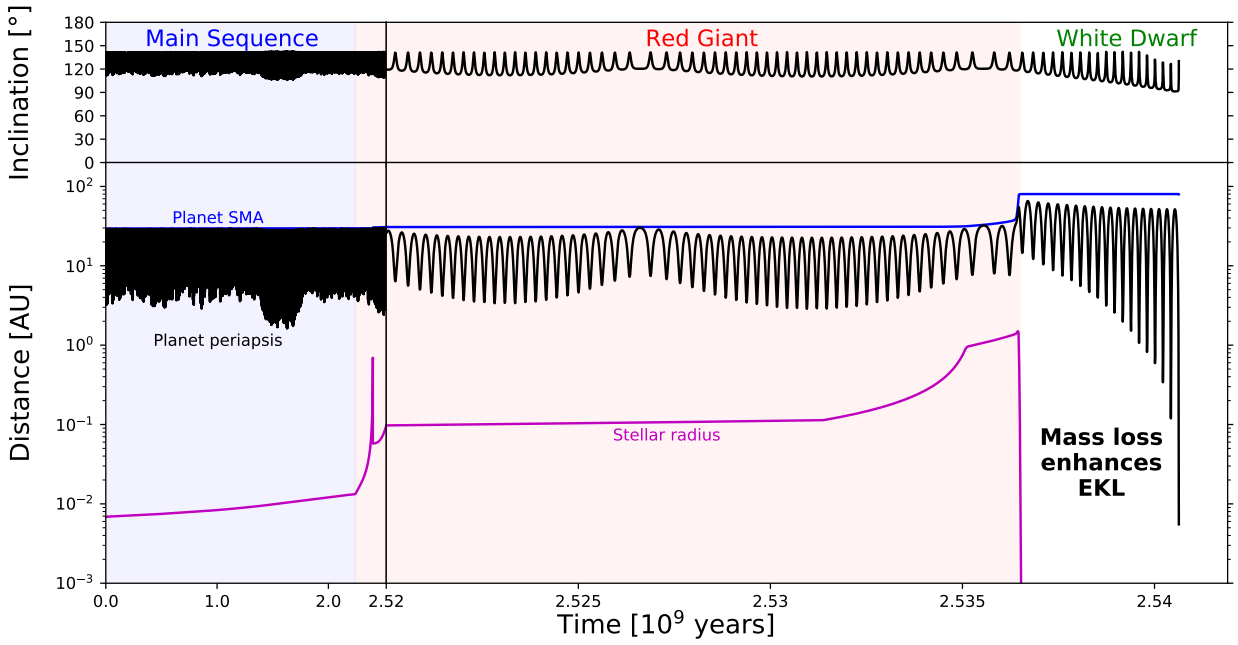

Figure 1.3: **Mass Loss triggering enhanced EKL Oscillations.** The figure presents the dynamical evolution of a Jupiter-sized planet orbiting in an evolving stellar binary system. The upper panels show the evolution of the inclination, while the lower panels show the evolution of the planet's semi-major axis (SMA, in blue) and periapsis (in black) over time. The left panels show the evolution for the first 2.52 Gyrs, while the right panels zoom in onto the last $\sim$ 20 Myrs of the shown evolution. The background colors signify the stellar evolution phases of the host star, also tracked by the main star radius (in magenta). As the star becomes a white dwarf, it loses a significant fraction of its mass, increasing the value of ϵ, and triggering enhanced EKL oscillations, leading to more extreme eccentricities. In this example, the planet is tidally disrupted at the end of the shown evolution. The initial parameters were $m_1 = 1.6$ M$_\odot$, $m_2 = M_{Jup}$ $m_3 = 0.534$ M$_\odot$, $R_p = R_{Jup}$, $a_{in} = 29.5$ AU, $a_{out} = 352$ AU, $e_{in} = 0.01$, $e_{out} = 0.322$, $inc = 120.3°$.

1.4 Application to Astrophysical Phenomena

For this dissertation, I have chosen to investigate two extreme astrophysical settings to explore the impact of combining the EKL mechanism with stellar evolution effects on the long-term dynamics of realistic triple system: exoplanet dynamics in stellar binary systems, and binary stars orbiting supermassive black holes (SMBHs) in galactic nuclei.

Exoplanets have become an important focus of astrophysical research over the last two decades, as observational surveys and new telescopes have determined that exoplanets are as common as stars in our galaxy. The study of exoplanets is a diverse field, including efforts to determine their formation, composition, long-term evolution, and to find Earth-like, habitable exoplanets that may harbor life. Some studies of planetary evolution had also considered the importance of stellar evolution (e.g., Spiegel and Madhusudhan 2012; Frewen and Hansen 2014, 2016). However, as binaries are common in the universe, with half of all sun-like stars residing in binary systems (e.g., Raghavan et al. 2010), hierarchical triple dynamics has to be included in the study of exoplanet evolution.

Most galactic nuclei are suspected or have been confirmed to contain SMBHs (e.g., Magorrian et al. 1998), which dominate the gravitational dynamics of the stellar clusters surrounding them with their immense mass. Our own Galactic Center has been observed to contain a SMBH of about 4×10^6 $M_\odot$ (e.g., Ghez et al. 2005), as well as a large population of exotic phenomena, such as infrared excess objects (Gillessen et al. 2012; Ciurlo et al. 2020), X-ray sources (e.g., Muno et al. 2005; Heinke et al. 2008), and peculiarly young stars not expected for such a dense environment (Ghez et al. 2005). Despite the high density of stars in the Galactic Center, several binary stars have been confirmed in the vicinity of the SMBH (e.g., Ott et al. 1999; Martins et al. 2006), which naturally form hierarchical triples with the SMBH as third companion. The dynamical evolution of such binaries can potentially explain many of the observed phenomena.

While these two settings, binaries with a planet and binaries orbiting a SMBH, appear to reside at two extreme ends of the astrophysical mass scales, they are still governed by the

same physics. Indeed, the mass ratios of planets to stars and of stars to SMBHs are of similar orders, making these systems mathematically similar. Studying the interplay of EKL, tides, general relativity, and stellar evolution is crucially important for understanding the long-term evolutionary outcomes of both types of systems. During my time as a PhD student, I have published five first-author research papers concerning exoplanets and SMBHs, which I include in the following two chapters as part of this dissertation. The publications are presented in a topical, rather than chronological, order.

1.5 Structure of the Dissertation

Chapter 2 discusses my studies on exoplanet systems, covered by three publications, beginning with Stephan et al. (2018), "A-type Stars, the Destroyers of Worlds: The Lives and Deaths of Jupiters in Evolving Stellar Binaries," in which we investigated how Jupiter-like planets in binary systems live, evolve, and get destroyed as they undergo the EKL mechanism and as their host stars age. The results predicted that Jupiter-like planets in many binary systems get destroyed, with some forming so-called "Temporary Hot Jupiters" around evolved stars.

The second publication in Chapter 2 is Stephan et al. (2020), "Eating Planets for Lunch and Dinner: Signatures of Planet Consumption by Evolving Stars," a study of some of the phenomena that can occur when planets are engulfed by their host stars during various stellar evolution stages. This study did not utilize the EKL-code directly, but rather focused on the physical processes that can occur in stellar envelopes as a consequence of planetary engulfment events predicted by the previously mentioned paper. Some of the phenomena that can occur are, for example, stellar spin-up, mass loss, extreme luminosity events, and chemical contamination of the stellar envelope.

The third and last publication in Chapter 2 is Stephan et al. (2017), "Throwing Icebergs at White Dwarfs." In this study, we investigated the pollution of white dwarf stars with heavy elements from planetary and cometary material, caused by the perturbations from

a wide stellar binary companion. In particular, this paper was able to explain pollution with icy, volatile-rich material from objects on extremely wide orbits around the host star. This scenario can also be seen as a special case of the scenarios discussed in Stephan et al. (2018) and Stephan et al. (2020), albeit with rather significant consequences for white dwarf pollution studies.

Chapter 3 is focused on my two publications related to the Galactic Center, beginning with Stephan et al. (2016), "Merging binaries in the Galactic Center: the eccentric Kozai–Lidov mechanism with stellar evolution," which was the first study in which I applied the combination of the EKL mechanism with stellar evolution effects. It investigates the dynamical evolution of binary stars that might orbit the SMBH in our Galactic Center, taking into account the binary's survival timescale against scattering effects from other stars. The results predicted that a rather large fraction of binaries in this environment (on the order of 25 %) collides or otherwise merges, often at advanced stages of stellar evolution, while the remaining binaries are separated into single stars.

The last publication in Chapter 3 is Stephan et al. (2019), "The Fate of Binaries in the Galactic Center: The Mundane and the Exotic." This study investigated the fates of the stellar mergers studied in Stephan et al. (2016) by using the binary stellar evolution code `BSE` (Hurley et al. 2002), improved by the COSMIC group (Breivik et al. 2019). The study predicted that many of these mergers can produce exotic phenomena, such as supernovae, cataclysmic variables, or gravitational wave sources.

Finally, In Chapter 4, I discuss the broader context of these five papers and their implications for current and future observations.

CHAPTER 2

Exoplanets in Evolving Binary Systems

Ground- and space-based telescope missions over the last decade, such as Kepler, WASP, HARPS, or the recently launched Transiting Exoplanet Survey Satellite (TESS), have revolutionized the field of exoplanet science with the discovery of thousands of exoplanets and exoplanet candidates. These exoplanets have been observed around a wide range of stellar types and ages, from the main sequence to red giants and white dwarfs (e.g., Charpinet et al. 2011; Johnson et al. 2011; Gettel et al. 2012; Howard et al. 2012; Barnes et al. 2013; Nowak et al. 2013; Niedzielski et al. 2015; Reffert et al. 2015; Vanderburg et al. 2015; Gänsicke et al. 2019). Indeed, the first exoplanet that was ever discovered is orbiting a millisecond pulsar (Wolszczan and Frail 1992). The existence of exoplanets in all these environments raises the question of how these exoplanets form, evolve, and survive during the various stellar evolution stages, especially around white dwarfs and pulsars, where the currently observed orbits would have been inside the stellar radius during the red giant phase.

As many stars, especially most stars more massive than the sun, have stellar binary companions (e.g., Raghavan et al. 2010), the long-term dynamical evolution of many exoplanets will be influenced by the EKL mechanism as well as tidal effects and the evolution of the stars themselves. Several problems in exoplanet research directly relate to the interplay of some or all of these effects, with some previous and concurrent studies covering topics such as Hot Jupiters (e.g., Fabrycky and Tremaine 2007; Wu et al. 2007; Naoz et al. 2011; Wu and Lithwick 2011; Naoz et al. 2012), planets around evolved stars (e.g., Johnson et al. 2007, 2008; Bowler et al. 2010; Gettel et al. 2012; Nowak et al. 2013; Niedzielski et al. 2015, 2016), or white dwarf pollution (e.g., Veras and Tout 2012; Vanderburg et al. 2015; Petrovich and Muñoz 2017). As a result, we know that many exoplanets in binary systems will eventually

collide or merge with their host stars, however, stellar evolution and tidal effects can make these processes more complicated. In particular, I have been investigating the circumstances and stellar evolution phases causing host binaries to destroy their planets and have studied the resulting effects and the probability to observe such events.

In the publications presented in this chapter, the dynamical evolution of exoplanets in binary systems is explored through all stages of their host stars' evolution. The first publication, Stephan et al. (2018), focuses on the dynamics of gas giants orbiting evolving A-type stars in binary systems. The second publication, Stephan et al. (2019), explores the physical processes that occur when a planet is engulfed by its host star as a result of the EKL or stellar evolution effects outlined in the first paper. The third publication, Stephan et al. (2017), investigated how the interplay of EKL and stellar evolution effects can lead to white dwarf pollution, a phenomenon that can provide details about exoplanet compositions and orbital architectures.

The Astronomical Journal, 156:128 (12pp), 2018 September https://doi.org/10.3847/1538-3881/aad6e5
© 2018. The American Astronomical Society. All rights reserved.

A-type Stars, the Destroyers of Worlds: The Lives and Deaths of Jupiters in Evolving Stellar Binaries

Alexander P. Stephan[1,2], Smadar Naoz[1,2], and B. Scott Gaudi[3]
[1] Department of Physics and Astronomy, University of California, Los Angeles, Los Angeles, CA 90095, USA; alexpstephan@astro.ucla.edu
[2] Mani L. Bhaumik Institute for Theoretical Physics, University of California, Los Angeles, Los Angeles, CA 90095, USA
[3] Department of Astronomy, The Ohio State University, Columbus, OH 43210, USA
Received 2018 June 9; revised 2018 July 24; accepted 2018 July 27; published 2018 August 29

Abstract

Hot Jupiters (HJs), gas giant planets orbiting their host stars with periods on the order of days, commonly occur in the Galaxy, including relatively massive (1.6–2.4 $M_{\odot}$, i.e., A-type main-sequence stars) and evolved stars. The majority of A-type main-sequence stars have stellar binary companions, that can strongly affect the dynamical evolution of planets around either star. In this work, we investigate the effects of gravitational perturbations by a far away stellar companion on the orbital evolution of gas giant planets orbiting A-type stars, the so-called Eccentric Kozai–Lidov mechanism, including the effects of general relativity, post-main-sequence stellar evolution, and tides. We find that only 0.15% of A-type stars will host HJs during their main-sequence lifetimes. However, we also find a new class of planets, Temporary Hot Jupiters (THJs), that form during the post-main-sequence lifetime of about 3.7% of former A-type main-sequence stars. These THJs orbit on periods of tens to a hundred days and only exist for a few 100,000 years before they are engulfed, but they reach similar temperatures as "classical" HJs due to the increased stellar luminosities. THJs' spin–orbit angles will mostly be misaligned. THJ effects on the host stars' evolution could also be observable for longer than a few 100,000 years. Overall, we find that approximately 70% of all gas giant planets orbiting A-type stars will eventually be destroyed or engulfed by their star, about 25% during the main-sequence lifetime, about 45% during post-main-sequence evolution.

Key words: binaries: general – planets and satellites: dynamical evolution and stability – stars: evolution – stars: kinematics and dynamics

1. Introduction

Exoplanets have been observed around a variety of host stars, with different masses, at all stages of stellar evolution, including main-sequence, subgiant and red-giant branch stages (e.g., Charpinet et al. 2011; Johnson et al. 2011b; Gettel et al. 2012; Howard et al. 2012; Barnes et al. 2013; Nowak et al. 2013; Niedzielski et al. 2015, 2016; Reffert et al. 2015). However, for massive, evolved stars, there appears to be a deficit in short-period or high-eccentricity planets (e.g., Johnson et al. 2007, 2008, 2010a, 2010b; Sato et al. 2008, 2013; Bowler et al. 2010; Schlaufman & Winn 2013). Furthermore, high metal abundances in so-called "polluted" white dwarf (WD) atmospheres indicate the presence of the remnants of planetary systems around these stars; the processes by which this material was brought onto the WDs is an active topic of research (e.g., Farihi et al. 2009, 2010; Klein et al. 2010, 2011; Melis et al. 2011; Zuckerman et al. 2011; Xu et al. 2013, 2017; Stephan et al. 2017).

The architectures of these planetary systems have become the focus of a rich field of research, as it was recently shown that dynamical processes play an important role in planetary system formation and evolution. These processes include resonant interactions (e.g., Lithwick & Wu 2012; Batygin & Morbidelli 2013; Petrovich et al. 2013; Goldreich & Schlichting 2014), planet–planet scattering (e.g., Rasio & Ford 1996; Chatterjee et al. 2008; Nagasawa et al. 2008; Beaugé & Nesvorný 2012; Boley et al. 2012), and secular perturbations from a companion (either a star or a planet; e.g., Fabrycky et al. 2007; Wu et al. 2007; Naoz et al. 2011, 2012, 2013a) or from multiple planets (e.g., Wu & Lithwick 2011; Denham et al. 2018).

A particularly interesting group of discovered exoplanets are the so-called "Hot Jupiters" (HJs), which are gas giants that orbit their host stars on very tight orbits with periods on the order of a few days. While this class of exoplanets seems ubiquitous in the galaxy, it is noticeably absent in our own solar system. Several models have been developed to explain the formation and existence of these HJs, including gravitational perturbations of the planets' original orbits to high eccentricities, followed by tidal dissipation and orbit circularization and shrinking (e.g., Fabrycky & Tremaine 2007; Naoz et al. 2011, 2012; Beaugé & Nesvorný 2012; Petrovich 2015; Frewen & Hansen 2016), as well as disk migration during giant planet formation (e.g., Armitage et al. 2002; Masset & Papaloizou 2003; Armitage 2007). The idea that outer companions have perturbed these planets and led to high-eccentricity migration is also supported by recent observational campaigns that have shown that most HJs have a far away companion, either a star or a planet (e.g., Knutson et al. 2014), though it remains unclear if most of these companions can trigger high-eccentricity migration (e.g., Ngo et al. 2016). For a three-body system consisting of star–planet–star to be long-term stable the inner two bodies, the main star and the gas giant, have to be on a much tighter orbit than the third, outer, object, leading to a hierarchical configuration.

In recent years, so-called "retired" A-type stars, which are observed as K-type giants, have been focused on by many studies in attempts to discover exoplanets (e.g., Johnson et al. 2007, 2008; Bowler et al. 2010; Johnson et al. 2010a, 2011a, 2011b). "Retired" A-type stars are stars that would be classified as A-type during their main-sequence

lifetimes, but that have evolved beyond the main sequence and are subgiant or giant K-type stars at their currently observed life stage. While main-sequence A-type stars usually rotate rapidly and have high surface temperatures, greatly impeding exoplanet detection through radial velocity measurements, "retired" A-type stars rotate slower, are cooler, and have allowed for the discovery of several exoplanets. Furthermore, several HJs have also been discovered around A-type main-sequence stars through exoplanet transits (e.g., Gaudi et al. 2017; Johnson et al. 2018).

The classification of "retired" A-type stars has been shown to be rather challenging, as different methods to determine stellar masses seem to yield different values (e.g., Lloyd 2011; Johnson et al. 2013; North et al. 2017; Stello et al. 2017; Ghezzi et al. 2018), implying that some of these stars might rather be "retired" F-type stars. There seems to be uncertainty over the validity of some methods when compared to precise astroseismological measurements. In this work, we avoid these classification problems by simply focusing on a particular range of stellar masses, between 1.6 and $3\,M_{\odot}$ (with masses above $\sim 2.4\,M_{\odot}$ technically belonging to the low-end B-type mass range). This intermediate stellar mass range broadly coincides with classical definitions of main-sequence A-type star masses (Adelman 2004), and we refer to this mass range when labeling a star as A-type. A further discussion concerning A-type star evolution is given in the Appendix.

Stars more massive than the Sun, like A-type stars, reach post-main-sequence evolution much faster than smaller stars, and the vast majority of them have stellar companions (e.g., Raghavan et al. 2010; Moe & Di Stefano 2017; Murphy et al. 2018). Indeed, several A-type stars with HJs have companion stars (e.g., Johnson et al. 2018; Siverd et al. 2018). This leads to an interesting interplay of dynamical and stellar evolution effects that needs to be considered for planets in such systems. On the one hand, a hierarchical star–planet–star configuration will lead to secular oscillations of the orbital parameters due to gravitational perturbations by the outer companion on the planet's orbit, often leading to extreme eccentricities, the so-called Eccentric Kozai–Lidov (EKL) mechanism (Kozai 1962; Lidov 1962; Naoz et al. 2016). On the other hand, post-main-sequence stellar evolution will lead to, for example, stronger tidal dissipation or engulfment of close-in planets due to stellar radial expansion, and expanded orbits due to stellar mass loss. In this work, we study the combined interplay of these dynamical and stellar effects for Jupiter-sized planets in stellar binaries with A-type star primaries. We find that short stellar evolution timescales, high prevalence of binary companions, and strong tides during post-main-sequence evolution result in the destruction of nearly 70% of Jupiters orbiting A-type stars, more than we would expect for lower mass single stars. We propose that observed planets around intermediate mass main- and post-main-sequence stars with stellar companions[4] are consistent with our predicted results.

2. Numerical Setup

We perform large Monte-Carlo simulations that follow the dynamical evolution of hierarchical three-body systems, consisting of a relatively tight *inner binary* pair of a star and a Jupiter-sized planet, which are orbited by another star on a distant orbit as *outer binary*. We solve the hierarchical secular triple equations up to the octupole level of approximation (the so-called EKL mechanism, e.g., Naoz et al. 2016), including general relativity effects on both inner and outer orbits (e.g., Naoz et al. 2013b), static tides between the primary star and the planet (following Hut 1980 and Eggleton et al. 1998; see Naoz et al. 2016 for the complete set of equations). Tides for radiative stars are also estimated to be much weaker than for convective stars, so we use different tidal models for (radiative) main-sequence and (convective) red-giant stars (e.g., Zahn 1977); however, observations are uncertain about their distinctiveness (Collier Cameron & Jardine 2018). The tidal Love numbers for stars and gas giants are set to 0.014 and 0.25, respectively (Kiseleva et al. 1998), and we choose a viscous timescale of 1.5 years for both. We also include the effects of stellar evolution on masses, radii, and spins on the two stars, as derived from the stellar evolution code SSE by Hurley et al. (2000). Unlike G- and F-type main-sequence stars, which exhibit magnetic braking due to their convective envelopes, A-type main-sequence stars are nearly completely radiative and do not experience significant magnetic braking (van Saders & Pinsonneault 2013). Their spin rates therefore do not substantially slow down during their main-sequence evolution lifetime, however, magnetic braking can occur during the red-giant phase after a convective envelope has formed, additionally to the slowing of the spin due to stellar expansion. These factors are included in the calculations performed with SSE and we also switch between tidal models for radiative and convective stars based on SSE determinations of evolutionary phases. Overall, the main differences between A-type stars and smaller stars lie in the much more rapid stellar rotation rate and the weaker tidal dissipation for radiative stars, which weaken the importance of stellar tides during the main-sequence lifetime. During post-main-sequence evolution, however, the massively expanded stellar radii, together with the more convective nature of red giants, greatly increase the strength of stellar tidal dissipation, beyond the strength of tides for less massive post-main-sequence stars. The interplay between the EKL mechanism and stellar evolution has previously been shown to play an important role in shaping the underlying dynamics and outcome of these systems (e.g., Kratter & Perets 2012; Shappee & Thompson 2013; Michaely & Perets 2014; Frewen & Hansen 2016; Naoz et al. 2016; Stephan et al. 2016, 2017; Toonen et al. 2016).

The mass of the primary star, $m_{\star,1}$, is taken from a Salpeter distribution with $\alpha = 2.35$ (Salpeter 1955); however, the mass range is restricted between 1.6 and $3.0\,M_{\odot}$ in order to ensure that the planet host star is an A-type or, at most, a small B-type star during its main-sequence lifetime (Adelman 2004). The stellar initial radii and spins are calculated using SSE by Hurley et al. (2000). Each primary star is given one planet, whose mass (m_p), size, and spin are set equal to those of Jupiter. The mass of the outer companion star, $m_{\star,2}$, is determined by the binary mass ratio distribution taken from Duquennoy & Mayor (1991). The semimajor axis, a_1 of the *inner binary* of the A-type star and Jupiter-sized planet is chosen uniformly between 1 and 10 au, while the *outer binary* orbit's semimajor axis, a_2, is again taken from the distribution in Duquennoy & Mayor (1991) for the stellar companion. The inner orbit's eccentricity is initially set to a small value, $e_1 = 0.01$, as are the stellar and planetary spin–orbit angles, since we assume that the planet was formed in a gaseous disk, while the outer orbit's

[4] Planetary companions might have different results.

eccentricity, e_2 is chosen uniformly between 0 and 1. To ensure long-term stability, we reject systems where a_2 is greater than ~10,000 au, as galactic tides will tend to separate such systems relatively quickly (Kaib et al. 2013), and we only consider hierarchical systems to ensure long-term stability, which requires:

$$\epsilon = \frac{a_1}{a_2}\frac{e_2}{1-e_2^2} < 0.1, \quad (1)$$

and $a_1/a_2 < 0.1$ (e.g., Naoz et al. 2016). The inclination, i between the inner and outer orbit's angular momenta is chosen isotropically in cosine.

In total, we simulate 4070 systems using these parameter conditions, 3000 of which have a primary star mass smaller than about 2.4 $M_\odot$ and therefore are safely classified as A-type stars during their main-sequence lifetimes. We calculate the dynamical evolution of these systems for 13 Gyr, or until a stopping condition is fulfilled. If a planet touches the surface of a star or crosses the Roche limit, we stop the integration. We define the Roche limit $R_{\mathrm{Roche},A}$ of a body of mass m_A and radius r_A with respect to an orbiting body of mass m_B as:

$$R_{\mathrm{Roche},A} = 1.66 \times r_A\left(\frac{m_A + m_B}{m_A}\right)^{1/3}. \quad (2)$$

Note that this equation simplifies to $R_{\mathrm{Roche},A} = 1.66 \times r_A$ and $R_{\mathrm{Roche},B} = 1.66 \times r_B\left(\frac{m_A}{m_B}\right)^{1/3}$ if $m_A \gg m_B$, as in the case of a star with mass m_A being orbited by a much smaller planet of mass m_B. The disruption of planets is highly sensitive to the Roche limit and thus to the numerical pre-factor value, chosen here to be 1.66. Numerical simulations by Guillochon et al. (2011) and Liu et al. (2013) suggested a larger value, (i.e., 2.7) while Faber et al. (2005) simulations found ~2.2. Thus, choosing here a fiducial value of 1.66 means that the number of engulfed planets represents a lower limit on the fraction of planets that can be engulfed during post-main-sequence radial stellar expansion. On the other hand, this value might lead us to overestimate the number of planets forming HJs during the main-sequence lifetime (see Petrovich 2015).

3. Results

3.1. Classification of Dynamical Evolution Outcomes

From our 4070 simulated systems, about 70% ended in the destruction of the Jupiter-like planet, while in only 30% of cases did the planet survive to the WD phase of its host star. We identify several distinct groups of orbital evolution behaviors and outcomes for Jupiters around A-type stars in stellar binaries. There are mainly four such groups (see Table 1 for percentages):

1. Classical Hot Jupiters (CHJs): These are HJs on orbits shorter than about 10 days, as one would expect from previous studies of high-eccentricity migration (e.g., Fabrycky & Tremaine 2007; Wu et al. 2007; Naoz et al. 2011, 2012; Petrovich 2015). These planets reach their short-period orbits during the host stars' main-sequence lifetime due to an interplay of EKL-caused high orbital eccentricities and tidal effects. They are ultimately engulfed and destroyed as the stars evolve and expand. About 1.5% of our systems experience this outcome. We further discuss this group in Section 3.2.
2. Roche-limit crossers: These are those planets that reach extremely large eccentricities through the EKL mechanism and cross their host stars' Roche limits or graze the stars' surfaces. We assume that they are destroyed upon crossing the Roche limit and end the computation of their orbital evolution. The actual fate of these planets might be more complicated, and some might even survive for an extended time after crossing the Roche limit (e.g., Faber et al. 2005; Dosopoulou et al. 2017; MacLeod et al. 2018); however, for simplicity, we mark them all as "RL-cross" in Figure 1. Some of the possible effects are discussed in Section 4.4. About 31% of our systems lead to Roche-limit crossing, 23% of which occur during main-sequence and 8% occur during post-main-sequence evolution. Those that cross the stellar Roche-limit during post-main-sequence evolution simply do not undergo high enough eccentricity excitations or are on initial orbits too wide to have short periapsis distances during the stellar main-sequence lifetime.
3. "Temporary" Hot Jupiters (THJs): These are planets that did not reach high enough eccentricities during the main-sequence lifetime of their host stars to experience tidal circularization and orbital shrinking, but which do so as the stars leave the main sequence and become giant stars. Virtually all of them only classify as "hot" Jupiters (in terms of temperature) for a short part of their total lifetime. They get engulfed as their host stars continue to expand and as tides continue to drive them to the stellar surface; however, their orbits usually do not fully circularize before engulfment. The engulfment process may result in energetic disturbances on the host star and might serve as an observable (e.g., MacLeod et al. 2018; see also Section 4.4). We find that about 37% of our systems experience this outcome; however, about a fifth of these (7% of all systems) reach this outcome even though the EKL perturbations by their companion stars are negligible, as their initial orbits are relatively close to the star, at about 1–3 au. Further details about this group are discussed in Section 3.3.
4. Surviving Jupiters: These are planets that never significantly interact with their host stars and survive until the stars become WDs. For this population, the companion stars' EKL perturbations were too weak to cause large eccentricities, and the planets' orbits were too

Table 1
Jupiter Evolution Outcome Percentages

Phase	CHJ	RL-cross	THJ	Survived up to t_{Hubble}
Total	1.5%	31%	37%	30%
MS	1.5%	23%	...	...
Post-MS	...	8%	37%	...
WD	...	0.3%	...	30%

Note. Listed are classical HJ (CHJ), RL-crossing Jupiter (RL-cross), temporary HJ (THJ), and surviving Jupiter (survived), up to Hubble time, outcomes as percentages of the whole population of simulated systems. The percentages are given for the whole evolution of the stars (total), and also split between main-sequence (MS), post-main-sequence (Post-MS), and white dwarf (WD) phases.

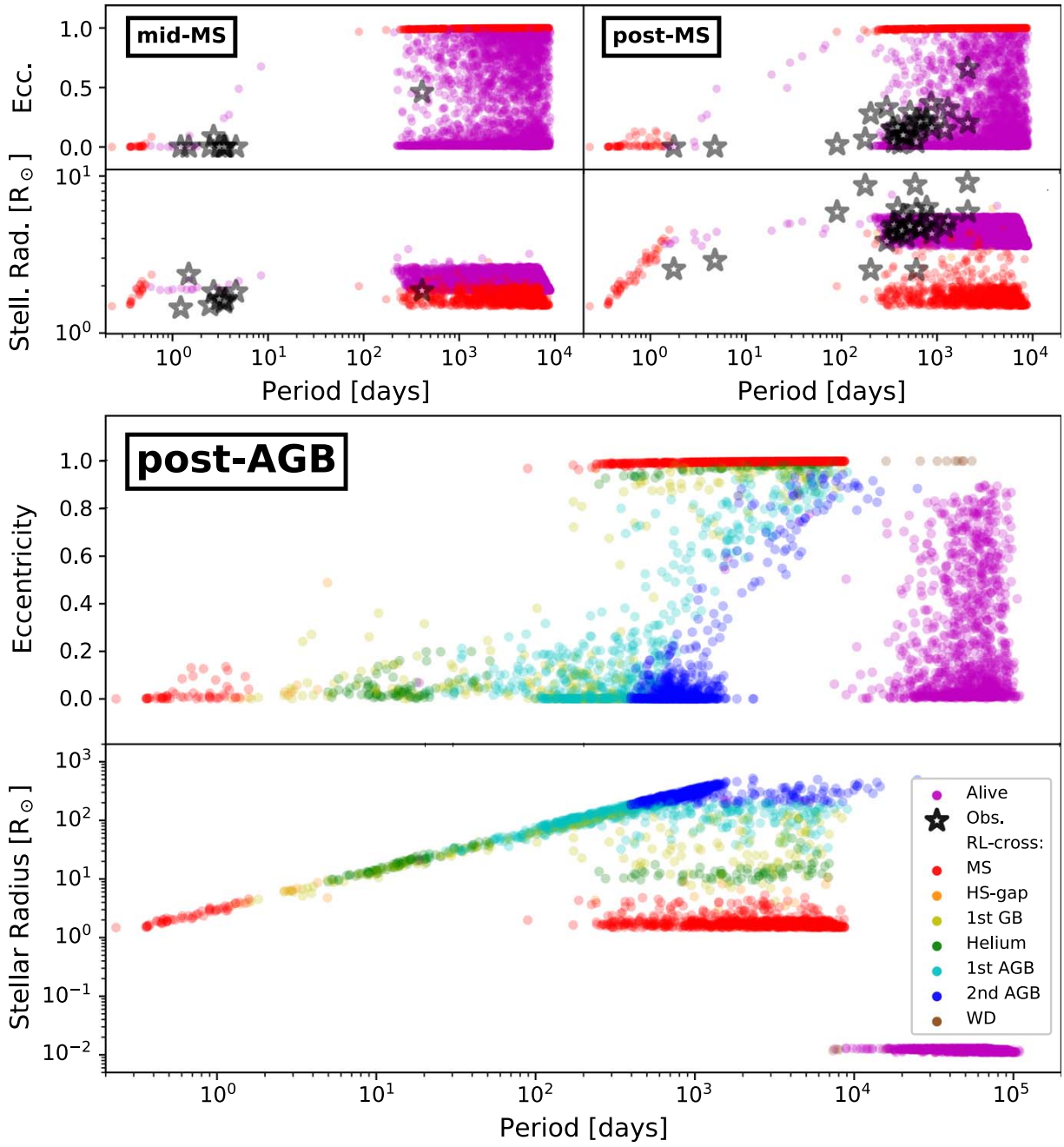

Figure 1. Dynamical evolution of Jupiters around A-type stars in binary systems. Top frame of each panel: Eccentricity vs. Orbital Period. Bottom frame of each panel: Stellar Radius vs. Orbital Period. The magenta dots show the parameters of Jupiters that survive to either the middle of the main-sequence (labeled mid-MS), the beginning of the post-main-sequence (labeled post-MS), or the white dwarf phase (labeled post-AGB). Differently colored dots show the final parameters for Jupiters that were destroyed by their stars either through EKL-induced high-eccentricity Roche-limit crossing or engulfment during stellar expansion. The colors represent the various stellar evolution phases at the time of planetary death: (red) main sequence, (orange) Hertzsprung gap, (yellow) first giant branch, (green) core helium burning, (cyan) first asymptotic giant branch, (blue) second asymptotic giant branch, and (brown) white dwarf phase. Out of 4070 planets, about 2870 were destroyed before 13 Gyr had passed, falling into two distinct main groups—(1) high-eccentricity, KL-driven deaths, and (2) low eccentricity, tidally, and stellar expansion driven deaths. The black stars are showing the positions of some observed Jupiters around A-type stars in this parameter space, see Section 3.2 for references.

wide to experience strong tidal effects during post-main-sequence evolution. This population mostly reflects our lack of knowledge on the initial conditions of these systems. About 30% of Jupiters survive to this stage. A small fraction of these (0.3% of all systems) gets destroyed and accretes onto the WDs as the stellar mass loss changes the orbital parameters of the systems, allowing extreme excitations of the orbital eccentricities through the EKL mechanism, ultimately driving these Jupiters to cross their own Roche limits and to get tidally

disrupted by the WDs. Examples of this potential WD pollution mechanism have been discussed in detail in Stephan et al. (2017). Recent work (van Lieshout et al. 2018) also indicates that some of the planet's material can be recycled into new planets and escape accretion.

In Figure 1, we show three snapshots of the different systems' realizations during the stars' lifetimes, mid-main-sequence (top left), at the beginning of post-main-sequence (top right), and post ABG phase (bottom). We consider the eccentricity as a function of the planet's period (top panels). For comparison, we also plot the observed systems (depicted as black stars) for the relevant snapshot. For context, we also show the stellar radii for all of our systems (bottom panels). When a planet crossed the Roche-limit, we stop the integration and mark its orbital parameters.

Note the slight offset between the distribution of red and magenta points on the right side of the lower frame of the mid-main-sequence panel. This offset is simply caused by the red points showing planets that have been destroyed via EKL-driven high-eccentricity Roche-lobe crossing. This happens quickly, before the host stars can significantly evolve and expand. All the planets that lie in the region of the parameter space that allow such large eccentricities to be reached do so and get tidally destroyed or engulfed early in the systems' lifetime. By the middle of the main-sequence lifetime of the star, the rest of the systems have evolved more and their stars have expanded; however, there simply are not many planets left in the correct parameter space to cross the new, expanded Roche limit; they have all already been destroyed. However, once the stars swell to become red giants, there is a new phase of destruction of planets that did not reach extreme eccentricities. The difference in behavior between these two different populations is due to the distinction between "quadrupole" and "octupole" types of EKL evolution (see Naoz et al. 2016, for a full review of the EKL mechanism). Thus, we predict an early "burst" of planet destruction during the early main-sequence evolution, followed by a pause until the stars become red giants, followed by another phase of planet destruction throughout post-main-sequence evolution.

3.2. CHJs and Surviving Jupiters

As we show in Figure 1 (see upper panels), by the middle of the main-sequence lifetime of the host stars, several classical HJs have been formed through high-eccentricity migration (shown in the upper left panels as purple dots, with periods shorter than about 10 days and eccentricities close to 0), or are still in the process of forming until the end of the main sequence. However, these more massive stars expand their radius during the main sequence by about a factor of two, which results in a higher rate of Roche-limit crossing than for less massive stars, since the more massive stars evolve and expand more quickly and the Roche-limit is proportional to the radius of the star (see Equation (2)). In total, we form 64 such HJs, or about 1.5% of our systems, which is broadly consistent with, though somewhat less efficient than, previous estimates of EKL-induced high-eccentricity migration models in stellar binaries, which considered smaller mass host stars (see, for example, Naoz et al. 2012, 2016; Petrovich 2015; Anderson et al. 2016). Some of these classical HJs only survive for short times at these orbits, as the interplay of the EKL mechanism and tides keeps driving them toward the stellar surface. However, many can exist for tens to hundreds of megayears after formation. Ultimately, though, all classical HJs get engulfed and destroyed as their host stars evolve and expand in radius. By the end of the main sequence, most of them have been destroyed (see the upper right panels of Figure 1; red dots show destroyed planets, with several red dots forming a line in the stellar radius versus orbital period parameter space where HJs were engulfed by their expanding host stars), with the remaining ones being destroyed as the stars evolve toward the giant phase (see the orange and yellow dots in the lower, large panels). In general, classical HJs around A-type main-sequence stars form at a lower frequency than HJs around smaller mass stars through high-eccentricity migration, and exist for shorter times due to faster stellar evolution, expansion, and tides.

The black stars in Figure 1 show the parameters of several observed Jupiters around A-type or retired A-type stars (Johnson et al. 2007, 2008, 2010a, 2010b, 2011a, 2011b, 2014, 2018; Collier Cameron et al. 2010; Sato et al. 2013; Bieryla et al. 2014; Wittenmyer et al. 2014, 2015a, 2015b; Hartman et al. 2015; Zhou et al. 2016; Beatty et al. 2017; Borgniet et al. 2017; Gaudi et al. 2017; Lund et al. 2017; Siverd et al. 2018; Talens et al. 2018), and they appear to be broadly consistent with our calculations. The observed HJs agree well with our predicted parameters at some time during the middle of the main-sequence lifetime of A-type stars (upper left panels), while observed Jupiters on wider orbits (periods beyond about 100 days) around retired A-type stars agree well with our predicted parameters for Jupiters that survive to the end of the main-sequence lifetime (upper right panels). Note that both observations and our predictions do not seem to show many Jupiters on intermediate orbits between 10 and 100 days. HJs migrate relatively fast through this part of the parameter space, on the order of a few million years (a very small fraction of the stars' total main-sequence lifetime), and are unlikely to be randomly observable.

3.3. Temporary Hot Jupiters

During post-main-sequence evolution, stars begin to expand, and those planets that have short pericenter distances are engulfed by their host stars. Furthermore, our calculations show that a large number of moderately eccentric giant planets will undergo significant tidal interactions with the expanding red-giant stars, leading to orbital shrinking and circularization before the eventual crossing of the Roche lobe or engulfment by the star, as shown by the example system evolution in Figure 2. During the red-giant phase, the strength of tidal effects on the star increases significantly due to the stellar radial expansion and the increased size of the convective envelope. During their main-sequence lifetime, A-type stars are mostly radiative, which severely reduces the effectiveness of their tides (Zahn 1977). We consequently observe a switch in the role of tides between the main-sequence and post-main-sequence evolution; while during the main sequence, the tidal effects on the planet were more significant, during post-main-sequence evolution, the tides on the star dominate. Tidal interactions and planet engulfment can be expected to have significant effects on the red-giant stars' envelope and mass-loss evolution, as well as changing the stellar rotation rate; such giant planet interactions with evolved stars have been used to explain observed irregularities in the shape of the horizontal branch in

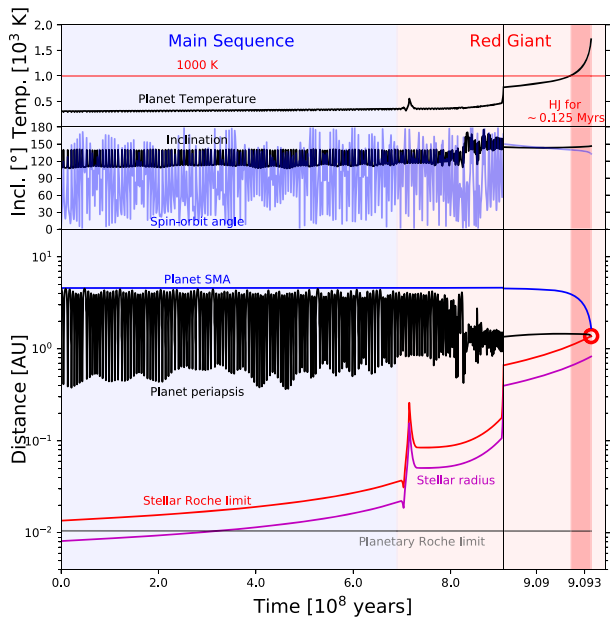

Figure 2. Orbital evolution of a Jupiter around an evolving A-type star in a stellar binary, leading to formation and destruction of a temporary hot Jupiter. The figure shows an example of Jupiter's equilibrium temperature (top frames), inclination, and spin–orbit angle (middle frames) and semimajor axis, periapsis, and stellar radius evolution (bottom frames) over time. In the bottom frames, the blue line shows the planet's semimajor axis, red and magenta show the host star's Roche limit and radius, and gray shows the planet's Roche limit. The blue shaded region marks the host star's main-sequence phase, while the red shaded area marks the post-main-sequence phase. The left frames of the figure show the first 908.8 Myr of evolution, while the right frames focus on the last 0.5 Myr before the planet enters the star's Roche lobe. Note that the planet's semimajor axis undergoes rapid tidal decay once the red-giant star has expanded sufficiently, on the very right edge of the figure. This rapid orbital decay lasts on the order of 300,000 years before the planet reaches the stellar Roche limit. The equilibrium temperature of the planet rises above 1000 K (marked by the red line in the top frames) for the last 125,000 years before entering the Roche lobe, rapidly increasing as the orbit decays, as highlighted by the darker red shaded area. Initial system parameters are $m_{*,1} = 2.39\,M_\odot$, $m_{*,2} = 1.95\,M_\odot$, $a_1 = 4.58$ au, $a_2 = 601.6$ au, $e_1 = 0.01$, $e_2 = 0.587$, spin–orbit angle $= 0°$, and $i = 108.^\circ 2$.

the Hertzsprung–Russel diagram (e.g., Soker 1998; Soker & Harpaz 2000; Livio & Soker 2002). Our "Temporary" HJs would most likely lead to such interactions, though we stop our calculations at the entering of the stellar Roche lobe. Further investigation would require a full hydro-dynamical treatment of the star–planet interactions. We assume that the further evolution of the stellar envelope and post-AGB remnant will be altered due to these interactions. THJ engulfment could also lead to lithium enrichment in the giant stars' atmospheres (e.g., Aguilera-Gómez et al. 2016).

The lower large panels in Figure 1 show the final orbital parameters of our systems in eccentricity versus period (upper frame) and host-star radius versus period space (lower frame). Those dots colored red, yellow, green, cyan, and blue show the final parameters before planets enter the stellar Roche lobe during the different post-main-sequence and pre-WD phases. The vast majority of these, those that form a distinct line on the left in the stellar radius versus period frame, experience at least some degree of high-eccentricity migration, and reach equilibrium temperatures comparable to classical HJs (see Figure 3). These planets begin to experience significant tidal interactions with their host stars as those stars expand in radius, facilitated by increasing orbital eccentricities due to the EKL mechanism. However, due to the continued stellar evolution of the host stars and the significantly enhanced tides, most of these THJs enter their host stars' Roche lobe even before they can be fully circularized, making their status as HJs very short-lived. We therefore name this class of HJs THJs. The THJ shown in Figure 2 only lives for about 300,000 years once tidal orbital decay becomes efficient before it reaches the stellar Roche limit. This process should, as mentioned above, have significant effects on the further evolution of the giant star's outer envelope.

While most (∼80%) of the THJs we discuss here are products of high-eccentricity migration caused by the EKL mechanism and tidal dissipation and therefore depend on the presence of a companion star, some THJs can also be formed without a companion. If a gas giant's initial orbit is sufficiently close, in general, smaller than about 3 au, post-main-sequence expansion of the host star will eventually lead to tidal interactions and engulfment of the planet even without increased orbital eccentricity, consistent with previous works investigating the evolution of gas giants around giant stars (e.g., Villaver & Livio 2009; Spiegel & Madhusudhan 2012; Lopez & Fortney 2016). However, one can distinguish between these two cases considering the spin–orbit alignment of the planet and the main star. If a THJ is formed without companion excitations, the orbital plane will not change from its initial orientation, which we assume to be aligned with the stellar spin. If the THJ was formed through the EKL mechanism, however, the spin–orbit angle will be from a nearly uniformly random distribution between 0° and 180°. We can see this in Figure 4. The two histograms on the right side of the figure show the distribution of spin–orbit angles among THJs. Both histograms show the same population, only that the far right one labeled "THJs (all)" includes THJs formed both with and without EKL effects, while the one labeled "THJs (EKL)" only shows those formed through EKL effects. Those THJs formed without EKL effects, for which the stellar companion was irrelevant, are all aligned and form the large peak at 0°, while those formed with EKL effects are nearly evenly spread across the whole range of angles between 0° and 180°. While the peak is large, it is extremely narrow and only includes ∼20% of our total number of THJs.

4. Observational Signatures

4.1. Equilibrium Temperature

The equilibrium temperature of planets is a potentially observable signature (e.g., Gaudi et al. 2017). We calculate the time-averaged equilibrium temperature for elliptical orbits for the planets in our simulations, following equations by Méndez & Rivera-Valentín (2017), namely:

$$\langle T_{\rm eq}\rangle \approx T_0\left[\frac{(1-A)L}{\beta\epsilon\, a^2}\right]^{\frac{1}{4}}\left[1-\frac{1}{16}e^2-\frac{15}{1024}e^4+\mathcal{O}(e^6)\right], \tag{3}$$

where $T_0 = 278.5$ K, Earth's equilibrium temperature, A is the planetary albedo (assumed to be zero), L is the host star's luminosity (in $L_\odot$), e and a are the planet orbit's eccentricity and semimajor axis (in au), respectively, and β and ϵ are coefficients for the planet's heat distribution and emissivity, respectively (both assumed to be ∼1 for simplicity).

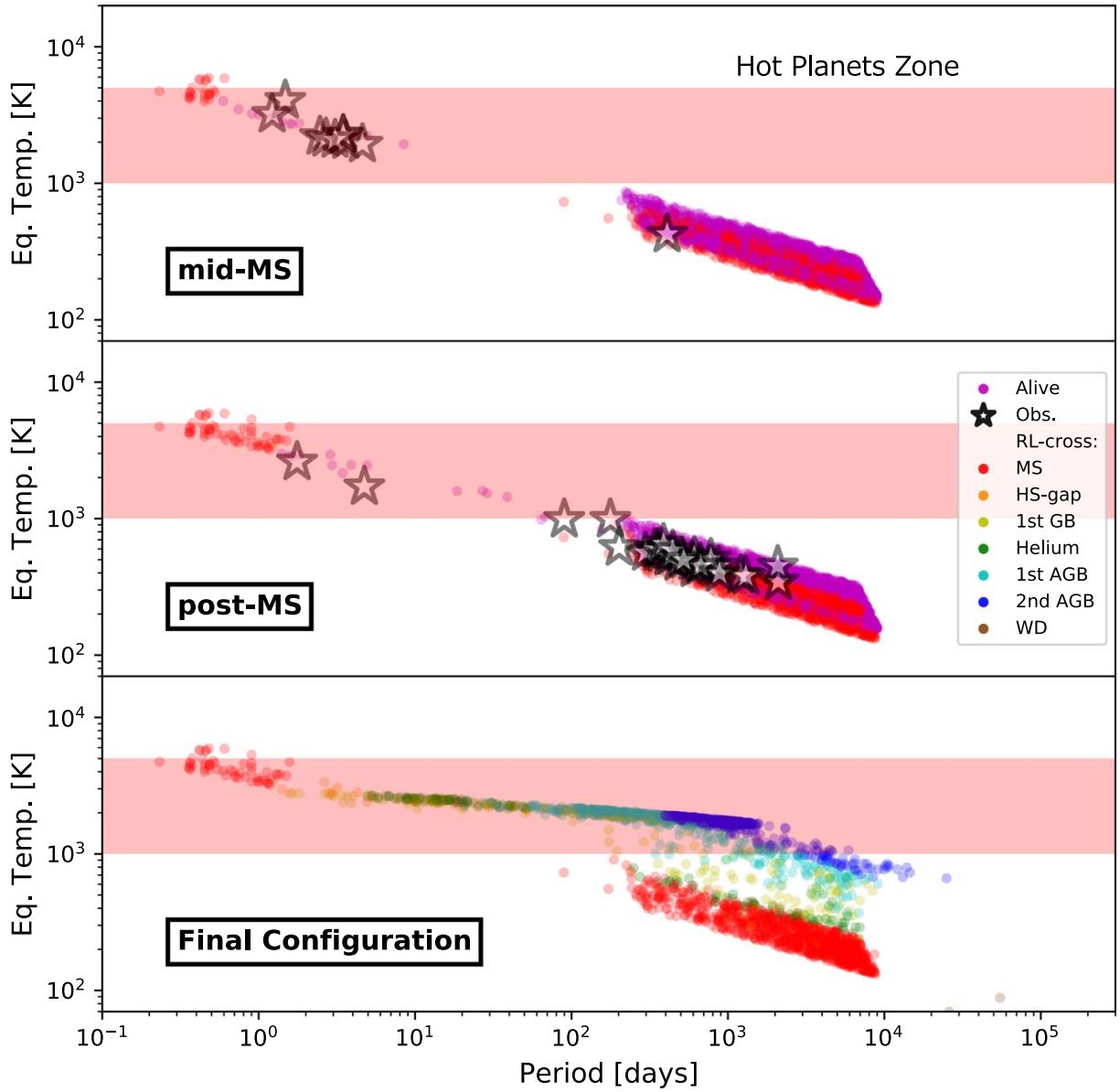

Figure 3. Equilibrium temperatures of Jupiters around A-type stars in binary systems. Equilibrium temperature vs. period of Jupiters for three evolutionary periods: middle of the main sequence (upper panel), beginning of the post-main-sequence (center panel), and the WD phase (bottom panel). Values for observed Jupiters around A-type stars are included as black stars. Dot colors have the same meaning as in Figure 1. The red shaded area shows the approximate parameter space of "hot" planet temperatures, from around 1000 to 5000 K. Note that THJs, which are within the red shaded area in the lower panel, can reach final equilibrium temperatures of several thousand Kelvin shortly before being destroyed, due to the intense stellar luminosity of the post-main-sequence host stars. Equilibrium temperatures were calculated using Equation (3) (Méndez & Rivera-Valentín 2017) for eccentric orbits, assuming zero albedo, or taken from papers cited in Section 3.2 for observed planets.

The classical hot Jupiters (CHJs) in our calculations have typical temperatures of about 2000–5000 K, consistent with estimated temperatures of observed HJs, as can be seen in the top frame of Figure 3, which shows our CHJs as magenta dots and observed HJs as black stars in the "Hot Planets Zone." CHJs remain at these temperatures for potentially millions of years, until they either evaporate or are engulfed by the host star as it leaves the main sequence (see the red dots in the middle frame of Figure 3. We find that THJs reach temperatures between 1000 and 3000 K just before entering the stellar Roche lobe, as shown in the bottom frame of Figure 3. The THJs only exist at such high temperatures for a short time, on the order of a few 100,000 years, as seen in the top right frame of Figure 2, as the increase in temperature follows from the planets' rapid orbital decay and the rapid increase in stellar luminosity due to post-main-sequence stellar evolution. Considering that the stellar luminosity increases tremendously during post-main-sequence stellar evolution, even THJs will produce a rather small contribution to the overall stellar spectra. At a wavelength of around 1 μm, the contrast between THJ and stellar emissions will be around 10^{-5}–10^{-7}. Additionally, the expanding stars' large size will

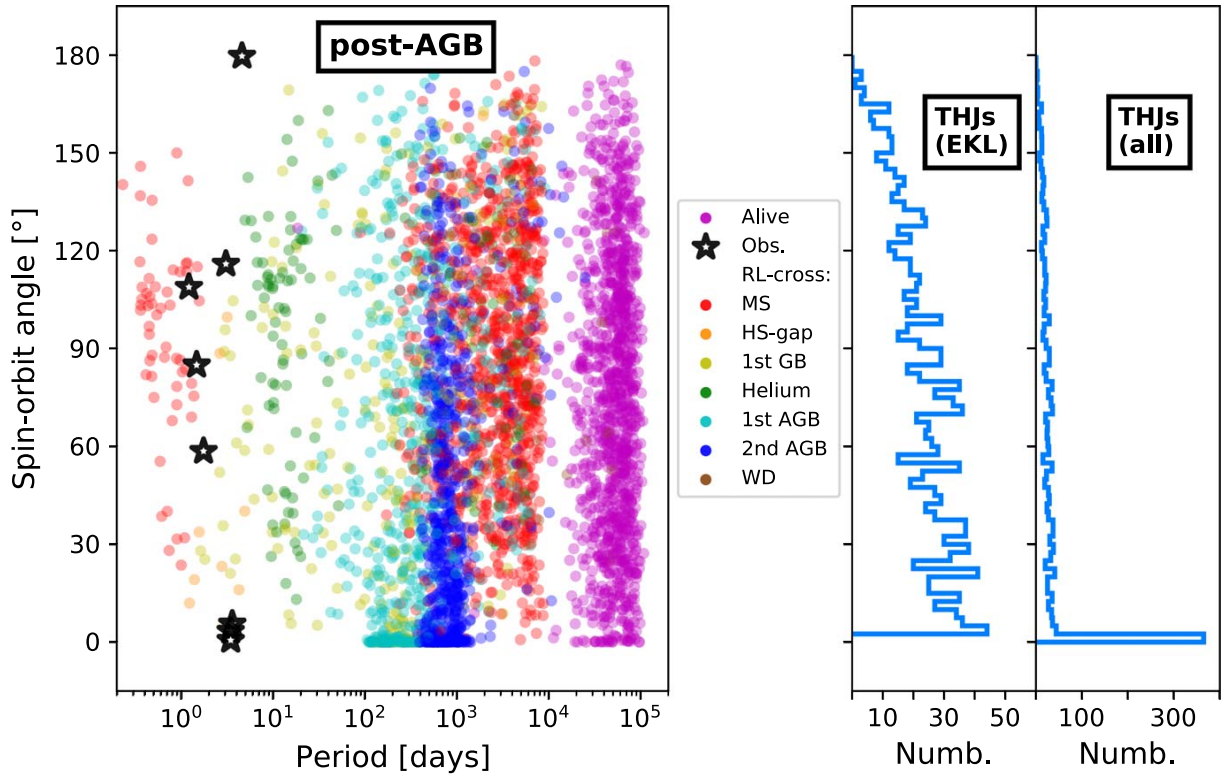

Figure 4. Spin–orbit misalignment angles for Jupiters around A-type stars in binary systems. Left large panel: Spin–orbit misalignment angle vs. period for Jupiters during the WD phase, with magenta dots showing survived Jupiters and differently colored dots showing destroyed Jupiters. Dot colors have the same meaning as in Figure 1. The plot shows that HJs, both classical and temporary, that form due to the EKL mechanism are most likely to have significantly misaligned orbits compared to their host stars' spin axes. This is broadly consistent with the few measured projected spin–orbit angles for HJs around A-type stars, shown by the black stars. THJs that form without the influence of the EKL mechanism are, in contrast, very well aligned (depicted by the blue and cyan points that are clustered near 0°). The two histograms in the right side panels show the distribution of misalignment angles for THJs. The far right histogram, labeled "THJs (all)," shows the spin–orbit angle distribution of all THJs, including both those formed with and without EKL effects, while the histogram to the left of it, labeled "THJs (EKL)," only shows those formed through EKL effects. Both histograms are practically identical except for the scale of the *x*-axis, which represents the number of simulated systems. The large peak at 0° inclination in the far right panel simply includes all non-EKL THJs. About 20% of THJs are in this peak and form without EKL effects, while about 80% of our THJs form through the EKL mechanism, spread across the rest of the spin–orbit angle parameter space.

make planet transit detection signals smaller as well; however, the larger size will also increase the chance that a transit can occur. At least for THJs around "small" giant stars ($R_* \sim 5\,R_\odot$), such as for stars during the helium burning phase, models suggest that transits are indeed observable (e.g., Assef et al. 2009), and some giant planets transiting giant stars of such sizes have indeed been observed (e.g., Lillo-Box et al. 2014), though it remains unclear if such transits would currently be observable for stars with sizes of hundreds of solar radii. However, if the increase in temperature leads to significant planetary inflation and if stellar high energy radiation or winds can drive a significant mass loss from the Jupiter, absorption lines from the stripped planetary material might be observable (e.g., Murray-Clay et al. 2009).

4.2. Stellar Obliquity

Detecting planets through the transit method makes it possible to observe the (projected) angle between the stellar spin axes and the planets' orbital planes through the Rossiter–McLaughlin effect (Gaudi & Winn 2007). Our calculations show that THJs, like CHJs, should preferentially be misaligned to the stellar spin axis, with a nearly uniform distribution of spin–orbit angles, showing only a small preference against fully retrograde orbits, as can be seen from the THJ spin–orbit angle histograms in Figure 4. Using the spin–orbit angle, it should also be possible to distinguish THJs born through EKL effects from THJs without that effect, as the later will remain aligned to their original spin–orbit angle, which can be assumed to be small, close to 0° in our case. As can also be seen from the left frame of Figure 4, observed projected spin–orbit angles for HJs also broadly confirm a broad range of misalignment angles, potentially caused by EKL effects.

4.3. Orbital Eccentricity

The eccentricities of planetary orbits is an important factor for understanding the architectures of planetary systems, as larger eccentricities can be indicators of significant dynamical interactions, such as planet–planet scattering events or secular perturbations, while small eccentricity values are expected from disk models of planetary formation and a subsequently quiescent dynamical history. Massive evolved stars show a deficiency of short-period eccentric planets (Johnson et al. 2007, 2008, 2010a, 2010b, 2013; Sato et al. 2008; Bowler et al. 2010; Schlaufman & Winn 2013). Our calculations show that this feature is in agreement with the dynamical evolution of giant planets in stellar binaries. As

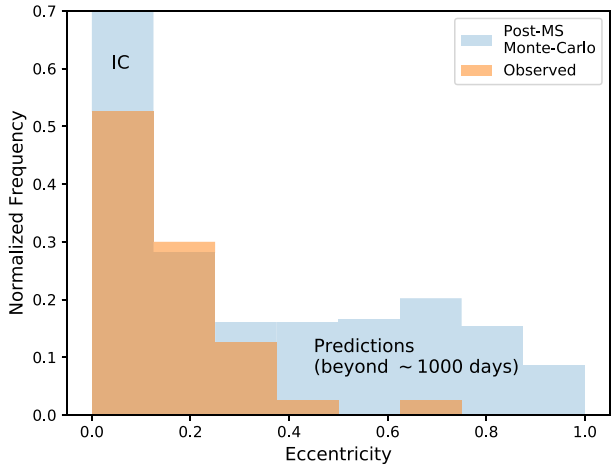

Figure 5. Simulated vs. observed eccentricity distributions for Jupiters around retired A-type stars. The plot shows the normalized frequencies of Jupiter eccentricities from observations (in orange) and from our simulations (in blue) during the post-main-sequence phase. Note that the high peak between eccentricities of 0 and 0.1 in the post-MS distribution continues beyond the frame; as we assumed very small eccentricities for all Jupiters at the beginning of our simulations, this is probably an artifact of our initial conditions. Furthermore, our simulations predict a more uniform distribution of eccentricities that continues toward higher values than currently observed. However, these higher eccentricity planets exist mostly beyond periods of ~1000 days, making them very difficult to observe with current methods (see Figure 1, top right frame). Note that the currently highest eccentricity Jupiter observed around a "retired" A-type star does indeed have an orbital period of about 2000 days (Sato et al. 2013).

shown in Figure 1, top panels, both the MS phase as well as the post-MS phase are in agreement with the observed giant planet eccentricities (the latter depicted as black stars). We predict that there is a large population of highly eccentric planets around main sequence and retired A-type stars, as shown in Figure 5 by the blue histogram; however, most of these high-eccentricity planets have orbits longer than ~1000 days (see Figure 1, top panels), making them difficult to observe with current methods. Interestingly, the highest eccentricity Jupiter-sized planet observed that orbits a retired A-type star, HD 120084, is very consistent with these predictions, having an eccentricity of 0.66 and a period of 2082 days (Sato et al. 2013).

Our results also indicate that most THJs will migrate to close-in orbits and get engulfed by their expanding host stars before the orbits can fully circularize, as seen in Figure 1. These planets will still have some residual eccentricities up until engulfment, consistent with a recent study of close-in planets around evolved stars (Grunblatt et al. 2018).

In our simulations, we assume that all giant planets start with very small eccentricities and treat them as singular planets around their host stars. This ignores the potential for planet–planet scattering during the further evolution. In the normalized histograms in Figure 5, we see that this artifact of our initial conditions produces an extremely high peak at small eccentricities for our simulated systems during the post-main-sequence phase (see blue histogram). This peak simply represents those systems that lie outside the parameter space that can undergo EKL oscillations. We propose that the actual initial eccentricity distribution should be more broad, probably caused by planet–planet interactions after dissipation of the planet-forming disk.

4.4. Effects of Post-MS Roche-lobe Crossing and Engulfment of THJs

A giant planet entering an expanding post-main-sequence star's Roche lobe, and subsequently the stellar envelope, can undergo and cause a multitude of effects. If the giant planet is massive and dense enough, it might resist dissipation and begin to accrete stellar material, potentially becoming a "stellar" companion undergoing complex common-envelope evolution with the main star (e.g., Soker et al. 1984). Planet engulfment should also lead to the deposition of angular momentum into the star, changing the spin rate (see Carlberg et al. 2009), which has similar consequences during the main-sequence phase (Carlberg et al. 2009; Qureshi et al. 2018), as well as the deposition of energy into the stellar envelope due to drag forces and orbital decay, increasing the luminosity of the star or producing bright UV and X-ray transients (e.g., Metzger et al. 2012; MacLeod et al. 2018). The strength of drag forces depends especially on the density of the stellar envelope and the orbital speed of the engulfed planet, which would lead to different strengths of this effect between main-sequence and post-main-sequence stars or between eccentric and circular planetary orbits. Furthermore, giant planets can have a range of masses beyond the simple Jupiter-analogs we have considered here, and can vary in density, especially if the planets are inflated due to increased temperatures (Lopez & Fortney 2016). This would lead to further variations in the possible merger outcomes (e.g., Metzger et al. 2012; Siverd et al. 2012), while also producing lithium enrichment through the engulfed giant planets of varying strengths (e.g., Aguilera-Gómez et al. 2016). The engulfment process could also lead to the ejection of material from the stellar envelope or planet, leading to the formation of dust around the star. A potential candidate for this scenario is the first-ascent giant star TYC 4144 329 2, which also has a wide separation binary companion consistent with our model (Melis et al. 2009). Overall, our predicted THJs should have a, potentially significant, influence on the evolution of their host stars post-engulfment, which could present another observable signature of THJs through increased spin rates, larger stellar luminosities, dust formation, and lithium enrichment. The effects on the further stellar evolution should also be more long-lived than the predicted few 100,000 years of existence as THJs, making indirect detection of THJs more promising than direct detection.

4.5. Occurrence Rate of HJs and THJs

To gain a better understanding of the importance of HJs and THJs as part of the overall planet population, we can estimate the fraction of systems that will produce HJs or THJs in the following way:

$$f_{\rm outcome} = f_b f_p f_{\rm event}, \quad (4)$$

where f_b is the fraction of stars in binary systems, close to 100% for A-type stars (e.g., Raghavan et al. 2010; Moe & Di Stefano 2017), f_p is the fraction of Jupiter-mass planets formed at distances of a few astronomical units from their stars, which is highly uncertain, and which we extrapolate here to be $f_p \sim 0.07$–0.1 from values for G-type stars (e.g., Wright et al. 2012; Bowler 2016). Lastly, $f_{\rm event}$ is the fraction of simulated systems that has undergone one of the possible events specified in Table 1. For example, the percentage of systems that form HJs (during the main sequence) of all A-type

stars is $f_{\rm HJ} \sim 0.15\%$ ($\sim$10% of stars have a Jupiter, and $\sim$1.5% of Jupiters become HJs), while the percentage for THJs is $f_{\rm THJ} \sim 3.7\%$. Interestingly, $\sim$2.5% of all A-type star systems will consume a Jupiter during their main-sequence lifetime and about $\sim$4.5% during their post-main-sequence evolution.

We estimate the number of stars in the galaxy as $N_\star \sim (100\text{–}400) \times 10^9$, of which about 1% are in the mass range we consider here (e.g., Salpeter 1955). Thus, we can also estimate the rate at which a post-main-sequence Roche-limit crossing will take place in the galaxy (and might result in a luminosity or spin rate signature). To first order, considering the average lifetime of an A-type star to be on the order of 1 Gyr and assuming roughly uniform formation and death rates, the post-MS Roche-limit crossing rate is approximately 0.045–0.18 per year. We predict that most of these events will be caused by THJ formation and engulfment and that, given that THJs go through their orbital decay phase on the order of a few 100,000 years, there will be a few to tens of thousands of THJs in the galaxy at any given moment. The length and strength of the increased luminosity signal in red-giant stars caused by THJ engulfment and orbital energy deposition is difficult to estimate, but if it is comparable to the Kelvin–Helmholtz timescale, which is on the order of a few 10,000 years for red giants, there should be thousands of such stars with enhanced luminosities in the galaxy at any given moment. These rates indicate that THJs and their effects on post-main-sequence stars should be observable and have a strong effect on the luminosity function of intermediate mass red-giant stars.

5. Discussion

In this work, we have explored the dynamical evolution of single giant planets around A-type stars in hierarchical binaries. Considering initially circular planetary orbits between 1 and 10 au, we identify four principal evolution outcomes:

1. Classical hot Jupiters (CHJs): Giant planets that undergo high-eccentricity migration to short-period orbits ($P < 10$ days) during the main-sequence lifetime of the main star, caused by an interplay of the EKL mechanism and tidal effects. These planets can typically reach temperatures of 2000–5000 K and are eventually engulfed by the star as it expands during post-main-sequence stellar evolution. About 1.5% of our giant planets in binaries lead to this result.
2. Temporary hot Jupiters (THJs): THJs form during post-main-sequence evolution, as the stars expand. These giant planets can either form like CHJs through high-eccentricity migration caused by EKL effects and tides, or their initial orbits were close enough to their stars to eventually be heated up and engulfed by their stars even with low eccentricities ($a_1 \lesssim 3$ au). These planets only exist as HJs for a few 100,000 years before Roche-lobe crossing and engulfment, but can have significant effects on the stellar envelope and can reach temperatures of 2000–3000 K before entering the stellar Roche lobe of the expanding star. About 37% of our systems lead to this outcome.
3. Roche-limit crossers: These are giant planets that undergo very strong EKL effects that are too strong to be counteracted by tidal forces, thus crossing the Roche limit or grazing the stellar surface at high eccentricities and velocities. About 23% of our giant planets experience this result during the stellar main sequence, while a further 8% do so in the post main sequence. During the AGB-phase, the stars lose a significant part of their mass, changing the orbital parameters of some systems enough to increase EKL strength significantly. This leads to about 0.3% of our giant planets to accrete and pollute the WD remnants through high-eccentricity Roche-limit crossing.
4. Surviving Jupiters: Gas giant planets that originally had large orbital periods and never underwent strong enough EKL effects to lead to significant interactions with their host stars. This is the case for about 30% of our systems.

Overall, only 30% of the planets will survive to the WD phase without stellar interactions, while 70% will be engulfed at some point in their evolution. The engulfed planets can have significant effects on the stellar rotation rates and luminosities. The EKL mechanism greatly enhances the fraction of planets that end up being engulfed; about 80% of engulfed planets have undergone significant EKL effects. Overall, we predict a THJ engulfment rate of $\sim$0.045–0.18 per year, which, depending on the length and strength of the engulfment effects onto the red-giant stars' envelopes, could translate to thousands or tens of thousands of red giants with THJ engulfment effects at any given moment in our galaxy.

From our calculation results, we also predict that there is a large population of high-eccentricity giant planets around A-type stars with orbital periods $\gtrsim$1000 days, which is difficult to observe, but is consistent with the known high-eccentricity giant planets. Our results are also consistent with the observed large, nearly isotropic spread of spin–orbit misalignment angles, further suggesting that stellar binary dynamics are crucial for the understanding of giant planet orbits around A-type star.

We thank the anonymous referee for helpful comments and questions that helped us to improve this paper. S.N. acknowledges the partial support from the Sloan foundation. S.N. and A.P.S. also acknowledge the partial support from the NSF through grant No. AST-1739160. We thank John Johnson for many inspiring conversations between him and S.N. during the time she was a postdoc at the ITC. We thank Ben Zuckerman, Michael Fitzgerald, and Ruth Murray-Clay for comments and discussions. We also thank Ahmed Qureshi for assisting in the continuing improvement of modeling the stellar spins. Calculations for this project were performed on the UCLA cluster *Hoffman2*.

Software: SSE (Hurley et al. 2000), Matplotlib (Hunter 2007).

Appendix
A-type Stars: Definitions and Evolution

Here we give a short overview of A-type stars' evolutionary phases. A-type main-sequence stars are usually defined to have masses between $\sim$1.6 and $\sim$2.4 $M_\odot$ with surface temperatures between about 7000 and 10,000 K (Adelman 2004). Figure 6 shows the evolution of temperature versus luminosity and radius for three example star masses (1.6, 2.0, and 2.4 $M_\odot$), calculated using `SSE` (Hurley et al. 2000).

As A-type stars evolve along the main sequence, shown in red in Figure 6, they slowly expand in radius by about a factor of two, cool down by $\sim$2000–3000 K, and increase in luminosity by about a factor of two as well. Note that this

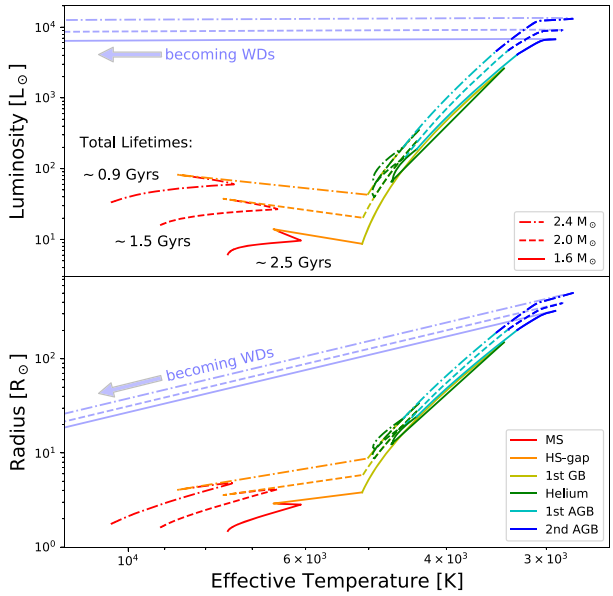

Figure 6. Stellar evolution temperature vs. luminosity and radius profiles of A-type stars. Shown are stellar evolutionary tracks for 1.6, 2.0, and 2.4 $M_\odot$ A-type stars, shown by a line, a dashed line, and a dotted–dashed line, respectively. The upper panel shows the evolution of temperature vs. luminosity, the lower panel shows temperature vs. radius. The colors of the curve segments represent different evolutionary phases, same as in Figure 1: (red) main sequence; (orange) Hertzsprung gap; (yellow) first giant branch; (green) core helium burning; (cyan) first asymptotic giant branch; (blue) second asymptotic giant branch. The light blue segment shows the evolution when the stars are becoming WDs. Lifetimes until becoming WDs for the three masses of stars are indicated in the upper panel. The lifetimes are, from low to high mass, 2.5, 1.5, and 0.9 Gyr. Tracks and times were calculated using SSE (Hurley et al. 2000).

evolution is slightly different from Sun-like G-type stars, which initially heat up during their main-sequence evolution before finally cooling down. The main-sequence phase lasts for about 2.2 Gyr for 1.6 $M_\odot$ A-type stars and 0.7 Gyr for 2.4 $M_\odot$. After they have expended their core hydrogen fuel, the stars then evolve through the Hertzsprung gap, shown in orange, rapidly expanding by another factor of two, cooling down to about 5000 K, and halving their luminosity over the course of 5–50 Myr (high to low mass).

Afterward, the first giant branch phase begins, shown in yellow, lasting for 6–100 Myr. This phase progresses very differently for low versus high mass A-type stars. A 1.6 $M_\odot$ star grows from 4 to 140 $R_\odot$, increases in luminosity from 8 to 2500 $L_\odot$ and cools down from 5000 to 3500 K, while a 2.4 $M_\odot$ star grows only from 8 to 33 $R_\odot$, increases in luminosity from 42 to 350 $L_\odot$ and cools down from 5000 to 4500 K. At the end of the first giant branch phase, the stars contract to their previous radius, luminosity, and temperature, as they begin to burn helium in their cores, shown in green. The helium burning phase lasts for about 200 Myr for 1.6 $M_\odot$ stars, 300 Myr for 2.0 $M_\odot$ stars, and 130 Myr for 2.4 $M_\odot$ stars. After expending their helium fuel, the stars rapidly evolve to become AGB giants, shown as in cyan (first ascent) and dark blue (second ascent), expanding to sizes of about 3000–4000 $R_\odot$, cooling down to 3000 K, and increasing their luminosities to about 10,000 $L_\odot$ over the course of 5–9 Myr. The stars then expel their outer layers and lose mass, becoming WDs.

In total, 1.6 $M_\odot$ stars need 2.5 Gyr, 2.0 $M_\odot$ stars need 1.5 Gyr, and 2.4 $M_\odot$ stars need 0.9 Gyr to reach the WD phase.

ORCID iDs

Alexander P. Stephan https://orcid.org/0000-0001-8220-0548
Smadar Naoz https://orcid.org/0000-0002-9802-9279
B. Scott Gaudi https://orcid.org/0000-0003-0395-9869

References

Adelman, S. J. 2004, in IAU Symp. 224, The A-Star Puzzle, ed. J. Zverko et al. (Cambridge: Cambridge Univ. Press), 1
Aguilera-Gómez, C., Chanamé, J., Pinsonneault, M. H., & Carlberg, J. K. 2016, ApJ, 829, 127
Anderson, K. R., Storch, N. I., & Lai, D. 2016, MNRAS, 456, 3671
Armitage, P. J. 2007, ApJ, 665, 1381
Armitage, P. J., Livio, M., Lubow, S. H., & Pringle, J. E. 2002, MNRAS, 334, 248
Assef, R. J., Gaudi, B. S., & Stanek, K. Z. 2009, ApJ, 701, 1616
Barnes, J. W., van Eyken, J. C., Jackson, B. K., Ciardi, D. R., & Fortney, J. J. 2013, ApJ, 774, 53
Batygin, K., & Morbidelli, A. 2013, AJ, 145, 1
Beatty, T. G., Stevens, D. J., Collins, K. A., et al. 2017, AJ, 154, 25
Beaugé, C., & Nesvorný, D. 2012, ApJ, 751, 119
Bieryla, A., Hartman, J. D., Bakos, G. Á., et al. 2014, AJ, 147, 84
Boley, A. C., Payne, M. J., & Ford, E. B. 2012, ApJ, 754, 57
Borgniet, S., Lagrange, A.-M., Meunier, N., & Galland, F. 2017, A&A, 599, A57
Bowler, B. P. 2016, PASP, 128, 102001
Bowler, B. P., Johnson, J. A., Marcy, G. W., et al. 2010, ApJ, 709, 396
Carlberg, J. K., Majewski, S. R., & Arras, P. 2009, ApJ, 700, 832
Charpinet, S., Fontaine, G., Brassard, P., et al. 2011, Natur, 480, 496
Chatterjee, S., Ford, E. B., Matsumura, S., & Rasio, F. A. 2008, ApJ, 686, 580
Collier Cameron, A., Guenther, E., Smalley, B., et al. 2010, MNRAS, 407, 507
Collier Cameron, A., & Jardine, M. 2018, MNRAS, 476, 2542
Denham, P., Naoz, S., Hoang, B.-M., Stephan, A. P., & Farr, W. M. 2018, arXiv:1802.00447
Dosopoulou, F., Naoz, S., & Kalogera, V. 2017, ApJ, 844, 12
Duquennoy, A., & Mayor, M. 1991, A&A, 248, 485
Eggleton, P. P., Kiseleva, L. G., & Hut, P. 1998, ApJ, 499, 853
Faber, J. A., Rasio, F. A., & Willems, B. 2005, Icar, 175, 248
Fabrycky, D., & Tremaine, S. 2007, ApJ, 669, 1298
Fabrycky, D. C., Johnson, E. T., & Goodman, J. 2007, ApJ, 665, 754
Farihi, J., Barstow, M. A., Redfield, S., Dufour, P., & Hambly, N. C. 2010, MNRAS, 404, 2123
Farihi, J., Jura, M., & Zuckerman, B. 2009, ApJ, 694, 805
Frewen, S. F. N., & Hansen, B. M. S. 2016, MNRAS, 455, 1538
Gaudi, B. S., Stassun, K. G., Collins, K. A., et al. 2017, Natur, 546, 514
Gaudi, B. S., & Winn, J. N. 2007, ApJ, 655, 550
Gettel, S., Wolszczan, A., Niedzielski, A., et al. 2012, ApJ, 745, 28
Ghezzi, L., Montet, B. T., & Johnson, J. A. 2018, arXiv:1804.09082
Goldreich, P., & Schlichting, H. E. 2014, AJ, 147, 32
Grunblatt, S. K., Huber, D., Gaidos, E., et al. 2018, ApJL, 861, L5
Guillochon, J., Ramirez-Ruiz, E., & Lin, D. 2011, ApJ, 732, 74
Hartman, J. D., Bakos, G. Á, Buchhave, L. A., et al. 2015, AJ, 150, 197
Howard, A. W., Marcy, G. W., Bryson, S. T., et al. 2012, ApJS, 201, 15
Hunter, J. D. 2007, CSE, 9, 90
Hurley, J. R., Pols, O. R., & Tout, C. A. 2000, MNRAS, 315, 543
Hut, P. 1980, A&A, 92, 167
Johnson, J. A., Bowler, B. P., Howard, A. W., et al. 2010a, ApJL, 721, L153
Johnson, J. A., Clanton, C., Howard, A. W., et al. 2011a, ApJS, 197, 26
Johnson, J. A., Fischer, D. A., Marcy, G. W., et al. 2007, ApJ, 665, 785
Johnson, J. A., Howard, A. W., Bowler, B. P., et al. 2010b, PASP, 122, 701
Johnson, J. A., Marcy, G. W., Fischer, D. A., et al. 2008, ApJ, 675, 784
Johnson, J. A., Morton, T. D., & Wright, J. T. 2013, ApJ, 763, 53
Johnson, J. A., Payne, M., Howard, A. W., et al. 2011b, AJ, 141, 16
Johnson, M. C., Cochran, W. D., Albrecht, S., et al. 2014, ApJ, 790, 30
Johnson, M. C., Rodriguez, J. E., Zhou, G., et al. 2018, AJ, 155, 100
Kaib, N. A., Raymond, S. N., & Duncan, M. 2013, Natur, 493, 381
Kiseleva, L. G., Eggleton, P. P., & Mikkola, S. 1998, MNRAS, 300, 292
Klein, B., Jura, M., Koester, D., & Zuckerman, B. 2011, ApJ, 741, 64
Klein, B., Jura, M., Koester, D., Zuckerman, B., & Melis, C. 2010, ApJ, 709, 950

Knutson, H. A., Fulton, B. J., Montet, B. T., et al. 2014, ApJ, 785, 126
Kozai, Y. 1962, AJ, 67, 591
Kratter, K. M., & Perets, H. B. 2012, ApJ, 753, 91
Lidov, M. L. 1962, P&SS, 9, 719
Lillo-Box, J., Barrado, D., Moya, A., et al. 2014, A&A, 562, A109
Lithwick, Y., & Wu, Y. 2012, ApJL, 756, L11
Liu, S.-F., Guillochon, J., Lin, D. N. C., & Ramirez-Ruiz, E. 2013, ApJ, 762, 37
Livio, M., & Soker, N. 2002, ApJL, 571, L161
Lloyd, J. P. 2011, ApJL, 739, L49
Lopez, E. D., & Fortney, J. J. 2016, ApJ, 818, 4
Lund, M. B., Rodriguez, J. E., Zhou, G., et al. 2017, AJ, 154, 194
MacLeod, M., Cantiello, M., & Soares-Furtado, M. 2018, ApJL, 853, L1
Masset, F. S., & Papaloizou, J. C. B. 2003, ApJ, 588, 494
Melis, C., Farihi, J., Dufour, P., et al. 2011, ApJ, 732, 90
Melis, C., Zuckerman, B., Song, I., et al. 2009, ApJ, 696, 1964
Méndez, A., & Rivera-Valentín, E. G. 2017, ApJL, 837, L1
Metzger, B. D., Giannios, D., & Spiegel, D. S. 2012, MNRAS, 425, 2778
Michaely, E., & Perets, H. B. 2014, arXiv:1406.3035
Moe, M., & Di Stefano, R. 2017, ApJS, 230, 15
Murphy, S. J., Moe, M., Kurtz, D. W., et al. 2018, MNRAS, 474, 4322
Murray-Clay, R. A., Chiang, E. I., & Murray, N. 2009, ApJ, 693, 23
Nagasawa, M., Ida, S., & Bessho, T. 2008, ApJ, 678, 498
Naoz, S. 2016, ARA&A, 54, 441
Naoz, S., Farr, W. M., Lithwick, Y., Rasio, F. A., & Teyssandier, J. 2011, Natur, 473, 187
Naoz, S., Farr, W. M., Lithwick, Y., Rasio, F. A., & Teyssandier, J. 2013a, MNRAS, 431, 2155
Naoz, S., Farr, W. M., & Rasio, F. A. 2012, ApJL, 754, L36
Naoz, S., Fragos, T., Geller, A., Stephan, A. P., & Rasio, F. A. 2016, ApJL, 822, L24
Naoz, S., Kocsis, B., Loeb, A., & Yunes, N. 2013b, ApJ, 773, 187
Ngo, H., Knutson, H. A., Hinkley, S., et al. 2016, ApJ, 827, 8
Niedzielski, A., Villaver, E., Nowak, G., et al. 2016, A&A, 589, L1
Niedzielski, A., Wolszczan, A., Nowak, G., et al. 2015, ApJ, 803, 1
North, T. S. H., Campante, T. L., Miglio, A., et al. 2017, MNRAS, 472, 1866
Nowak, G., Niedzielski, A., Wolszczan, A., Adamów, M., & Maciejewski, G. 2013, ApJ, 770, 53
Petrovich, C. 2015, ApJ, 799, 27
Petrovich, C., Malhotra, R., & Tremaine, S. 2013, ApJ, 770, 24
Qureshi, A., Naoz, S., & Shkolnik, E. 2018, arXiv:1802.08260
Raghavan, D., McAlister, H. A., Henry, T. J., et al. 2010, ApJS, 190, 1
Rasio, F. A., & Ford, E. B. 1996, Sci, 274, 954
Reffert, S., Bergmann, C., Quirrenbach, A., Trifonov, T., & Künstler, A. 2015, A&A, 574, A116
Salpeter, E. E. 1955, ApJ, 121, 161
Sato, B., Izumiura, H., Toyota, E., et al. 2008, PASJ, 60, 539
Sato, B., Omiya, M., Harakawa, H., et al. 2013, PASJ, 65, 85
Schlaufman, K. C., & Winn, J. N. 2013, ApJ, 772, 143
Shappee, B. J., & Thompson, T. A. 2013, ApJ, 766, 64
Siverd, R. J., Beatty, T. G., Pepper, J., et al. 2012, ApJ, 761, 123
Siverd, R. J., Collins, K. A., Zhou, G., et al. 2018, AJ, 155, 35
Soker, N. 1998, AJ, 116, 1308
Soker, N., & Harpaz, A. 2000, MNRAS, 317, 861
Soker, N., Livio, M., & Harpaz, A. 1984, MNRAS, 210, 189
Spiegel, D. S., & Madhusudhan, N. 2012, ApJ, 756, 132
Stello, D., Huber, D., Grundahl, F., et al. 2017, MNRAS, 472, 4110
Stephan, A. P., Naoz, S., Ghez, A. M., et al. 2016, MNRAS, 460, 3494
Stephan, A. P., Naoz, S., & Zuckerman, B. 2017, ApJL, 844, L16
Talens, G. J. J., Justesen, A. B., Albrecht, S., et al. 2018, A&A, 612, A57
Toonen, S., Hamers, A., & Portegies Zwart, S. 2016, ComAC, 3, 6
van Lieshout, R., Kral, Q., Charnoz, S., Wyatt, M. C., & Shannon, A. 2018, arXiv:1805.04429
van Saders, J. L., & Pinsonneault, M. H. 2013, ApJ, 776, 67
Villaver, E., & Livio, M. 2009, ApJL, 705, L81
Wittenmyer, R. A., Gao, D., Hu, S. M., et al. 2015a, PASP, 127, 1021
Wittenmyer, R. A., Horner, J., Tinney, C. G., et al. 2014, ApJ, 783, 103
Wittenmyer, R. A., Wang, L., Liu, F., et al. 2015b, ApJ, 800, 74
Wright, J. T., Marcy, G. W., Howard, A. W., et al. 2012, ApJ, 753, 160
Wu, Y., & Lithwick, Y. 2011, ApJ, 735, 109
Wu, Y., Murray, N. W., & Ramsahai, J. M. 2007, ApJ, 670, 820
Xu, S., Jura, M., Klein, B., Koester, D., & Zuckerman, B. 2013, ApJ, 766, 132
Xu, S., Zuckerman, B., Dufour, P., et al. 2017, ApJL, 836, L7
Zahn, J.-P. 1977, A&A, 57, 383
Zhou, G., Rodriguez, J. E., Collins, K. A., et al. 2016, AJ, 152, 136
Zuckerman, B., Koester, D., Dufour, P., et al. 2011, ApJ, 739, 101

The Astrophysical Journal, 889:45 (11pp), 2020 January 20 https://doi.org/10.3847/1538-4357/ab5b00
© 2020. The American Astronomical Society. All rights reserved.

Eating Planets for Lunch and Dinner: Signatures of Planet Consumption by Evolving Stars

Alexander P. Stephan[1,2], Smadar Naoz[1,2], B. Scott Gaudi[3], and Jesus M. Salas[1,2]
[1] Department of Physics and Astronomy, University of California, Los Angeles, Los Angeles, CA 90095, USA; alexpstephan@astro.ucla.edu
[2] Mani L. Bhaumik Institute for Theoretical Physics, University of California, Los Angeles, Los Angeles, CA 90095, USA
[3] Department of Astronomy, The Ohio State University, Columbus, OH 43210, USA
Received 2019 September 11; revised 2019 November 21; accepted 2019 November 21; published 2020 January 23

Abstract

Exoplanets have been observed around stars at all stages of stellar evolution, in many cases orbiting in configurations that will eventually lead to the planets being engulfed or consumed by their host stars, such as hot Jupiters or ultrashort period planets. Furthermore, objects such as polluted white dwarfs provide strong evidence that the consumption of planets by stars is a common phenomenon. This consumption causes several significant changes in the stellar properties, such as changes to the stellar spin, luminosity, chemical composition, or mass-loss processes. Here, we explore this wide variety of effects for a comprehensive range of stellar and planetary masses and stages of stellar evolution, from the main sequence over red giants to white dwarfs. We determine that planet consumption can cause transient luminosity features that last on the order of centuries to millennia, and that the post-consumption stellar spins can often reach breakup speeds. Furthermore, stellar mass loss can be caused by this spin-up, as well as through surface grazing interactions, leading to to the formation of unusual planetary nebula shapes or collimated stellar gas ejections. Our results highlight several observable stellar features by which the presence or previous existence of a planet around a given star can be deduced. This will provide future observational campaigns with the tools to better constrain exoplanet demographics, as well as planetary formation and evolution histories.

Unified Astronomy Thesaurus concepts: Stellar evolution (1599); Stellar rotation (1629); Tidal interaction (1699)

1. Introduction

Exoplanets have been observed around a variety of host stars, at all stages of stellar evolution, including main-sequence (MS), subgiant, and red giant branch stars (e.g., Charpinet et al. 2011; Johnson et al. 2011; Gettel et al. 2012; Howard et al. 2012; Barnes et al. 2013; Nowak et al. 2013; Reffert et al. 2015; Niedzielski et al. 2015, 2016). Additionally, white dwarf pollution signatures may indicate the presence of planetary systems in a large fraction of white dwarf systems (about 25% to 50%, e.g., Jura et al. 2009; Klein et al. 2010, 2011; Zuckerman et al. 2010; Melis et al. 2011). Planets that stray too close to their host star may get disrupted and finally consumed by the star (e.g., WASP-12b Patra et al. 2017), leading, for example, to the observed white dwarf pollution (e.g., Vanderburg et al. 2015).

Dynamical processes play an important role in planetary system formation and evolution, in particular planet consumption. Interactions between planets may result in orbital instability, possibly plunging planets into the star (e.g., Rasio & Ford 1996; Chatterjee et al. 2008; Nagasawa et al. 2008; Naoz et al. 2011; Teyssandier et al. 2013; Denham et al. 2019) Furthermore, the fraction of stellar binaries in the field is high ($\sim$40%–70% for $\gtrsim 1\,M_{\odot}$ stars, e.g., Raghavan et al. 2010). The stellar companions may also cause planets to plunge into their host stars (e.g., Lithwick & Naoz 2011; Naoz et al. 2012, 2013a; Veras & Tout 2012; Veras et al. 2013, 2017a, 2017b; Naoz 2016; Veras 2016; Stephan et al. 2017, 2018; Martinez et al. 2019; Veras & Wolszczan 2019).

The interplay between dynamical effects and post-MS evolution can be very rich. An evolving and expanding star may not only engulf planets on initially close-in orbits, but also faraway planets that have had their eccentricities excited due to perturbations from a third companion. Furthermore, an expanding star will experience stronger tidal forces (that scale with its radius) and may shrink a faraway planet's orbit enough to consume it. In either case, the vicinity to the star will heat the planets significantly prior to contact, turning them into "temporary hot Jupiters" (Stephan et al. 2018). However, the mass loss an evolving star undergoes can also expand the orbits, preventing consumption (Valsecchi et al. 2014). This orbital expansion can change the dynamical stability of a system, especially in the presence of companions, which can lead to star–planet collisions at later times (e.g., Hamers & Portegies Zwart 2016; Petrovich & Muñoz 2017; Stephan et al. 2017). The interplay of stellar evolution with dynamical processes can therefore explain a variety of interesting observations (e.g., Xu et al. 2017; Huber et al. 2019; Wang et al. 2019).

Here, we explore the physical processes that a star undergoes as it consumes a planet, for a range of stellar masses and evolutionary phases. The consumption of a planet by a star was considered in the literature as a way to explain a variety of astrophysical phenomena. For example, a planet grazing a stellar surface has been suggested as the cause for the peculiar gas ejections observed from the red giant star V Hydrae (Sahai et al. 2016; Salas et al. 2019). Furthermore, as a planet enters a star's atmosphere, its interaction with the stellar gas has been suggested to result in transit phenomena such as strong stellar wind, as well as strong optical, UV, and X-ray radiation (e.g., Herbig 1977; Retter & Marom 2003; Metzger et al. 2012). Consumption of planets or protoplanetary disk material has also been considered to explain the FU Orionis phenomenon, where a pre-main-sequence star undergoes a relatively fast increase in brightness followed by a gradual decline (e.g., Herbig 1977; Larson 1980; Elbakyan et al. 2019). Moreover,

planet engulfment, similar to binary star interactions, has been considered as a cause for nonspherical planetary nebulae systems (e.g., Morris 1981; Soker 1992, 1994, 1995, 1996, 1998a, 2001; Mastrodemos & Morris 1998; Soker & Harpaz 2000; Livio & Soker 2002; Morris et al. 2006; Kim et al. 2017; Sabach & Soker 2018).

When a star consumes a planet, it may have significant effects on the physical properties of the star. For example, it has been shown that the consumption of a Hot Jupiter by a young star can explain some observed patterns of spin–orbit misalignments in planetary systems (Matsakos & Königl 2015). Recently, a proof-of-concept calculation for main-sequence G- and K-type stars by Qureshi et al. (2018) showed that a consumption of a planet can significantly spin-up a star (lowering the spin period). Furthermore, they showed that this spin period change is consistent with the observed bifurcation of spin periods in young open clusters.

In this work, we integrate all the aforementioned aspects of planet consumption by stars for a comprehensive range of stellar masses and evolutionary phases. We calculate a range of observational signatures that can be used to infer active planetary consumption events (Section 2). In particular, we determine the phase space of planetary and stellar mass and radius that allow the ejection of stellar gas due to grazing interactions (Section 2.1); we calculate the duration and intensity of high-energy UV radiation emitted over the planet's migration through the stellar atmosphere (Section 2.2); and we estimate the new spin periods of post-consumption stars due to angular momentum conservation (Section 2.3).

2. Observable Signatures of Planet Consumption

The consumption of planets by stars involves a multitude of processes and effects as a consequence of angular momentum and energy conservation. As a planet begins to graze and contact the stellar surface, gravitational and tidal interactions can disturb or even eject stellar surface material (e.g., Dosopoulou et al. 2017; Salas et al. 2019). When the planet eventually migrates deeper into the stellar envelope, drag interactions will heat the stellar gas, producing additional luminosity (e.g., Retter & Marom 2003; Bear et al. 2011; Metzger et al. 2012), and transfer angular momentum from the planet's orbit onto the star, changing the stellar spin rate and orientation (e.g., Qureshi et al. 2018). Eventually, the planet will be disrupted and its material will be added to the star, changing its chemical composition. In this section, we investigate all of these consumption signatures and determine their strengths and relevance for different stellar types and evolutionary phases.

2.1. Surface Grazing Interactions

As a planet grazes the surface of a star, it can be expected that stellar surface material will be gravitationally disturbed by the planet, assuming that the planet did not get tidally disrupted beforehand. A planet with radius R_p can approach its host star as close as

$$R_{\rm Roche} \sim kR_p\left(\frac{M_*}{M_p}\right)^{1/3} \sim kR_\odot\left(\frac{R_p}{R_{\rm Jup}}\right)\left(\frac{M_*}{M_\odot}\right)^{1/3}\left(\frac{M_p}{M_{\rm Jup}}\right)^{-1/3} \quad (1)$$

without being disrupted, where M_* and M_p are the star's and planet's masses, respectively, and k is a numerical factor on the order of 1.6–2.4. In general, for any star of solar or heavier mass that has at least slightly evolved toward the later stages or past the main sequence, and which has not yet become a white dwarf or other compact object, this tidal disruption distance is smaller than or on the same order as the radius of the star itself, allowing a planet to reach the stellar surface and to undergo grazing interactions. The star V Hya is very likely an example of this type of interaction.

Over recent decades, the carbon star V Hya has been observed to periodically eject "bullets" of gaseous material (Sahai et al. 2016). These ejections can be explained by the close periastron passage of a substellar companion that grazes the stellar surface, scooping up surface material and ejecting some of it as "bullets" (Salas et al. 2019). A variety of mechanisms have been suggested as the cause of the ejections; however, here we consider a simple ballistic model (e.g., Dosopoulou et al. 2017), where the velocity of the bullets v_b is approximately equal to the sum of the planet's periastron passage velocity and the planet's escape velocity

$$v_b \sim \sqrt{G(M_* + M_p)\frac{1+e_p}{a_p(1-e_p)}} + \sqrt{\frac{2GM_p}{R_p}}, \quad (2)$$

where a_p and e_p are the orbital semimajor axis and eccentricity, respectively.

However, for a bullet to actually leave the star, the bullet velocity must be larger than the stellar escape velocity $v_{\rm esc,*}$ from the periastron, such that

$$v_b \geqslant v_{\rm esc,*}, \quad (3)$$

where v_b is defined in Equation (2) and the escape velocity is simply

$$v_{\rm esc,*} = \sqrt{\frac{2GM_*}{a_p(1-e_p)}}. \quad (4)$$

Equation (3) can yield a specific relation on the mass to radius ratio of planets and stars. Specifically, assuming that the star is much more massive than the planet and that the periastron distance must be approximately the same as the radius of the star, R_*, Equation (3) leads to the condition

$$\frac{M_p}{R_p} \geqslant \frac{M_*}{R_*}\left(\frac{3}{2} + \frac{e_p}{2} - \sqrt{2(1+e_p)}\right), \quad (5)$$

which needs to be fulfilled for ballistic ejections to efficiently leave the stellar system. Note that for extremely eccentric orbits ($e_p \sim 1$), the right side of Equation (5) approaches zero, greatly enhancing ejection likelihood. Figure 1 shows how different types of planets are able to cause V Hya-like ejections, depending on their masses and the stellar evolutionary phases. If a planet does not fulfill Equation (5), its interaction with the stellar surface can only eject stellar material onto bound orbits around the star. This could produce a gas and dust disk or cloud around the star whose mass and extend would depend on the planet's mass.

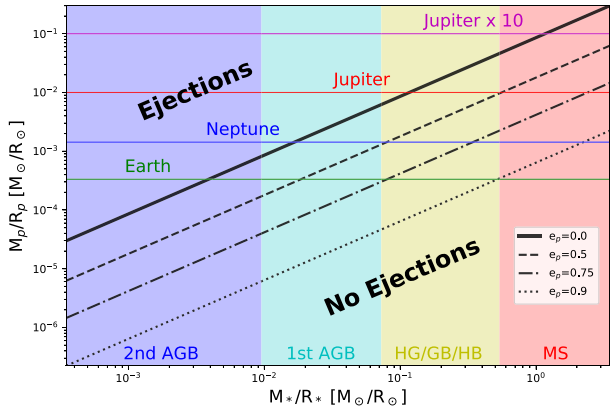

Figure 1. Ejection conditions for a range of planetary masses, stellar types, and orbital eccentricities. The figure plots the ejection conditions outlined in Equation (5), for four different orbital eccentricities e_p: 0 (solid black line), 0.5 (dashed black line), 0.75 (dotted–dashed black line), and 0.95 (dotted black line). Planets whose masses divided by their radius lie above these lines are able to cause V Hya-like ejections for a given star with the corresponding value of its mass divided by its radius. The shaded regions show approximate value ranges of mass divided by radius for different stellar evolutionary phases, for a range of stellar masses. The red region marks values for MS stars, yellow for Hertzsprung gap, giant branch, and helium-burning stars, cyan for first asymptotic giant branch (AGB) stars, and blue for 2nd AGB stars. Note that ejections become easier the more evolved a star is, as its ratio of mass to radius decreases. Values for different example planets are shown as vertical lines: Earth in green, Neptune in blue, Jupiter in red, and a massive Jupiter or small brown dwarf in magenta. While a brown dwarf can cause ejections for any type of star or orbital eccentricity, an Earth-sized planet can only cause them for extremely enlarged AGB stars or at extremely high eccentricities.

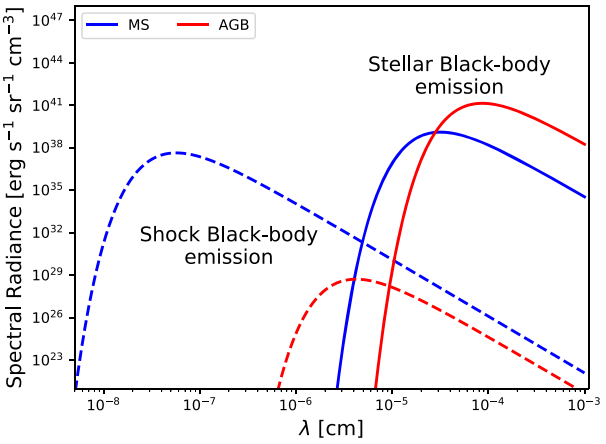

Figure 2. Blackbody Emission of a 2 $M_\odot$ Star vs. (unobscured) shock front blackbody emission during the MS and AGB Phases. The figure shows the blackbody emission spectrum approximating the emission of a 2 $M_\odot$ star (solid lines), compared with the blackbody emission spectrum approximating the possible emission of the hot shock front as a Jupiter-sized planet is consumed by the star (dashed lines). Shown are the spectra during the main sequence (blue lines) and the AGB phases (red lines). Note that as the shock is extremely hot, it emits much stronger in the UV and X-ray than the star itself. However, one would probably not actually see most of this emission; during the main sequence, the power dissipated in the shock can actually surpass the total luminosity of the star, which should drive a wind that eventually obscures the UV emission, turning it into lower temperature thermal emission (Metzger et al. 2012). The energy of the shock would also spread and heat surrounding gases as they mix, reducing the emission temperature. During the AGB phase, as the planet migrates further inward into the stellar envelope, the shock's emission is unlikely to penetrate all the way to the surface of the red giant to be observable. As such, these UV signals would most likely be indicators of extremely recent and ongoing consumption events. For example, for a MS star the energy dissipated in the shock should begin to drive a wind and be obscured about 20 yr into the merger.

2.2. Luminosity and Energy Signatures

After a planet has grazed a stellar surface, it will eventually orbit fully inside the stellar envelope, shedding orbital energy and angular momentum as it spirals further into the star. The planet will interact with the stellar gas through the drag force $f_d = C_d \rho_* {v_k}^2/2$, where C_d is a dimensionless drag coefficient of order unity, ρ_* is the stellar density, and v_k is the relative velocity of the planet within the stellar atmosphere (Metzger et al. 2012). This drag force acts on the planet's effective cross-section A_p, which depends on the size of the stellar scale height $H = k_B T/(\mu \mathrm{m}_H g)$ (here, k_B is the Boltzmann constant, T is the gas temperature, μ is the mean molecular mass of the gas, m_H is the mass of a hydrogen atom, and g is the local gravity), as a difference in distance H inward into the star will increase the density, and thus drag force, by a factor of e. If H is much smaller than the planet's radius R_p, most of the drag will be caused by the part of the planet most inward into the star, and A_p will be of order ${R_p}^{1/2} H^{3/2}$. The drag torque at a given radius r from the stellar center, $f_d A_p \times r$, will thus contribute to the inward migration of the planet with inward radial speed,

$$v_r \sim C_d A_p \frac{\rho_*(r)}{M_p} r v_k(r). \tag{6}$$

The inward radial speed due to drag contributes to the rate of orbital energy dissipation via

$$\dot{E}_\mathrm{orb} = \frac{G M_* M_p v_r}{2r^2}, \tag{7}$$

(Metzger et al. 2012). This energy is added to the stellar gas, heating it up. In general, the travel speed v_k of the planet upon entering the star will be much larger than the stellar atmosphere's sound speed $c_s = \sqrt{\gamma P_*/\rho_*}$; here, γ is the adiabatic index, with a value of 5/3 for ideal gases, and P_* is the gas pressure in the star. The planet will therefore produce a strong shock front as it travels through the stellar atmosphere by which it is orbital energy is dissipated.[4] Assuming the standard Rankine–Hugoniot jump conditions and a strong shock, we can estimate the temperature of the gas behind the shock front as

$$T_\mathrm{shock} = A \frac{\mu \mathrm{m}_H}{k_\mathrm{B}} v_k^2, \tag{8}$$

where A is a numerical factor of order unity depending on the nature of the gas (~3/16 for an ideal gas). Note that for fully ionized gas in a star $\mu = 0.62$; however, the gas in a red giant is generally not fully ionized preshock, and has a larger value for μ, which has to be taken into account.

The temperature of the shock can be extremely high, potentially reaching several 10,000 K, producing a lot of X-ray and far-UV radiation, as the peak emission strength will occur at $\lambda_\mathrm{max} = b_W/T$, where $b_W \sim 0.28978$ cm K is Wien's displacement constant. The radiation intensity as a function of wavelength for blackbodies with the stellar and shock front temperatures are also shown in Figure 2, following Planck's law. However, the radiation will not necessarily be able to

[4] Note that there is also a contribution to the inward migration speed and energy dissipation due to tidal forces. This energy is added to the bulk of the star, not the shock front.

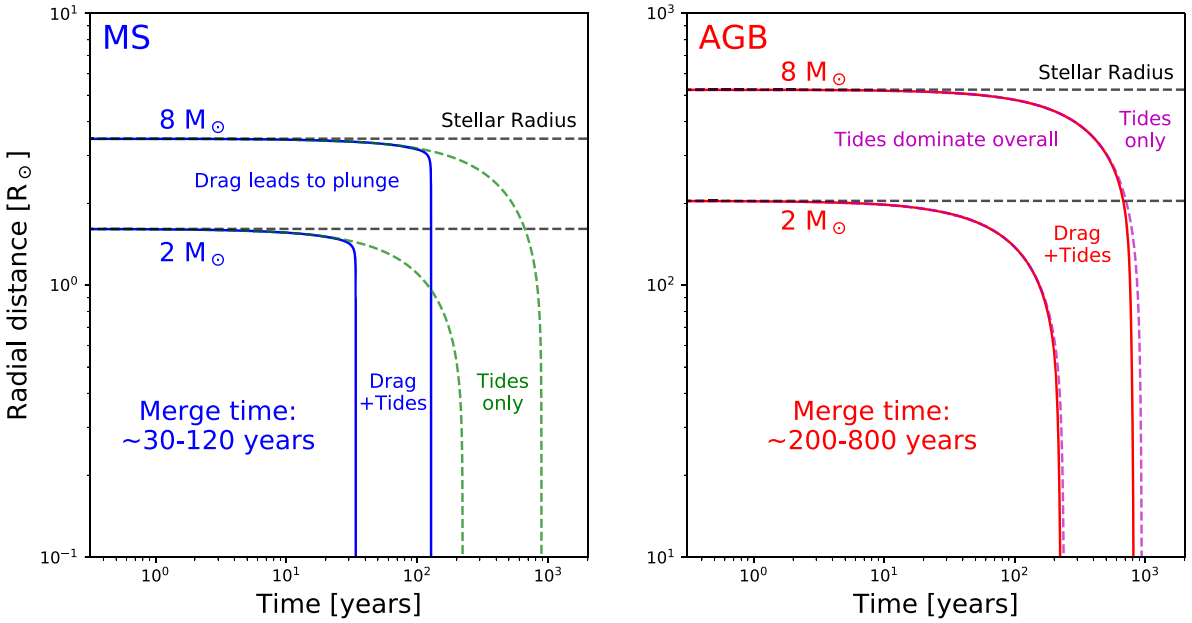

Figure 3. Merging of a Jupiter with a 2 (8) $M_{\odot}$ Star. This figure shows the inward radial position over time of a Jupiter-sized planet entering either a MS star (left panel) or an AGB star (right panel). Shown are both the migration due to tides alone (dashed green and magenta lines) and due to drag and tides combined (solid blue and red lines), as well as the radius of the star (dashed black lines). Overall, the planet will have fully merged with the MS star after about 30–120 yr, and after about 200–800 yr with the AGB star. The exact time, in all cases, depends strongly on the viscous timescale t_v assumed for the star, as tidal effects dominate while the planets are in the outer layers of the stellar envelope. Here, we assumed $t_v = 1.5$ yr (Hansen 2010; Fabrycky et al. 2007). Indeed, while for MS stars drag forces overtake tidal forces after the planets have migrated to about 90% of the stellar radius, for AGB stars drag forces only begin to dominate at about 50% of the radius. In either case, once drag forces become dominant, the planets will "plunge" into the stellar core on timescales comparable to the planets' orbital periods.

escape the stellar envelope, depending on the optical thickness or ionization state of the gas. Furthermore, the luminosity added to the star can be so large that the immediate region of the shock exceeds its local Eddington limit, which will lead to a wind that will drive an outflow of material from the stellar envelope. This material, in turn, can efficiently block the high-energy radiation emitted by the shock (Metzger et al. 2012), and can also emit additional infrared radiation as it reradiates intercepted stellar radiation. For different stellar types and phases, the reached temperatures and luminosity emitted by the shock vary, as indicated in Figure 2.

We note here that we ignore the potential feedback on stellar structure due to the large amount of energy transferred into the stellar envelope. This feedback would be most relevant for compact stars absorbing large planets. The luminosity generated by the orbital decay, estimated from Equations (6) and (7), can surpass the stellar luminosity by orders of magnitude for a short time during the final "plunge" of the planet into the star (compare also with Figure 2 in MacLeod et al. 2018). This plunge occurs over timescales of hours to days, as can be seen in Figure 3 (see also Metzger et al. 2012). It can therefore be assumed that the interior structure for main-sequence stars or stars in the Hertzsprung gap (i.e., subgiants) would be majorly impacted by the sudden injection of energy, or that the planet itself disintegrates, making our calculations inaccurate to describe the planet's orbital behavior during this final plunge. For evolved and red giant stars on the AGB, however, the energy dissipated due to orbital decay is always much smaller than the star's luminosity and stellar structure should remain mostly unchanged. Stars on the first giant branch (GB) or in the core helium-burning phase (HeB) represent an intermediate case, where we expect the generated orbital decay power to be of similar order to the stellar luminosity during the final plunge. The structure of these stars might therefore be affected by the injected energy, albeit to a lesser degree than for main-sequence or Hertzsprung gap stars.

2.3. Angular Momentum Transfer and Stellar Spin-up

A planet will transfer angular momentum to its star either through tidal forces, mostly important when the planet is still outside or in the outer regions of the star, or through drag forces, especially important when the planet has reached denser interior layers of the star. The tidal friction timescale of the star can be described by (e.g., Hut 1981; Eggleton et al. 1998; Kiseleva et al. 1998; Naoz 2016)

$$t_{\rm TF} = \frac{t_v}{9}\left(\frac{a_p}{r_*}\right)^8 \frac{m_*(r_*)^2}{(m_*(r_*)+M_p)M_p}\frac{1}{(1+k_l)^2}, \quad (9)$$

with t_v and k_l being the stellar viscous timescale and Love number, respectively, a_p being the planet's semimajor axis, M_p being the planetary mass, and m_* being the star's mass interior to the radius r_*. Note that r_* is equal to R_*, the star's outer radius, if the planet has not entered the stellar envelope yet, and is equal to a_p otherwise. This approximation ignores the tidal effects of the stellar material outside of the planet's orbit, as it should generally be insignificant compared to the effects of the stellar interior. The timescale associated with the gas drag forces outlined in Section 2.2 can be described by

$$t_{\rm drag} \sim \frac{R_*}{v_r} \sim {C_d}^{-1}\frac{M_p}{\rho_* A_p v_k}\frac{R_*}{a_p}, \quad (10)$$

(Metzger et al. 2012).

We can apply the timescales for drag and tidal migration, using realistic models of stellar structure for internal density profiles, to estimate the time needed for a planet to fully merge with a star of given mass and evolutionary stage. Here, we assume that the stellar envelope is an $n = 3$ polytrope, with an additional compact core in the case of the red giant. While a MS star might only require a few tens of years to fully merge with a planet, a red giant star might need hundreds of years to do the same, as shown in Figure 3.

In general, drag forces overcome tidal friction eventually after a planet enters a star, both for MS and red giant stars, as can be seen in Figure 3. Indeed, the inward migration speed can become even faster than the orbital speed of the planet, leading to a "plunge," with subsequent disruption of the planet and mixing into the stellar core. Overall, however, an engulfed planet spends the vast majority of its time in the outer layers of the star, where tides dominate over drag. This makes the total lifetime of the planet before the "plunge" highly dependent on the assumed tidal parameters. Once the planet reaches the "plunge" distance, it quickly falls into the core. For a MS star the plunge distance is about one-tenth of the stellar radius (from the surface), for a red giant star the plunge distance is at about half the stellar radius, as can be seen in Figure 3.

Regardless of the mechanism that contributes most to angular momentum transfer and the planet's migration in the stellar envelope, the angular momentum of the planet's orbit will change the spin of the star. Here, we calculate the new spin rates after such spin-up events and estimate under which conditions the spin-up would actually lead to stellar breakup or envelope loss.

The orbital angular momentum of a planet orbiting a star with semimajor axis a_p and eccentricity e is

$$J_{\rm orb} = \frac{M_* M_p}{M_* + M_p}\sqrt{G(M_* + M_p)a_p(1 - e^2)}. \quad (11)$$

Assuming that the planet is much less massive than the star, which is reasonable given the mass ratio of Jupiter to the Sun, and that the planet orbit's closest approach distance $a_p(1 - e)$ must be the same as the size of the star's Roche limit $R_{*,\rm Roche}$, this equation can be simplified to

$$J_{\rm orb} \sim m\sqrt{GM_p R_{*,\rm Roche}(1 + e)}, \quad (12)$$

where we note that e can only vary between values of 0 and 1, thus changing the magnitude of the angular momentum at most by a factor of $\sqrt{2}$. The rotational angular momentum of a spinning star is

$$J_* = I_* \Omega_*, \quad (13)$$

where I_* is the stellar moment of inertia and Ω_* its rotation frequency. Here, we ignore potential differential rotation profiles. For simplicity, we assume that a MS star or a red giant's envelope have a polytropic index of about 3, and basically reaches all the way from the stellar surface to the stellar core, giving the numerical factor 0.08 for the angular moment of inertia calculations. From this, we determine that the stellar angular momentum is about

$$J_{*,\rm env} = I_{*,\rm env}\Omega_{*,\rm env} \sim 0.08 M_{*,\rm env} R_*^2 \Omega_{*,\rm env}, \quad (14)$$

with $I_{*,\rm env}$, $\Omega_{*,\rm env}$, $M_{*,\rm env}$ being the stellar envelope's moment of inertia, rotation rate, and mass, respectively.

When the star's expanding envelope's Roche limit grows past the planet's orbit, the planet will impart its angular momentum onto the star as it eventually spirals inward. The angular momenta must add up such that the envelope's new angular momentum is

$$\begin{aligned} \boldsymbol{J}_{*,\rm env,new} &= \boldsymbol{J}_{*,\rm env} + \boldsymbol{J}_{\rm orb} \\ &= 0.08 M_{*,\rm env} {R_*}^2 \boldsymbol{\Omega}_{*,\rm env,new} \\ &= \Omega_{*,\rm env} + M_p\sqrt{GM_* R_{*,\rm Roche}(1 + e)}\hat{\boldsymbol{h}}, \end{aligned} \quad (15)$$

assuming here that the stellar radius does not change due to consumption, no differential rotation, and that the planet's mass, as well as the angular momentum of the planetary spin, are negligible. Note also that the stellar Roche limit can be expressed as

$$R_{*,\rm Roche} = qR_*\left(\frac{M_* + M_p}{M_*}\right)^{1/3} \sim qR_*, \quad (16)$$

with q being a numerical factor assumed here to be about 2.7. The new spin rate $\Omega_{*,\rm env,new}$ is the observable factor, which now becomes

$$\boldsymbol{\Omega}_{*,\rm env,new} = \boldsymbol{\Omega}_{*,\rm env} + 12.5 \times M_p\sqrt{\frac{qGM_*(1 + e)}{M_{*,\rm env}^2 R_*^3}}\hat{\boldsymbol{h}}. \quad (17)$$

Using Equation (17), we can now calculate the changes on a red giant star's spin in a variety of scenarios. We use the stellar evolution code SSE (Hurley et al. 2000) to evolve stars of masses between 1 and 8 $M_\odot$ from the beginning of the MS to their widest possible stellar radius during the AGB phase. SSE gives information about the stars' radii, masses, core masses, temperatures, and spin rates during all evolutionary phases. SSE provides fitting formulae based on the stellar evolution models produced by Pols et al. (1998), giving evolution tracks for a wide range of stellar masses and metallicities. In these models, stellar spins are calculated considering the potential division of a star into core and envelope, which is also taken into account in Equation (17), while also considering effects such as magnetic braking for the spin evolution. We adjusted SSE's magnetic braking coefficients by using values from Dobbs-Dixon et al. (2004) for Sun-like stars. We calculate the changes in stellar spin rates and periods upon consumption of planets with varying masses, orbital eccentricities, and spin–orbit angles. The full ranges of tested parameters are shown in Table 1. We compare the changes in spin periods due to consumption during different stellar evolutionary phases, including the MS, GB, the HeB, and the first and second AGB phases. We note here that generally the stellar radius of a star during the HeB phase is smaller than during the GB phase; however, giant planets can still plunge into their host stars during that phase due to effects such as the Eccentric Kozai–Lidov mechanism, in which a companion star can induce high orbital eccentricity on a planet due to gravitational perturbations (e.g., Naoz et al. 2011, 2012, 2013b; Naoz 2016; Stephan et al. 2018). In Figure 4 we show the effects of stellar consumption of prograde-orbiting gas giant planets by stars of different masses and evolutionary phases on the stars' spin periods. In Figures 5 and 6 we show the same for more evolutionary phases and for retrograde planet orbits.

We note here that we calculate the new spin periods only for the time immediately following the planets' consumption and do not predict the further evolution of the spins. Magnetic

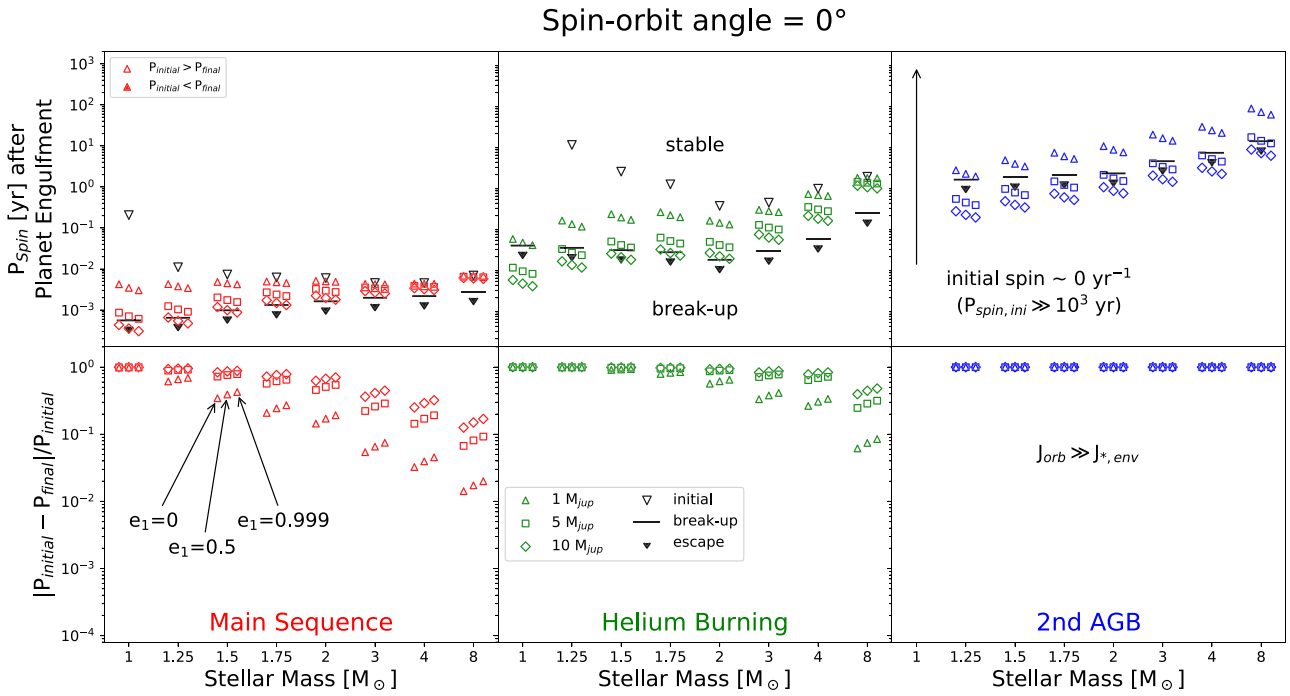

Figure 4. Consumption of prograde-orbiting planets. Shown are the spin periods (upper panels) and fractional changes of the spin periods (lower panels) due to the consumption of prograde-orbiting planets of various masses and various eccentricities for a variety of stellar masses and evolutionary phases. The shown evolutionary phases are main sequence (red), core helium burning (green), and second AGB (blue). The empty black downward triangles show the initial stellar spin periods before consumption, calculated with SSE or based on observations in the case of white dwarfs (Kawaler 2003). The tested planetary masses were 1 $M_{\rm Jup}$ (upward triangles), 5 $M_{\rm Jup}$ (squares), and 10 $M_{\rm Jup}$ (diamonds). For each planetary mass, three orbital eccentricities were tested, shown by groups of three identical symbols; from left to right, the eccentricities were 0, 0.5, and 0.999. The black lines mark the minimum spin periods possible before a star would begin to either lose surface material or be significantly inflated around its equator due to centrifugal forces. The filled-in black downward triangles show spin periods below which surface material would reach escape speeds, being completely lost from the star. These effects are generally more relevant, as shown, for relatively massive planets being consumed by relatively low-mass stars, and for more evolved stars.

Table 1
Parameters

Parameters	Values
M_* [$M_\odot$]	1, 1.25, 1.5, 1.75, 2, 3, 4, 8
M_p [$M_{\rm Jupiter}$]	1, 5, 10
Spin–orbit angle [rad]	0, $\pi/2$, π
e_1	0, 0.5, 0.999

Note. Listed are the relevant parameters for Equation (17) to determine the new stellar spin rate after consumption of a planet.

braking, stellar winds, and further radial inflation or contraction will change the spin periods as the stars continue to evolve. Some previous studies have indicated that the spin-up of red giant stars due to planet consumption could cause important changes to the magnetic fields generated by the stellar envelopes (e.g., Soker 1998b; Privitera et al. 2016b, 2016a), which could strongly impact magnetic braking and mass-loss processes.

2.4. Critical Spin Rates and Stellar Breakup

When calculating the new stellar spins ,we also need to compare it with the rotational breakup speed of the stars, i.e., the rotation rate at which material on the surface of a given star would be launched into orbit, leaving that surface. The simplest definition of this breakup spin period can be written as

$$P_{*,\rm break-up} = 2\pi\sqrt{\frac{{R_*}^3}{GM_*}}. \quad (18)$$

At this spin period, a particle on the stellar surface would remain in circular orbit around the star, ignoring potential additional forces such as radiation pressure or similar effects. If the star spins with a smaller period, material from the stellar surface will be launched into orbit. If the spin period is shorter by a factor of $\sqrt{2}$, material launched from the surface will have escape velocity and leave the star completely. At spin periods between $P_{\rm break-up}$ and $P_{\rm break-up}/\sqrt{2}$, material would be launched onto eccentric orbits, effectively leading to the formation of an extreme equatorial bulge and potentially a gaseous disk around the star. As this takes place the spin periods calculated here would obviously need to be adjusted as the shape of the star changes and potentially loses surface material. We note here that calculated spin speeds beyond the breakup speeds are therefore only an indicator for the formation of oblate stars or circumstellar gaseous disks, not for the actual final observable spins.

As Figures 5 and 6 show, for a wide variety of stellar and planetary masses the addition of the planetary orbital angular momentum would lead to stellar spins exceeding the spin frequencies required for stellar surface material to be ejected, in particular for more evolved stars past GB, but also some

lesser-evolved stars. It therefore seems reasonable to assume that such object might already have been observed by previous surveys. Indicators, for example, would be the presence of infrared-excess radiation from debris disks or ejected stellar gas, together with fast stellar spins. Indeed, some observed systems (e.g., Melis et al. 2009) seem to be good candidates for this process.

2.5. Stellar Chemical Enrichment

The consumption of a planet by a star would also enrich the stellar gas with planetary material. However, at least for gas giants planets, the bulk composition of the planet and the star can be assumed to be very similar, as they are formed from the same protostellar gas and dust disk. Still, there are some cases where the consumption could produce detectable chemical alterations, including lithium enrichment, rocky material enrichment, and white dwarf pollution.

Lithium is easily destroyed in stellar nuclear fusion processes through adding a proton to ^{7}Li, producing two alpha particles. As such, lithium is heavily depleted in fully convective low-mass stars, where material is continuously mixed back into the core fusion zone, and moderately depleted in more massive stars, where lithium is mostly burned during the pre-MS phase but can survive in the stellar atmosphere (e.g., Thévenin et al. 2017). However, many observations have shown that a small number of stars, in particular red giants, show abnormally high lithium abundances, with ideas about the cause including dredge-up, new lithium production, or pollution from interstellar gas, brown dwarfs, or planets (e.g., Alexander 1967; Brown et al. 1989; Montalbán & Rebolo 2002; Aguilera-Gómez et al. 2016; Bharat Kumar et al. 2018; Yan et al. 2018).

Apart from lithium enrichment, it has been suggested that a stellar envelope's metallicity could also be enhanced by absorbing a super-earth or other rocky planetary body (Church et al. 2019). Unfortunately, for a star in isolation, it might be difficult to deduce that the observed metallicity is larger than the primordial metallicity. However, in the case of binary stars, which presumably form with the same primordial metallicities, metal enrichment of one member versus the other might be much easier to determine. Indeed, the binary star pair of HD 240430 and HD 240429 has been suggested to be an example of this scenario, where HD 240430 is estimated to have consumed about 15 $M_\oplus$ of rocky material (Oh et al. 2018).

Elements heavier than hydrogen and helium are expected to sink to the cores of white dwarfs, however about one-quarter to one-third of all white dwarfs still show such heavy elements in their atmospheric spectra (e.g., Zuckerman et al. 2003, 2010; Koester et al. 2014). In general, it is thought that white dwarfs are being polluted by planetary bodies, usually rocky in composition (e.g., Debes & Sigurdsson 2002; Jura 2003; Jura et al. 2009; Zuckerman et al. 2011; Vanderburg et al. 2015; Xu et al. 2016; Veras et al. 2017a, 2017b), though some icy bodies containing volatile compounds have also been shown to contribute (Stephan et al. 2017; Xu et al. 2017). Furthermore, even gas giants could theoretically be brought onto extremely eccentric orbits, getting close enough to the white dwarfs for tidal disruption and eventual pollution (Stephan et al. 2017, 2018). The material brought onto a white dwarf from such a massive pollution source could majorly alter the composition of the white dwarf; many white dwarfs are so called helium white dwarfs, with little to no hydrogen left in their atmosphere. A gas giant planet with a mass in the range or 1 to 10 $M_{\rm Jup}$, roughly 0.001–0.01 $M_\odot$, could cover the white dwarf with a hydrogen atmosphere. Some of the material could also produce second-generation planets or planetary nebulae (e.g., Bear & Soker 2015; van Lieshout et al. 2018).

3. Discussion

We have studied the variety of consequences due to planetary consumption throughout a star's lifetime. Planetary consumption is expected to be a common outcome of dynamically hot systems (e.g., Rasio & Ford 1996; Chatterjee et al. 2008; Nagasawa et al. 2008; Veras & Ford 2010; Naoz et al. 2012; Valsecchi et al. 2014; Petrovich 2015; Petrovich & Muñoz 2017; Stephan et al. 2017, 2018; Denham et al. 2019).

Considering a wide range of stellar masses (1–8 $M_\odot$) and a wide range of planetary masses (1 $M_\oplus$–10 $M_{\rm J}$), we examined the effects of planet consumption on a host star. We note here that these calculations are agnostic to the process leading to Roche-limit crossing. The initial stage of star–planet interaction, where the planet interacts with the surface of the star, can have large observable effects. It may lead to ejections of material, either resulting in winds and planetary nebulae (e.g., Livio & Soker 2002), or even violent, periodic ejections (as was shown for the case of V Hydrae ejections Salas et al. 2019). The ejection of stellar material due to grazing interactions depends on the star's and planet's mass and size, as well as the orbital eccentricity. We quantified the phase space, considering ballistics ejections,[5] at which ejection of material is expected at any given point of a star's lifetime (see Figure 1). In particular, we find that Jupiter mass planets (or higher masses) are efficient in ejecting material over most of the stellar lifetime and for most stellar masses, even for circular orbits. Smaller planets on eccentric orbits can also lead to material ejection rather efficiently. Because the escape velocity from the surface of a star on its second AGB phase is relatively low (a few tens of km s^{-1}), even small, Earth-like planets are sufficient to cause ejections, albeit small ones.

As a planet migrates further into a star's atmosphere, it begins to experience gas drag and creates a hot shock as it loses orbital energy. This shock can produce observable UV radiation. For MS stars (blue lines in Figure 2) the shock's blackbody emission intensity can be comparable to the star's radiation (as was shown previously in Metzger et al. 2012). However, the large amount of energy released can drive a wind, obstructing direct observation of the UV emission and converting it into cooler thermal radiation. During the AGB phase the planet's shock radiation is much less intense than the stellar emission. Thus, while it has less power, it may add a small far-UV component to a predominantly visual emission (see red lines in Figure 2). We estimated the timescales over which the consumption takes place and over which the additional UV signals might be observable. The migration of a planet just inside the surface of a star will mostly be dominated by tides (as shown in Figure 3) until drag becomes dominant and "plunges" the planet into the stellar core. To reach this phase, it takes on the order of a few decades for MS stars and on the order of a few centuries for red giant stars, over which UV signals and shock effects should be visible.

[5] Note that there are variety of processes that may lead to ejections (e.g., Goodson & Winglee 1999; Fendt 2003). Here we adopted the simplest one, which makes no assumptions on magnetic fields or accretion disks.

Once the planet is finally consumed by the star, we estimated the resulting stellar spin periods from angular momentum conservation.[6] We found that MS stars, post-consumption, should be rapidly spinning (consistent with Qureshi et al. 2018) and that the consumption can significantly alter the star's axis of rotation (consistent with Matsakos & Königl 2015). Red giant stars, post-consumption, can often reach spin speeds at or beyond breakup speeds, indicating that these stars would undergo mass loss from their surface or are strongly tidally distorted into a flattened shape or will become enshrouded by ejected gas. This can also apply to smaller mass stars consuming massive planets or brown dwarfs. Finally, we also showed that white dwarfs can also be significantly spun up, if the angular momentum of a planet can be efficiently transferred to the star. This feature may explain some observed white dwarfs with very short spin periods, such as SDSS J0837 +1856 (e.g., Hermes et al. 2017a, 2017b).

Already, observations of short-period planets show that some may have decaying orbits that will eventually let them be consumed by their host star. For example, WASP-12b is a Jupiter size planet that is on a decaying orbit around a 1.35 $M_{\odot}$ star (e.g., Li et al. 2010; Patra et al. 2017). Based on our calculations (e.g., Figures 4 and 6), we predict that the spin period of WASP-12, upon consumption of this planet, may decrease by a factor of two (prograde orbit), or would be completely flipped (retrograde orbit). Additional planets that are estimated to be on decaying orbits have also been observed (e.g., Gaudi et al. 2017; Johnson et al. 2018; Johns et al. 2019; Labadie-Bartz et al. 2019; Rodriguez et al. 2019).

While the observation of an active consumption event might be challenging for a MS star, given the short timescale of a few decades per consumption event, for a red giant star the timescales are relatively favorable, as consumption events would last for centuries or even millennia. Given lifetimes of a few hundred thousand to a few million years for the AGB phase, the chance to observe an engulfment (assuming that every AGB star engulfs a planet) would be on the order of a few tenths to about 1%. Beyond direct observations, the pre- and post-consumption signatures described in this work may provide several avenues to indirectly infer the existence of a planet around a given star. Future *Hubble Space Telescope* (*HST*) and *James Webb Space Telescope* (*JWST*) observations may detect some of the signatures described here (similar to the gas ejections from V Hydrae described by Sahai et al. 2016).

We thank the anonymous referee for their comments and suggestions to improve this paper. A.P.S. and S.N. acknowledge partial support from the NSF through grant No. AST-1739160. S.N. thanks Howard and Astrid Preston for their generous support. We thank Noam Soker and Brian Metzger for helpful comments and discussions.

Appendix
Post-planet-consumption Spin Periods

Here, we provide expanded versions of Figure 4, showing the stellar pre- and post-consumption spin periods for stars during the main sequence, first giant branch, helium burning, first asymptotic giant branch, second asymptotic giant branch, and as white dwarfs. The values are calculated for a range of stellar and planetary masses, and varying orbital eccentricities. Figure 5 shows the values assuming a prograde orbit of the planet during engulfment, Figure 6 assumes a retrograde orbit. We also show the fractional change in spin periods due to engulfment, and mark spin periods that would surpass breakup speed, highlighting engulfment events that would most likely lead to stellar mass loss through gas ejections or decretion disks.

[6] Note that angular momentum may not be strictly conserved due to mass losses and winds. The consequences of these processes are beyond the scope of this paper.

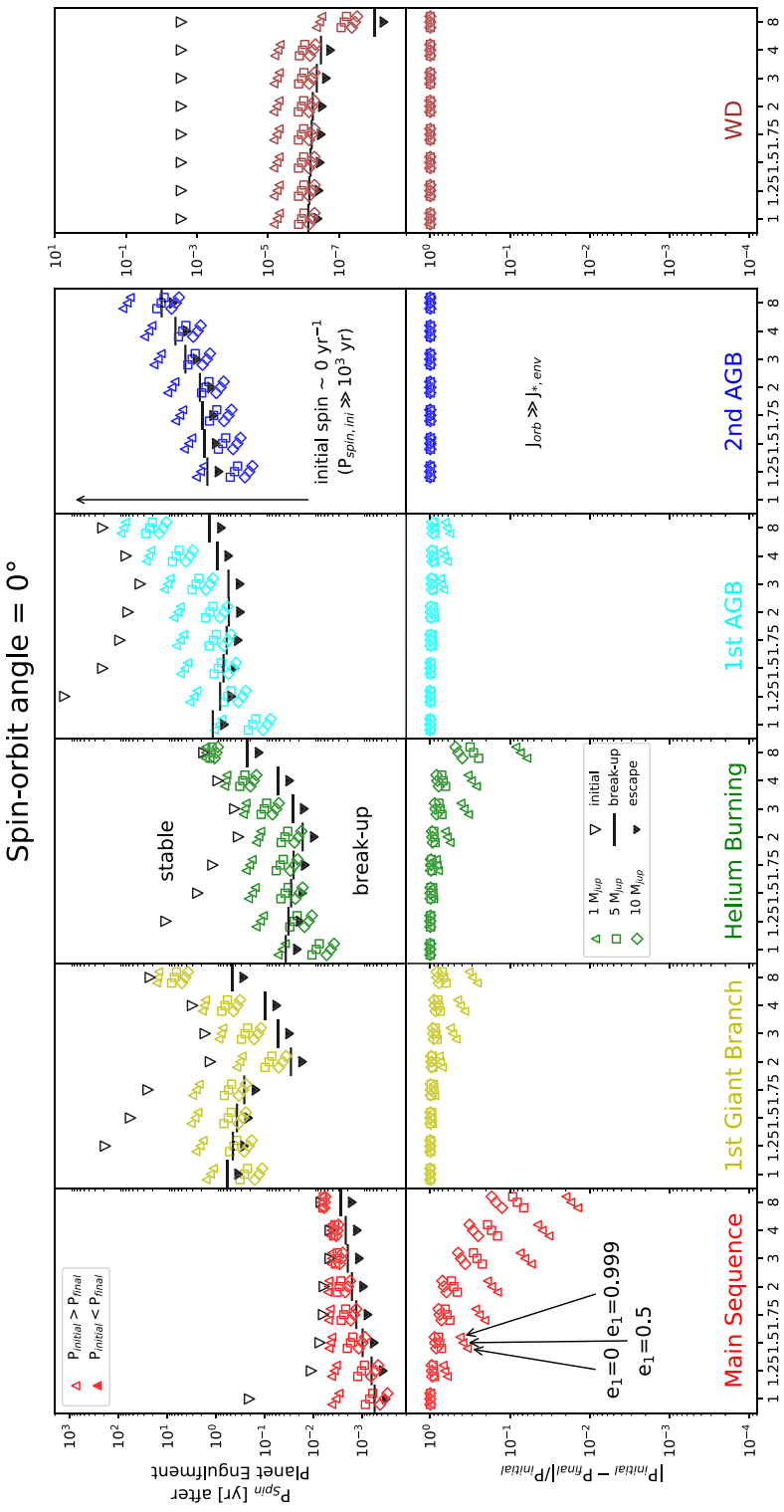

Figure 5. Consumption of prograde-orbiting Planets (extended). This figure is similar to Figure 4, however it also includes the results for a larger number of stellar evolution phases. The shown evolutionary phases are main sequence (red), first giant branch (yellow), core helium burning (green), first AGB (cyan), second AGB (blue), and white dwarfs (brown). The empty black downward triangles show the initial stellar spin periods before consumption, calculated with SSE or based on observations in the case of white dwarfs (Kawaler 2003). The tested planetary masses were 1 M_{Jup} (upward triangles), 5 M_{Jup} (squares), and 10 M_{Jup} (diamonds). For each planetary mass, three orbital eccentricities were tested, shown by groups of three identical symbols; from left to right, the eccentricities were 0, 0.5, and 0.999. The black lines mark the minimum spin periods possible before a star would begin to either lose surface material or be significantly inflated around its equator due to centrifugal forces. The filled-in black downward triangles show spin periods below which surface material would reach escape speeds, being completely lost from the star. These effects are generally more relevant, as shown, for relatively massive planets being consumed by relatively low-mass stars, and for more evolved stars.

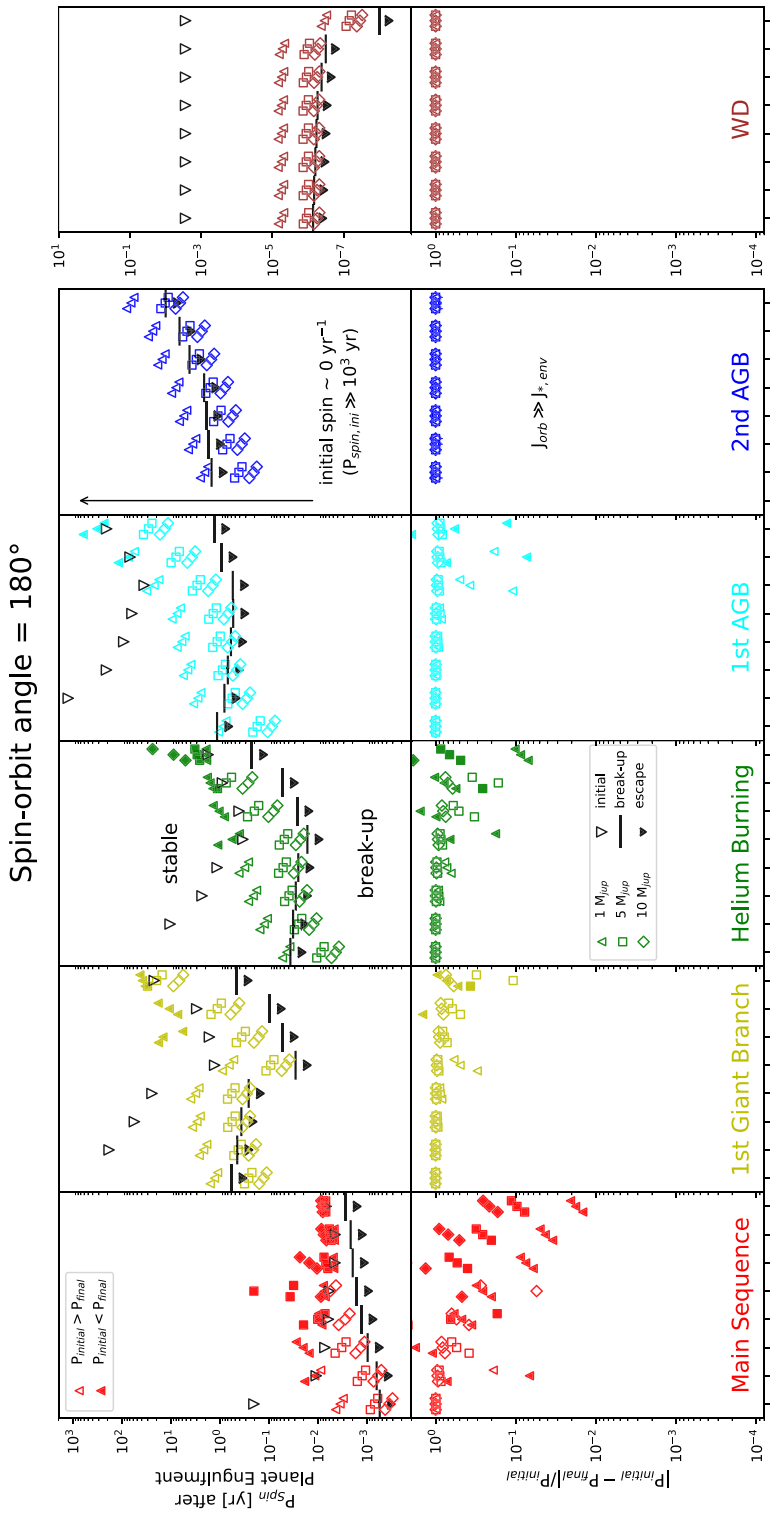

Figure 6. Consumption of retrograde-orbiting planets. This figure is similar to Figure 5, however here the planets orbited the stars in retrograde orbits relative to the preconsumption stellar spin orientation. As a result, it is possible to not just increase a star's spin velocity due to the planets' consumption, but also to instead slow them down. This is shown by the filled-in symbols in the upper and lower panels and appears to be most relevant for massive pre-AGB stars. In all other cases, the angular momentum added by the planets overcomes the stars' own angular momentum, resulting in still faster rotation; however, in that case, the spin direction is reversed relative to the initial spin.

ORCID iDs

Alexander P. Stephan https://orcid.org/0000-0001-8220-0548
Smadar Naoz https://orcid.org/0000-0002-9802-9279
B. Scott Gaudi https://orcid.org/0000-0003-0395-9869

References

Aguilera-Gómez, C., Chanamé, J., Pinsonneault, M. H., & Carlberg, J. K. 2016, ApJ, 829, 127
Alexander, J. B. 1967, Obs, 87, 238
Barnes, J. W., van Eyken, J. C., Jackson, B. K., Ciardi, D. R., & Fortney, J. J. 2013, ApJ, 774, 53
Bear, E., Kashi, A., & Soker, N. 2011, MNRAS, 416, 1965
Bear, E., & Soker, N. 2015, MNRAS, 450, 4233
Bharat Kumar, Y., Singh, R., Eswar Reddy, B., & Zhao, G. 2018, ApJL, 858, L22
Brown, J. A., Sneden, C., Lambert, D. L., & Dutchover, E. J. 1989, ApJS, 71, 293
Charpinet, S., Fontaine, G., Brassard, P., et al. 2011, Natur, 480, 496
Chatterjee, S., Ford, E. B., Matsumura, S., & Rasio, F. A. 2008, ApJ, 686, 580
Church, R. P., Mustill, A. J., & Liu, F. 2019, MNRAS, 491, 2391
Debes, J. H., & Sigurdsson, S. 2002, ApJ, 572, 556
Denham, P., Naoz, S., Hoang, B.-M., Stephan, A. P., & Farr, W. M. 2019, MNRAS, 482, 4146
Dobbs-Dixon, I., Lin, D. N. C., & Mardling, R. A. 2004, ApJ, 610, 464
Dosopoulou, F., Naoz, S., & Kalogera, V. 2017, ApJ, 844, 12
Eggleton, P. P., Kiseleva, L. G., & Hut, P. 1998, ApJ, 499, 853
Elbakyan, V. G., Vorobyov, E. I., Rab, C., et al. 2019, MNRAS, 484, 146
Fabrycky, D. C., Johnson, E. T., & Goodman, J. 2007, ApJ, 665, 754
Fendt, C. 2003, A&A, 411, 623
Gaudi, B. S., Stassun, K. G., Collins, K. A., et al. 2017, Natur, 546, 514
Gettel, S., Wolszczan, A., Niedzielski, A., et al. 2012, ApJ, 745, 28
Goodson, A. P., & Winglee, R. M. 1999, ApJ, 524, 159
Hamers, A. S., & Portegies Zwart, S. F. 2016, MNRAS, 462, L84
Hansen, B. M. S. 2010, ApJ, 723, 285
Herbig, G. H. 1977, ApJ, 217, 693
Hermes, J. J., Gänsicke, B. T., Kawaler, S. D., et al. 2017b, ApJS, 232, 23
Hermes, J. J., Kawaler, S. D., Romero, A. D., et al. 2017a, ApJL, 841, L2
Howard, A. W., Marcy, G. W., Bryson, S. T., et al. 2012, ApJS, 201, 15
Huber, D., Chaplin, W. J., Chontos, A., et al. 2019, AJ, 157, 245
Hurley, J. R., Pols, O. R., & Tout, C. A. 2000, MNRAS, 315, 543
Hut, P. 1981, A&A, 99, 126
Johns, D., Reed, P. A., Rodriguez, J. E., et al. 2019, AJ, 158, 78
Johnson, J. A., Apps, K., Gazak, J. Z., et al. 2011, ApJ, 730, 79
Johnson, M. C., Rodriguez, J. E., Zhou, G., et al. 2018, AJ, 155, 100
Jura, M. 2003, ApJL, 584, L91
Jura, M., Muno, M. P., Farihi, J., & Zuckerman, B. 2009, ApJ, 699, 1473
Kawaler, S. D. 2003, arXiv:astro-ph/0301539
Kim, H., Trejo, A., Liu, S.-Y., et al. 2017, NatAs, 1, 0060
Kiseleva, L. G., Eggleton, P. P., & Mikkola, S. 1998, MNRAS, 300, 292
Klein, B., Jura, M., Koester, D., & Zuckerman, B. 2011, ApJ, 741, 64
Klein, B., Jura, M., Koester, D., Zuckerman, B., & Melis, C. 2010, ApJ, 709, 950
Koester, D., Gänsicke, B. T., & Farihi, J. 2014, A&A, 566, A34
Labadie-Bartz, J., Rodriguez, J. E., Stassun, K. G., et al. 2019, ApJS, 240, 13
Larson, R. B. 1980, MNRAS, 190, 321
Li, S.-L., Miller, N., Lin, D. N. C., & Fortney, J. J. 2010, Natur, 463, 1054
Lithwick, Y., & Naoz, S. 2011, ApJ, 742, 94
Livio, M., & Soker, N. 2002, ApJL, 571, L161
MacLeod, M., Cantiello, M., & Soares-Furtado, M. 2018, ApJL, 853, L1
Martinez, M., Stone, N. C., & Metzger, B. D. 2019, MNRAS, 489, 5119
Mastrodemos, N., & Morris, M. 1998, ApJ, 497, 303
Matsakos, T., & Königl, A. 2015, ApJL, 809, L20
Melis, C., Farihi, J., Dufour, P., et al. 2011, ApJ, 732, 90
Melis, C., Zuckerman, B., Song, I., Rhee, J. H., & Metchev, S. 2009, ApJ, 696, 1964
Metzger, B. D., Giannios, D., & Spiegel, D. S. 2012, MNRAS, 425, 2778
Montalbán, J., & Rebolo, R. 2002, A&A, 386, 1039
Morris, M. 1981, ApJ, 249, 572
Morris, M., Sahai, R., Matthews, K., et al. 2006, in IAU Symp. 234, Planetary Nebulae in our Galaxy and Beyond, ed. M. J. Barlow & R. H. Méndez (Cambridge: Cambridge Univ. Press), 469
Nagasawa, M., Ida, S., & Bessho, T. 2008, ApJ, 678, 498
Naoz, S. 2016, ARA&A, 54, 441
Naoz, S., Farr, W. M., Lithwick, Y., Rasio, F. A., & Teyssandier, J. 2011, Natur, 473, 187
Naoz, S., Farr, W. M., Lithwick, Y., Rasio, F. A., & Teyssandier, J. 2013a, MNRAS, 431, 2155
Naoz, S., Farr, W. M., & Rasio, F. A. 2012, ApJL, 754, L36
Naoz, S., Kocsis, B., Loeb, A., & Yunes, N. 2013b, ApJ, 773, 187
Niedzielski, A., Villaver, E., Nowak, G., et al. 2016, A&A, 588, A62
Niedzielski, A., Wolszczan, A., Nowak, G., et al. 2015, ApJ, 803, 1
Nowak, G., Niedzielski, A., Wolszczan, A., Adamów, M., & Maciejewski, G. 2013, ApJ, 770, 53
Oh, S., Price-Whelan, A. M., Brewer, J. M., et al. 2018, ApJ, 854, 138
Patra, K. C., Winn, J. N., Holman, M. J., et al. 2017, AJ, 154, 4
Petrovich, C. 2015, ApJ, 799, 27
Petrovich, C., & Muñoz, D. J. 2017, ApJ, 834, 116
Pols, O. R., Schröder, K.-P., Hurley, J. R., Tout, C. A., & Eggleton, P. P. 1998, MNRAS, 298, 525
Privitera, G., Meynet, G., Eggenberger, P., et al. 2016a, A&A, 593, A128
Privitera, G., Meynet, G., Eggenberger, P., et al. 2016b, A&A, 593, L15
Qureshi, A., Naoz, S., & Shkolnik, E. L. 2018, ApJ, 864, 65
Raghavan, D., McAlister, H. A., Henry, T. J., et al. 2010, ApJS, 190, 1
Rasio, F. A., & Ford, E. B. 1996, Sci, 274, 954
Reffert, S., Bergmann, C., Quirrenbach, A., Trifonov, T., & Künstler, A. 2015, A&A, 574, A116
Retter, A., & Marom, A. 2003, MNRAS, 345, L25
Rodriguez, J. E., Quinn, S. N., Huang, C. X., et al. 2019, AJ, 157, 191
Sabach, E., & Soker, N. 2018, MNRAS, 473, 286
Sahai, R., Scibelli, S., & Morris, M. R. 2016, ApJ, 827, 92
Salas, J. M., Naoz, S., Morris, M. R., & Stephan, A. P. 2019, MNRAS, 487, 3029
Soker, N. 1992, ApJ, 386, 190
Soker, N. 1994, PASP, 106, 59
Soker, N. 1995, MNRAS, 274, 147
Soker, N. 1996, ApJL, 460, L53
Soker, N. 1998a, AJ, 116, 1308
Soker, N. 1998b, MNRAS, 299, 1242
Soker, N. 2001, MNRAS, 324, 699
Soker, N., & Harpaz, A. 2000, MNRAS, 317, 861
Stephan, A. P., Naoz, S., & Gaudi, B. S. 2018, AJ, 156, 128
Stephan, A. P., Naoz, S., & Zuckerman, B. 2017, ApJL, 844, L16
Teyssandier, J., Naoz, S., Lizarraga, I., & Rasio, F. A. 2013, ApJ, 779, 166
Thévenin, F., Oreshina, A. V., Baturin, V. A., et al. 2017, A&A, 598, A64
Valsecchi, F., Rasio, F. A., & Steffen, J. H. 2014, ApJL, 793, L3
Vanderburg, A., Johnson, J. A., Rappaport, S., et al. 2015, Natur, 526, 546
van Lieshout, R., Kral, Q., Charnoz, S., Wyatt, M. C., & Shannon, A. 2018, MNRAS, 480, 2784
Veras, D. 2016, RSOS, 3, 150571
Veras, D., Carter, P. J., Leinhardt, Z. M., & Gänsicke, B. T. 2017a, MNRAS, 465, 1008
Veras, D., & Ford, E. B. 2010, ApJ, 715, 803
Veras, D., Georgakarakos, N., Dobbs-Dixon, I., & Gänsicke, B. T. 2017b, MNRAS, 465, 2053
Veras, D., Mustill, A. J., Bonsor, A., & Wyatt, M. C. 2013, MNRAS, 431, 1686
Veras, D., & Tout, C. A. 2012, MNRAS, 422, 1648
Veras, D., & Wolszczan, A. 2019, MNRAS, 488, 153
Wang, S., Jones, M., Shporer, A., et al. 2019, AJ, 157, 51
Xu, S., Jura, M., Dufour, P., & Zuckerman, B. 2016, ApJL, 816, L22
Xu, S., Zuckerman, B., Dufour, P., et al. 2017, ApJL, 836, L7
Yan, H.-L., Shi, J.-R., Zhou, Y.-T., et al. 2018, NatAs, 2, 790
Zuckerman, B., Koester, D., Dufour, P., et al. 2011, ApJ, 739, 101
Zuckerman, B., Koester, D., Reid, I. N., & Hünsch, M. 2003, ApJ, 596, 477
Zuckerman, B., Melis, C., Klein, B., Koester, D., & Jura, M. 2010, ApJ, 722, 725

The Astrophysical Journal Letters, 844:L16 (8pp), 2017 August 1 https://doi.org/10.3847/2041-8213/aa7cf3
© 2017. The American Astronomical Society. All rights reserved.

Throwing Icebergs at White Dwarfs

Alexander P. Stephan, Smadar Naoz[1], and B. Zuckerman
Department of Physics and Astronomy, University of California, Los Angeles, CA 90095, USA; alexpstephan@astro.ucla.edu
Received 2017 April 25; accepted 2017 June 29; published 2017 July 25

Abstract

White dwarfs (WDs) have atmospheres that are expected to consist nearly entirely of hydrogen and helium, since heavier elements will sink out of sight on short timescales. However, observations have revealed atmospheric pollution by heavier elements in about a quarter to a half of all WDs. While most of the pollution can be accounted for with asteroidal or dwarf planetary material, recent observations indicate that larger planetary bodies, as well as icy and volatile material from Kuiper belt analog objects, are also viable sources of pollution. The commonly accepted pollution mechanisms, namely scattering interactions between planetary bodies orbiting the WDs, can hardly account for pollution by objects with large masses or long-period orbits. Here we report on a mechanism that naturally leads to the emergence of massive body and icy and volatile material pollution. This mechanism occurs in wide binary stellar systems, where the mass loss of the planets' host stars during post main sequence stellar evolution can trigger the Eccentric Kozai–Lidov mechanism. This mechanism leads to large eccentricity excitations, which can bring massive and long-period objects close enough to the WDs to be accreted. We find that this mechanism readily explains and is consistent with observations.

Key words: binaries: general – planetary systems – stars: evolution – stars: kinematics and dynamics – stars: mass-loss – white dwarfs

1. Introduction

Most stars ($\leqslant 8\,M_{\odot}$) that have exhausted their nuclear fuel end up as white dwarfs (WDs). Over the last few decades, many WDs have been observed with spectra that show the presence of significant amounts of elements heavier than hydrogen or helium in their atmospheres (Zuckerman et al. 2003, 2010; Koester et al. 2014). These heavy elements are expected to sink rapidly to the core of WDs, which implies a recent replenishment (Paquette et al. 1986). The commonly expected source for this replenishment is material from asteroidal or minor planet-sized bodies (Debes & Sigurdsson 2002; Jura 2003; Veras et al. 2017a), some of which have been observed in the process of tidal break-up (Vanderburg et al. 2015; Xu et al. 2016). However, some observations have suggested that planetary bodies, with sizes of the order of Mars or larger, can also contribute to WD pollution (Jura et al. 2009; Zuckerman et al. 2011). Furthermore, for the first time a WD (WD 1425+540) has shown signs of pollution by icy and volatile material from a Kuiper belt analog object that was initially on a very wide orbit (Xu et al. 2017). Here we report on a mechanism that naturally leads to the emergence of both of these observed features, large planetary mass and icy and volatile material pollution. In this mechanism we utilize the observed high binary fraction of stars (Raghavan et al. 2010) that facilitates the accretion of long-period planets and Kuiper belt analog objects onto WDs. Secular (i.e., long-term coherent) gravitational perturbations exerted by a stellar companion on such objects can excite their eccentricities to extreme values, and even lead to accretion onto the host star. If these extreme eccentricity excitations take place after the host star has evolved to the WD phase, the WD can be polluted by a planet or a Kuiper belt analog object.

Most efforts to explain the aforementioned polluted WD observations have focused on mechanisms to bring rocky asteroids onto a WD, either through scattering or secular effects (Veras et al. 2013; Hamers & Portegies Zwart 2016; Petrovich & Muñoz 2017; Veras et al. 2017b). These can explain small-mass object accretion by material that orbits the WD on relatively close orbits, as well as Fe, Mg, O, and Si signatures in the WD atmosphere (Veras et al. 2013; Farihi 2016; Hamers & Portegies Zwart 2016; Veras 2016; Petrovich & Muñoz 2017; Veras et al. 2017b). However, they cannot readily account for, or have not been used to explain, accretion of planet-sized objects (Jura et al. 2009; Zuckerman et al. 2011) or icy and volatile material (Xu et al. 2017) from wide orbits. Here, we consider a potential polluter (PP), the mass of which can be anywhere between several times the mass of Jupiter to the mass of a large asteroid, orbiting its host star on a relatively wide orbit that is being gravitationally perturbed by a much more distant stellar companion through the Eccentric Kozai–Lidov (EKL) mechanism.

In this paper, planetary material refers to rocky and metallic material in large amounts (i.e., from Mars-sized or larger bodies), icy material refers to water ice, and volatile material refers to volatile chemicals based largely on nitrogen, carbon, or sulfur. Neptune-like ice giants and Kuiper belt analog objects contain both icy and volatile material, while ice giants also have large rocky and metallic cores. Volatile material, and thus nitrogen, is difficult to bring onto a WD as its snow line is much further from a star than for planetary or icy material. While the accretion of volatile material most noticeably enriches a WD's atmosphere in carbon and nitrogen (Xu et al. 2017), the accretion of icy material will over time accumulate hydrogen in the atmosphere (especially noticeable for helium-dominated WDs), since hydrogen always remains in the atmosphere (e.g., Gentile Fusillo et al. 2017).

The majority of WD progenitors have a binary companion (Raghavan et al. 2010) that can excite the eccentricities of PPs to extreme values (Naoz 2016). This can cause some of these

[1] Mani L. Bhaumik Institute for Theoretical Physics, University of California, Los Angeles, CA 90095, USA.

Table 1
Initial Parameters before Applying Stability Criteria

Parameter	Neptune-runs	Kuiper-runs	WD 1425+540 Runs
# of runs	3000	1500	1500
$a_{\mathrm{PP},i}$ [au]	20–50	40–100	120–300
$a_{c,i}$ [au]	$\gtrsim$200[a]	$\gtrsim$400[a]	1120
$m_{\star,i}$ [$M_\odot$]	1–8[b]	1–8[b]	2
$m_{\mathrm{PP},i}$ [$M_\odot$]	5.149×10^{-5}	8.345×10^{-9}	8.345×10^{-9}
$m_{c,i}$ [$M_\odot$]	0.1–8[a]	0.1–8[a]	0.75
$e_{\mathrm{pp},i}$	0.01	0–0.15	0–0.15

Notes. Listed are the initial semimajor axis (a), mass (m), and eccentricity (e) distributions for potential polluters (subscript PP), primary stars (subscript $\star$), and companion stars (subscript c). Unless stated differently, all of the parameters distributions are uniform within the given ranges. The eccentricity of the companion star's orbit is picked from a uniform distribution between 0 and 1, while i_{tot} is chosen isotropically, for all three runs.
[a] Binary separation and companion mass distributions are taken from Duquennoy & Mayor (1991), determined from binary observations.
[b] Primary stellar mass distribution taken from the Salpeter Initial Mass Function (Salpeter 1955).

PPs to accrete onto the primary star during its main sequence lifetime or to be engulfed by the star as it becomes a red giant. During the Asymptotic Giant Branch (AGB) stage, stars lose mass, which causes the orbits of surviving PPs and distant stellar companions to expand. After this stage, if a companion can trigger extreme eccentricity excitations, accretion onto and pollution of WDs can occur.

The paper is organized as follows: we begin by describing the numerical setup of our calculations and Monte Carlo simulations (Section 2), followed by a description of the orbital parameters that lead to accretion (Section 3). We end the paper by discussing the implications of our results and our conclusions (Section 4).

2. Initial Conditions and Numerical Setup

2.1. Monte Carlo Simulations

We perform large Monte Carlo simulations of two representative example scenarios covering different mass scales, Neptune-like planets (denoted Neptune-runs; Howard 2013) and Kuiper belt analogs (denoted Kuiper-runs), and give a proof of concept for the proposed pollution mechanism. The initial parameters for these systems are chosen to be consistent with observed main sequence binary stars (see Table 1 for an overview of the parameters). As such we choose the primary stellar mass from a Salpeter distribution (Salpeter 1955), limited between 1 and 8 $M_\odot$. More massive stars are not expected to evolve into WDs, while less massive stars have not had enough time to evolve to become WDs over the age of the Galaxy. The mass of the companion star is chosen from a normal distribution of mass ratios consistent with observations of field binaries (Duquennoy & Mayor 1991). The masses and radii of Neptune-like planets are set equal to Neptune's, while the mass and radius of Kuiper belt dwarf planet Eris is used for the Kuiper belt analog objects.

The semimajor axis (SMA) values (a_{pp}) of the Neptune-like planets are chosen from a uniform distribution between 20 and 50 au and set with initially very low eccentricities ($e_{\mathrm{pp}} = 0.01$), while Kuiper belt analog objects' SMA values are chosen from a uniform distribution between 40 and 100 au with eccentricities chosen from a uniform distribution between 0 and 0.15

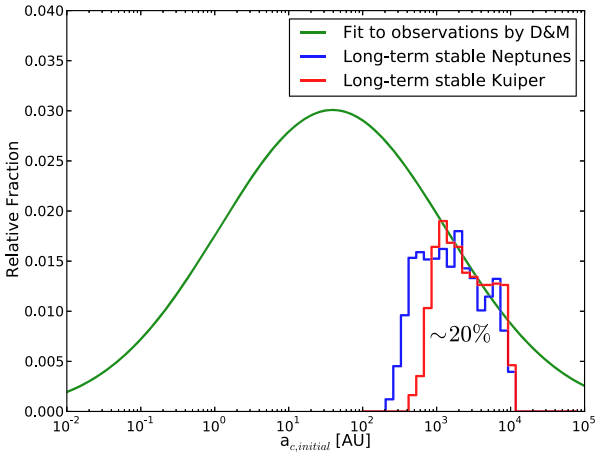

Figure 1. Initial distribution of a_c. We show the initial distribution of binary star separations based on a fit to observations by Duquennoy & Mayor (1991) in green. Overplotted are the distributions of the companion star separation, a_c, for which PP orbits are long-term stable. The blue histogram shows stable systems for Neptunes, the red one shows stable systems for Kuiper belt analogs. The systems in the stable distributions represent ~20% of the total binary population.

(e.g., Trujillo et al. 2001). Long-term stability requires:

$$\epsilon = \frac{a_{\mathrm{pp}}}{a_c}\frac{e_c}{1-e_c^2} < 0.1 \quad (1)$$

and $a_{\mathrm{pp}}/a_c < 0.1$ (e.g., Naoz 2016) so that the orbits of the PP and outer companion do not ever lead to dynamical instability and strong short-term interactions, such as, for example, scattering. This restricts the potential binary companions to wide orbits ($a_c \gtrsim 200$ au), as shown in Figure 1. We still use observational estimates from field binaries for the orbital separation (Duquennoy & Mayor 1991). Note that we also reject systems with initial a_c values of $\gtrsim$10,000 au, as galactic tides become strong enough to efficiently dissolve binaries of such separations. Due to the wide binary restriction, our simulations describe only about 20% of the entire binary population parameter space. The companion's orbital eccentricity, e_c, is picked from a uniform distribution between 0 and 1, as long as the orbits still fulfill the long-term stability criteria. Overall we performed 3000 Neptune-runs and 1500 Kuiper-runs, about 15% of which started with an initial companion star more massive than the initial primary star and which served as test systems. For these test systems no WD pollution is expected, as explained in Section 2.2.

We also perform a separate Monte Carlo simulation for the example system of WD 1425+540, which shows signs of volatile pollution suspected to stem from an accreting Kuiper belt analog object (Xu et al. 2017). This WD has a known K-dwarf companion star (Wegner 1981), and we use the simulation to determine the likelihood that our mechanism is producing the observed pollution. The WD progenitor mass is estimated to be around 2 $M_\odot$ (Xu et al. 2017), and the K-dwarf companion has a B–V color of about 1.29 (Zacharias et al. 2012), from which we estimate its mass to be approximately 0.75 $M_\odot$. A 2 $M_\odot$ star loses about two-thirds of its mass before becoming a WD (Hurley et al. 2000), meaning that the total system lost about half its mass. Given that the current visual separation of the binary is 40 arcsec (Wegner 1981; Xu et al. 2017), which

corresponds to ∼2240 au, the separation before mass loss would have been ∼1120 au. We use this value as the minimum possible apoapsis value for the initial binary orbital parameters, which restricts the minimum possible SMA and eccentricity value for the stellar companion. The Kuiper belt analog's SMA is uniformly chosen between 120 and 300 au. The lower limit of 120 au is the roughly estimated closest distance for which a Kuiper belt analog object can retain a large amount of volatiles around a 2 $M_{\odot}$ star (Xu et al. 2017). The objects' initial eccentricities are uniformly chosen between 0 and 0.15. The inclination between the Kuiper belt analog's orbit and the stellar companion's orbit is chosen isotropically. After mass loss has occurred, the Kuiper belt analog objects' SMA values increase by a factor of ∼3, while the SMA value of the companion star only increases by a factor of ∼2, which leads to the increasing value of ϵ. We perform 1500 runs of possible system configurations.

2.2. Numerical Methods and Triggering EKL

We solve the hierarchical three-body Hamiltonian up to the octupole order of approximation and average over the orbits to obtain the hierarchical secular dynamical evolution equations, also called the EKL mechanism (e.g., Naoz et al. 2013a; Naoz 2016). In this framework the three-body system consists of an inner binary formed by the host star and a PP, with an initial SMA of $a_{\rm pp}$, and which is orbited by the stellar binary companion on a much wider orbit with SMA a_c, forming an outer binary.

We consider as a proof of concept two representative examples, which vary in the mass of the PPs; one is Neptune-sized planets and the other is Kuiper belt analogs. We include equilibrium tidal models for the inner binary following Hut (1980) and Kiseleva et al. (1998); see Naoz (2016) for complete equations. We also implement general relativity precessions for the inner and outer binary (Naoz et al. 2013b). Finally, we include radial expansion, contraction, structure changes, and mass loss due to stellar evolution for the two stars following the stellar evolution code SSE (Hurley et al. 2000),[2] where we follow Dobbs-Dixon et al. (2004) and Barker & Ogilvie (2009) for the magnetic braking coefficients.

We adopt the nominal tidal coefficent parameters for our calculations. The tidal Love number of Kuiper belt analog objects is set to 5×10^{-5}, since they are icy solid objects (Grundy et al. 2007; Goldreich & Sari 2009), for stars it is set to 0.014 and for gas giants to 0.25 (Kiseleva et al. 1998). The tidal viscous evolution timescale, t_V, for stars, Neptune-like planets, and Kuiper belt analog objects is set to 1.5 years. However, we tested different t_V values over a range of several orders of magnitudes and found that they have no measurable influence on our results. In particular, once a star evolves to become a WD, its small radius suppresses tidal effects on the WD, unless the orbiting planet reaches extremely close separations, at which point the planet itself will already be tidally disrupted.

The inclusion of the octupole level of approximation leads to qualitatively different behaviors from the quadrupole level, including extreme eccentricity spikes and inclination flips from prograde to retrograde, and a generally more chaotic evolution (see Naoz 2016 for review). During the evolution of the system, the companion induces eccentricity and inclination oscillations on the orbit of a PP. In many cases the PP's eccentricity increases until it is accreted onto the evolving primary star during or before stellar expansion. However, in most cases the eccentricity excitations are not large enough to plunge the PP onto the star before the WD phase, since the octupole effects are not strong enough. The strength of the octupole oscillations are estimated by the pre-factor of the octupole level of the Hamiltonian, ϵ, which is given by Equation (1); see Naoz (2016) for a detailed explanation. The onset of this behavior can be estimated in the ϵ-inclination phase space (Katz et al. 2011; Lithwick & Naoz 2011; Teyssandier et al. 2013; Li et al. 2014). This parameter space is depicted in Figure 2, where the solid black line marks the predicted onset of octupole induced inclination flips (for the high inclination ($\geqslant 61.^{\circ}7$) test particle case, Katz et al. 2011).

Adiabatic (slow and uniform) mass loss in gravitationally bound two-body systems of total mass m leads to the expansion of the SMA a according to

$$a_f = \frac{m}{m_f} a, \tag{2}$$

where f subscripts denote post-mass loss values. In hierarchical three-body systems, the mass loss in one of the inner binary members will lead to SMA expansion for both the inner binary and the outer companion. However, the total masses to consider for each SMA are different. In our case, the PP's SMA changes to

$$a_{{\rm pp},f} = \frac{m_\star + m_{\rm pp}}{m_{\star,f} + m_{\rm pp}} a_{\rm pp} \sim \frac{m_\star}{m_{\star,f}} a_{\rm pp}, \tag{3}$$

while the companion's star SMA changes to

$$a_{c,f} = \frac{m_\star + m_{\rm pp} + m_c}{m_{\star,f} + m_{\rm pp} + m_c} a_c \sim \frac{m_\star + m_c}{m_{\star,f} + m_c} a_c. \tag{4}$$

To simplify the description of the mechanism, we present a case for which the companion does not lose mass. However, we note that, throughout the rest of the calculation, we do account for any mass lost by the companion. With these expressions we calculate the final value of ϵ, which is

$$\epsilon_f = \frac{m_\star}{m_{\star,f}} \frac{m_{\star,f} + m_c}{m_\star + m_c} \epsilon. \tag{5}$$

As $m_{\star,f}$ is always going to be smaller than $m_\star$ and m_c is larger than zero, the value of $m_\star/m_{\star,f}$ is always going to increase faster than the value of $(m_{\star,f} + m_c)/(m_\star + m_c)$ will decrease, due to the fact that ϵ_f will always be larger than ϵ. This can move systems that were in the quadrupole-dominated regime before mass loss occurred into the part of the parameter space that is octupole dominated, as shown in Figure 2. The red shaded area in the left panel shows the estimated area of the ϵ-inclination parameter space that shifts from quadrupole to octupole-dominated behavior for an example case (see figure caption for details). The possibility of increasing the strength of the octupole behavior through mass loss during stellar evolution has been shown before in the context of triple stars (Shappee & Thompson 2013), as well as WD pollution by non-volatile material of objects smaller than Mars (Hamers & Portegies Zwart 2016). If, however, the companion star is more

[2] We have tested the inclusion of post main sequence evolution to the secular code in the past and showed that it played an important role in three-body dynamical evolution (e.g., Naoz et al. 2016; Stephan et al. 2016).

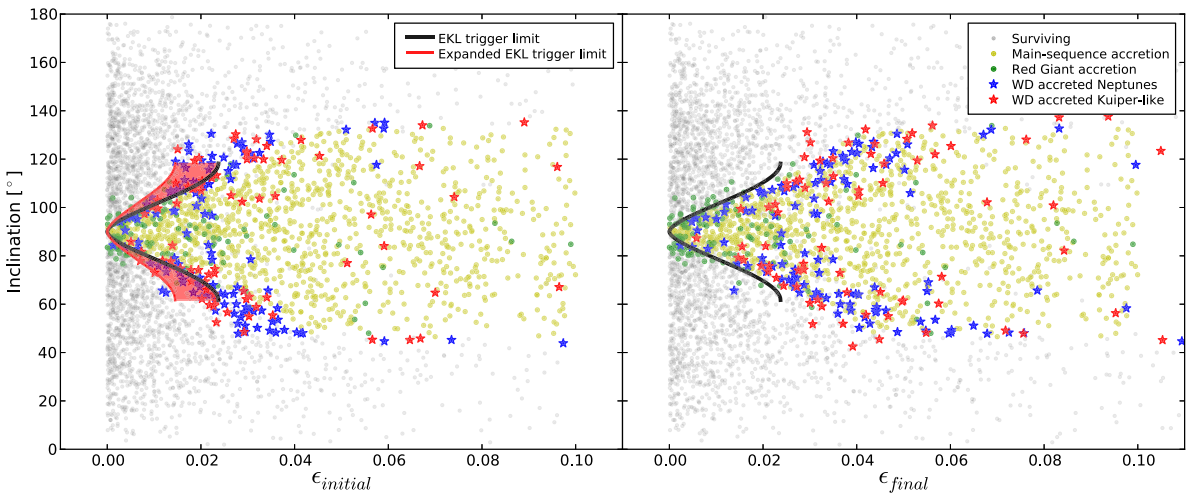

Figure 2. Octupole behavior strength within the ϵ-inclination phase space. We show the initial inclination as a function of ϵ for our Monte Carlo simulations before (left) and after (right) mass loss has occurred. Systems that survive the full 13 Gyr evolution are shown in gray, systems where the PP was accreted or destroyed during the main sequence are shown in yellow, and green marks PPs that were destroyed during the host star's red giant phase. Neptune-like planets and Kuiper belt analog objects that accrete onto WDs are shown as blue and red stars, respectively. The solid black line shows the theoretically predicted flip condition in the test particle case (e.g., Katz et al. 2011), which corresponds to high eccentricity spikes, as seen, for example, on the far right side of Figures 3(a) and (b). The red shaded area in the left panel shows the approximate part of the parameter space that shifts from non-EKL to EKL behavior through mass loss in an example case ($m_\star = 2\ M_\odot$ and $m_c = 0.75\ M_\odot$, such as WD 1425+540 and its K-dwarf companion, see Wegner 1981; Xu et al. 2017).

massive than the host star and evolves first beyond the main sequence phase, the effect will be opposite. ϵ will become smaller and the strength of octupole level perturbations decreases. Likewise, once a companion star to a WD becomes a WD itself, the mass loss might move the system from the octupole-dominated regime back to the quadrupole-dominated one.

In Figures 3(a) and (b), we show two example evolutions where the ϵ values increase by a factor of 2, leading to large eccentricity excitations during the WD phase (see the far right side of the lower parts of the plots). Note that periapsis distance and inclination oscillations (both in black) are fairly regular during the main sequence phase of the host stars (see blue shaded and red shaded parts of the plots). The periapsis distance also does not reach extreme values, and the PPs never cross the stellar Roche limit (in red) or the stellar surface (in purple) to be destroyed or accreted. However, as shown in the parts of the plots with a white background, this behavior changes after the stars have lost most of their mass during post main sequence evolution, as marked by the expanding semimajor axes of the PPs and companion stars (in blue and green, respectively, with the companion stars' periapsis distances in cyan). The eccentricities can now reach extreme peak values, at which the periapsis distances can become small enough such that the PPs cross their Roche limits (in gray, see red circles) and disintegrate around the WD, forming rings of material that can be accreted (Veras et al. 2014, 2015). The stellar Roche limit is

$$R_{\mathrm{Roche},\star} = 1.66 \times r_\star \left(\frac{m_\star + m_{\mathrm{PP}}}{m_\star}\right)^{1/3}, \quad (6)$$

while the PP's Roche limit is

$$R_{\mathrm{Roche,PP}} = 1.66 \times r_{\mathrm{PP}} \left(\frac{m_\star + m_{\mathrm{PP}}}{m_{\mathrm{PP}}}\right)^{1/3}. \quad (7)$$

Here, $r_\star$ and r_{PP} are the stellar and PP radius, respectively. When a PP crosses either Roche limit we halt the simulation. We assume that the PP is lost if it crosses the stellar Roche limit during the main sequence and red giant phases. If it crosses its own Roche limit during the WD phase, we assume that the PP will be accreted onto the WD.

3. EKL-induced WD Pollution

From the Kuiper and Neptune set of Monte Carlo runs we predict the orbital properties of binary stars that can lead to WD pollution through planets or Kuiper belt analog objects. Stellar companions that facilitate this mechanism are likely to have an SMA on the order of a few thousand au and are fairly eccentric (>0.2), as depicted in Figure 4, top and middle left panels. Furthermore, the mass of the companion is most likely slightly less than a solar mass (Figure 4, bottom left). Such lower-mass stars have a long main sequence lifetime, which is beneficial for the EKL mechanism. Once the companion stars evolve past the main sequence phase, they lose mass, increasing the SMA of the outer binary, a_c. As can be seen from Equation (5), ϵ will decrease, and further EKL evolution is suppressed. We also find that accretion can take place over a large range of WD cooling ages with a higher accretion likelihood during the first few 100 Myr to first few Gyr (Figure 4, bottom right). The distribution of the initial masses of host stars that lead to WD pollution was not found to differ substantially from the initial Salpeter distribution and was therefore omitted in Figure 4.

We note that nearly all Neptune-like planets that were later accreted onto the WD reached periapsis distances, during their host stars' AGB phase, within a few au of the expanding host star, as seen in the example in Figure 3(a). During this phase the planet can potentially lose part of its gaseous envelope due to the strong radiation from the evolving star, which heats up the planet. This may inflate the planet's atmosphere and remove gas until only the planet's rocky core and a diminished atmosphere remain (e.g., Owen & Wu 2013; Valsecchi et al. 2014). The

(a) Neptune-like Planet

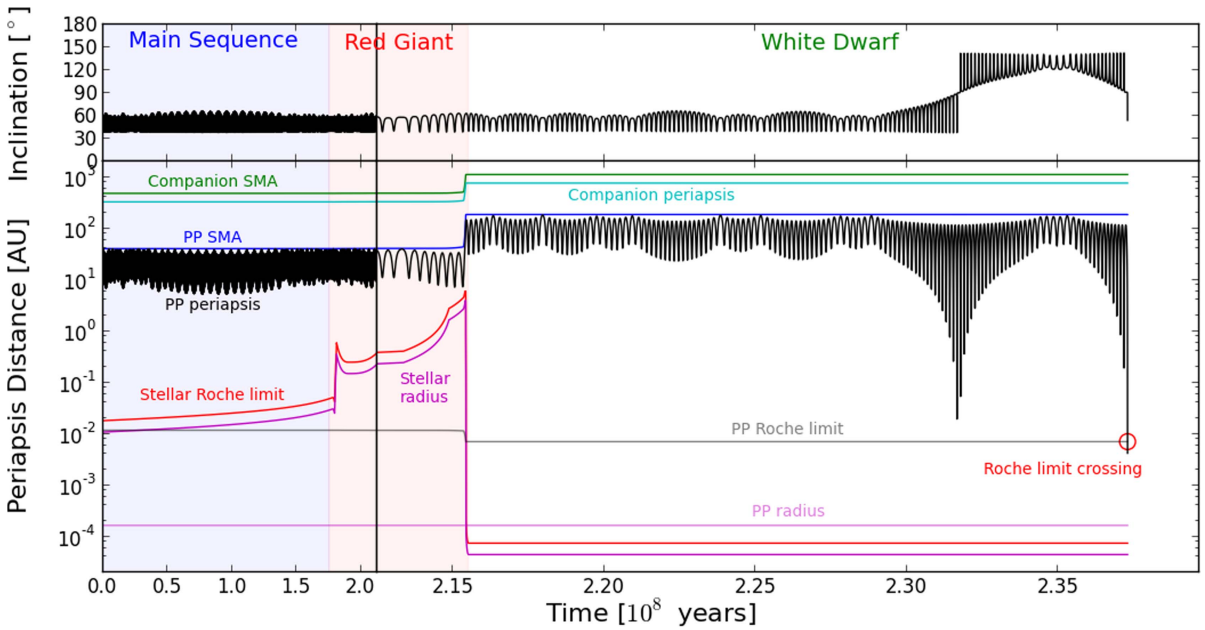

(b) Kuiper Belt Analog Object

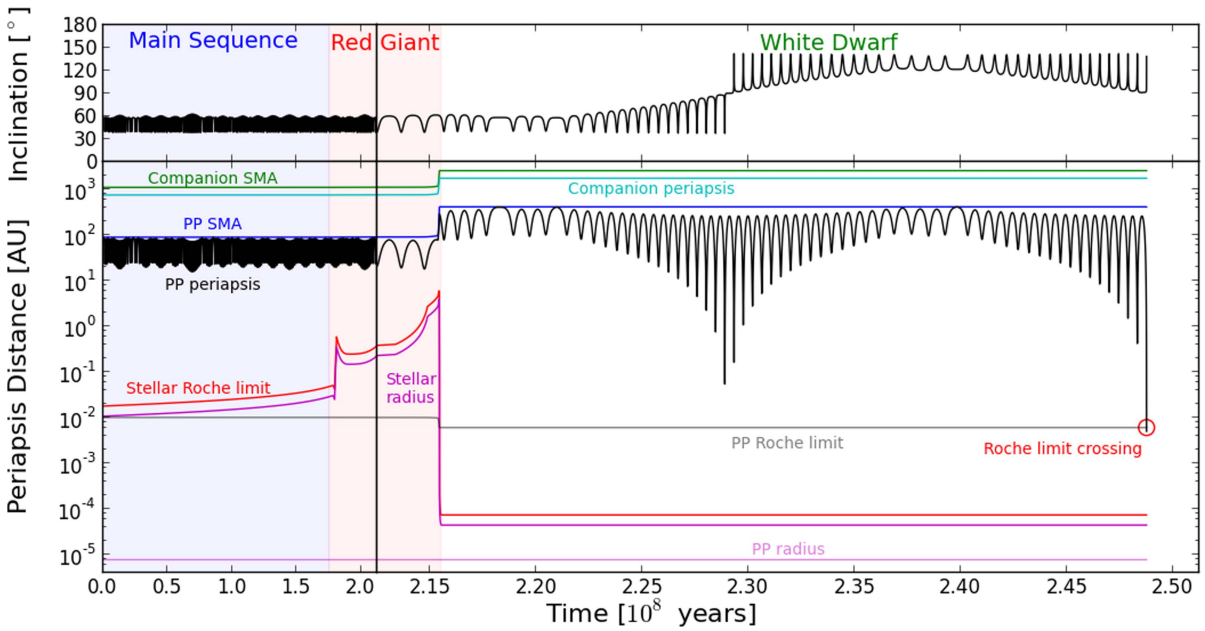

Figure 3. Dynamical evolution of a Neptune-like planet (a) and a Kuiper belt analog object (b) in wide binary star systems. Top parts of each figure show the evolution of the inclination of the PP. Bottom parts show the evolution of PP periapsis distance and SMA (in black and blue, respectively), stellar companion periapsis distance and SMA (in cyan and green, respectively), host star radius and Roche limit (in magenta and red, respectively), and the PP Roche limit (in gray). Left panels show the evolution during the fist 212.5 Myr of the binary systems' lifetime, while right panels zoom in on the last (a) ∼25 Myr and (b) ∼35 Myr of the systems' evolution. Note that there is no gap in the time-axis, only the scale changes at 212.5 Myr. The blue shaded area marks the main sequence phase, while the red shaded area approximately marks the red giant and asymptotic red giant branch phases. The white background marks the WD phase. The initial system parameters are: (a) $m_\star = 4\ M_\odot$, $m_c = 1.5\ M_\odot$, $a_{\rm pp} = 40$ au, $a_c = 480$ au, $e_{\rm pp} = 0.01$, $e_c = 0.318$, and inclination $i_{\rm tot} = 58.^\circ265$. (b) $m_\star = 4\ M_\odot$, $m_c = 1.5\ M_\odot$, $a_{\rm pp} = 90$ au, $a_c = 1110$ au, $e_{\rm pp} = 0.01$, $e_c = 0.318$, and inclination $i_{\rm tot} = 58.^\circ265$. Inclination is defined as the angle between the inner and outer orbits' angular momenta. The value of ϵ increases by a factor of ∼2 in both examples.

body that will accrete onto the WD will therefore consist mostly of this core, not of the gaseous envelope. Furthermore, if these planets were able to retain most of their envelopes during this phase, once they plunge inwards of their Roche limit around the WD the remaining gaseous envelope will be the first part to be tidally stripped off of the planets.

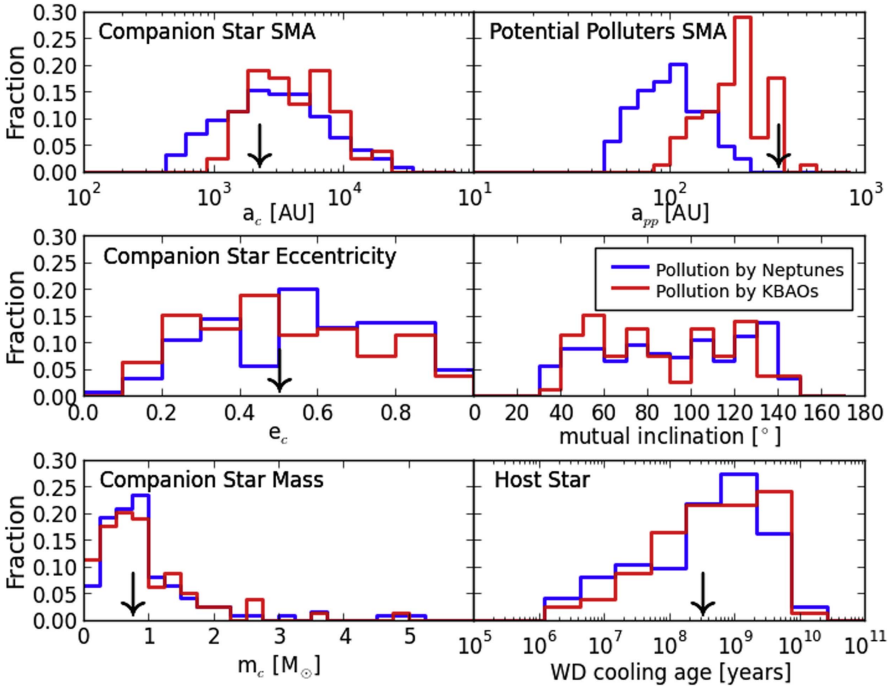

Figure 4. Orbital parameter space for polluted WDs. We show the orbital parameter likelihood distributions for systems associated with WDs polluted by the Eccentric Kozai–Lidov mechanism, after the host star has gone through mass loss and become a WD. Shown are the parameter distributions for inducing pollution by Neptune-like planets (in blue) and Kuiper belt analog objects (in red). Shown are (left to right, top to bottom): SMA of the companion star and of the PP; eccentricity of the companion star and mutual inclination between inner and outer orbits' angular momenta; mass of the companion star and WD cooling age at time of accretion. The histograms are normalized such that the integral of each one is unity. The black arrows mark the known and estimated parameters for the WD 1425+540 system (see Figure 5 for tighter estimation of the parameter space of this system). We note that the position of our Neptune polluters are consistent with the HR 8799 (Marois et al. 2008) planetary system.

In contrast to Neptune-like planets, because of their wider initial SMA, Kuiper belt analog objects that accrete during the WD phase do not typically reach periapsis distances closer than a few dozen au during the main sequence and red giant phase, as seen in the example in Figure 3(b). It is therefore highly likely that these objects will retain most or at least a significant part of their volatile material. In some cases the closest approach distance, combined with extreme radiation during the red giant phase, might trigger a comet-like behavior of the Kuiper belt analog object. For a more detailed discussion of the thermal evolution of these objects, see Jura & Xu (2010, 2012) and Malamud & Perets (2016, 2017).

We estimate the likelihoods of accretion using binary configurations that are otherwise consistent with field binaries (Duquennoy & Mayor 1991), disregarding the test systems with more massive companions than host stars, for which no WD pollution is expected and for which none occurred (see Section 2). We find that 5% of our Neptune-runs result in accretion of the planet onto the WD, as well as 6.5% of our Kuiper-runs. However, our Kuiper-runs do not actually reflect the probability of WDs accreting volatile material, as they do not account for different Kuiper belt analog orbital configurations per system. A given Kuiper belt analog can be expected to contain thousands of objects with different orbital configurations, such as the solar system's Kuiper belt. For any given Kuiper belt analog in a wide binary system, at least some objects of the belt can be expected to accrete onto the WD, as long as the initial inclination of the belt to the stellar companion lies in the favorable regime (inclinations between ∼40° and ∼140°, see also Figure 2). Thus, we conducted a proof-of-concept simulation for a single example system that is in the favorable part of the parameter space,[3] and found that up to one-third of the objects of a given Kuiper belt analog can over time accrete onto the WD. We estimate that about 75% of wide binary systems systems lie in this favorable initial inclination regime, based on an inclination distribution initially uniform in cosine. Our simulations represent about 20% of the stellar binary population, since we are restricted to wide binaries (Figure 1), and we adopt a 50% binary fraction, consistent with observations for main sequence stars (Raghavan et al. 2010). Toonen et al. (2017) show that the binary fraction of WDs with main sequence stellar companions is lower than 50%; they suggest that this is mostly due to stellar mergers of tight binaries, which should not influence our results. Based on these assumptions, our simulations are applicable to about 10% of the entire WD population. Assuming that an average star system starts out with a Neptune-like planet (the solar system, for example, has two, Uranus and Neptune), we estimate from our results that about 1% of all WDs should accrete such Neptune-like planets. Assuming that an average star system possesses a Kuiper belt analog, our results indicate that up to ∼7.5% of all WDs should accrete Kuiper belt analog objects. This may be consistent with observations of volatile and planetary material pollution.

[3] We chose a fixed inclination of 70°, a WD initial progenitor mass of 1.5 $M_{\odot}$, a companion star mass of 0.75 $M_{\odot}$, a companion orbit SMA of 2000 au and orbital eccentricity of 0.5, and SMAs and eccentricities for the Kuiper belt analog objects from uniform distributions between 40 and 100 au and 0 and 0.15, respectively. 1000 objects were tested, with about equal contributions to object survival, destruction during main sequence or red giant phases, and WD accretion.

The total number of confirmed polluted WDs is on the order of ∼200, while the overall pollution rate for all WDs is about 25–50% (e.g., Farihi 2016; Veras 2016).[4] However, there have been detailed abundance measurements for only about 15 polluted WDs so far (see Jura & Young 2014; Jura et al. 2015; Wilson et al. 2015; Farihi et al. 2016; Gentile Fusillo et al. 2017; Melis & Dufour 2017; Xu et al. 2017, and references therein), two of which show signs of planetary pollution in terms of composition and amount (see Section 1 for planetary pollution; Jura et al. 2009; Zuckerman et al. 2011), and one with signs of volatile material pollution in the form of nitrogen (Xu et al. 2017). While these are so far very small number statistics, these current results could imply that the planetary and volatile pollution rates are relatively high, on the order of ∼10%, roughly consistent with our findings that ∼7.5% of all WDs could be polluted by Kuiper belt analog objects, while about 1% could be polluted by Neptune-like planets. More detailed abundance measurements are needed for a larger number of WDs to determine the exact occurrence rates of volatile and planetary pollution. We note here that our pollution mechanism generally operates on any objects that are large enough to avoid major orbital changes by non-gravitational forces (see Hamers & Portegies Zwart 2016, for a discussion on maximum asteroid sizes sensitive to radiative forces) and are smaller than a significant fraction of the host star's mass (up to a few Jupiter masses). If any such objects commonly exist on long-period orbits in wide binary systems, they would also accrete onto WDs with a chance of ∼1%, and could potentially be the sources of planetary material pollution. Given the large uncertainty in observed planetary and volatile pollution rates, our results are consistent with the observations.

Our additional Monte Carlo simulation for the example system of WD 1425+540 leads to the accretion of icy material onto the WD for about 12.5% of tested configurations. From our results we estimate that the current periapsis distance of the K-dwarf companion should be about 3500 au, and that the mutual inclination between the Kuiper belt analog and companion star can be anywhere between ∼30° and 150° (see also Figure 5). Within these loose parameter constraints our mechanism can efficiently deliver Kuiper belt analog objects onto the WD. WD 1425+540 has an age estimate of a few 100 Myr (Xu et al. 2017), consistent with our estimated pollution likelihood over time (Figure 5, lower right panel).

4. Discussion and Conclusions

We have shown that WD pollution by icy and volatile material from Neptune-like planets and Kuiper belt analog objects can naturally be explained through the EKL evolution in wide binary systems. The mass loss during post main sequence stellar evolution enhances the strength of EKL eccentricity excitations, which can lead to the accretion of PPs onto WDs (see Figures 3(a) and (b) as examples). Systems that are more likely to facilitate this type of pollution have had an increase in ϵ value (where ϵ describes the strength of the octupole level perturbations, see Equation (1)) due to stellar mass loss during the AGB phase. These systems occupy a specific part in the ϵ-inclination parameter space (where inclination is defined as the angle between the inner and outer orbits' angular momenta), as shown in Figure 2. We note that we find some PPs that were initially in the octupole-favored regime were able to avoid accretion onto the WD progenitor during the main sequence and red giant phases. Accretion only took place in the WD phase for these PPs, after mass loss had occurred (Figure 2).

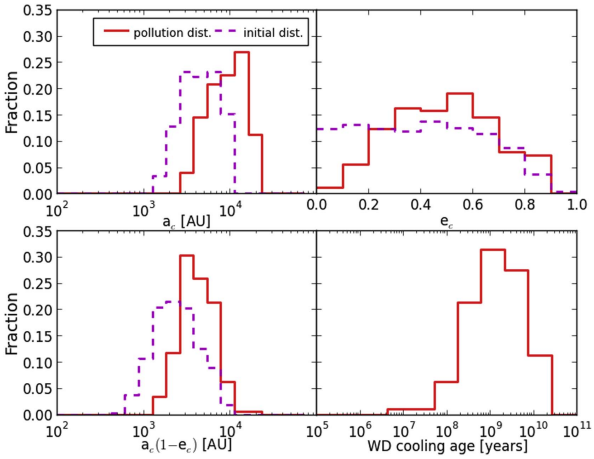

Figure 5. Orbital parameter likelihood distribution for the stellar companion of WD 1425+540. We show the orbital parameter likelihood distributions for the K-dwarf companion to WD 1425+540 if the observed volatile pollution was caused by the Eccentric Kozai–Lidov mechanism. Shown are the initial overall tested parameter distributions (dashed, in magenta) and the post-mass loss parameter distributions that led to pollution (in red).

Zuckerman (2014) studied WD pollution in binary systems and showed that pollution should preferentially occur if the binary companion was on a wide pre-mass loss orbit of at least about 1000 au, which indicates that binary separations closer than that either suppress planetary system formation or prohibit long-term stability and survival into the WD phase. This is consistent with our results, where we find that the bulk of polluted WDs had initial binary separations of about 1000 au, as shown in Figure 1. This is related to the previously discussed stability criterion, which constrained our initial system architectures to be long-term stable. However, this criterion still allows for systems that are in the octupole-favored regime (as depicted in Figures 1 and 2). In these systems, the eccentricity excitations will drive the PPs to be accreted during the main sequence or red giant phases, before the star can become a WD. As mentioned before, only systems with mild eccentricity excitations before mass loss can occur are able to result in WD pollution. These systems correspond to the a_c distribution shown in Figure 4, upper left panel.

We note here also that we ignored the effects of galactic tides on the orbital parameters of the binaries. It has been shown that galactic tides can excite eccentricities of wide stellar binaries such that their pericenter distance can get sufficiently close to scatter planetesimals onto a WD (Bonsor & Veras 2015). However, this galactic tides mechanism acts on extremely long timescales, on the order of a few to ten Gyr, while the EKL mechanism is most efficient for the first one or two Gyr. In our case galactic tides would change the companion stars' eccentricity, e_c, which would change ϵ (see Equation (1)), and thus the strength of the octupole level of approximation. This could lead to both suppression and enhancement of EKL

[4] Note that there are ∼1000 polluted WD candidates known from *SDSS* data (e.g., Zuckerman et al. 2003, 2007, 2010; Kleinman et al. 2013; Koester et al. 2014; Gentile Fusillo et al. 2015; Kepler et al. 2015, 2016).

oscillations over time. Tides might thereby increase the efficiency of our pollution mechanism, as binaries that are outside of the appropriate inclination-ϵ parameter space could be moved inside of it. Furthermore, comparing our mechanism directly to the one in Bonsor & Veras (2015), it appears that galactic tides will be most relevant at polluting WDs in very wide binaries ($a_c \gtrsim 3000$ au), while our mechanism is also effective at modestly wide separations ($a_c \gtrsim 500$ au), for which galactic tides are weak and slow. Given that the number of binary systems drops rapidly with separation (see distribution from Duquennoy & Mayor 1991, as plotted in Figure 1), our mechanism appears to be sufficient to describe the general WD population.

The implications of our results for multi-planet systems broadly fall into two categories. In general, if a multi-planet system is packed tightly enough with massive enough planets, we expect EKL and large eccentricity excitations to be mostly suppressed by the planets' mutual gravitational interactions (Innanen et al. 1997). However, if the system is not tightly packed or if the objects are not very massive, such as, for example, in a debris disk or a Kuiper belt analog, EKL excitations should still occur for each object in the disk or belt. In such systems the eccentricity and inclination changes can lead to the crossing of orbits, and potentially planet collisions or strong scattering. WD pollution should still occur for those systems. As we have discussed in Section 3, the presence of multiple objects exhibiting a range of orbital parameters indeed increases the chance of WD accretion for a given system in the favorable regime.

WD 1425+540, which exhibits volatile material pollution signatures (Xu et al. 2017), has a low-mass stellar companion on a wide orbit (Wegner 1981), consistent with our proposed pollution model. We are able to make additional predictions for its orbital parameters, as shown in Figure 5.

We predict that WDs polluted by planets or volatile material are more likely to have a binary companion with orbital parameters consistent with the distributions in Figure 4, in particular large companion separations and low companion masses. Future observations of these systems and their pollution signatures can be used to gain insights into the outer planetary and Kuiper belt analog architectures of wide stellar binary systems. By using upcoming *GAIA* data releases it should be possible to find more WDs with wide binary companions due to detailed proper motion measurements. These WDs will be excellent observational targets for finding more volatile pollution signatures and investigating the long-period planetary architectures of wide binary systems.

The authors would like to dedicate this paper to the late UCLA Professor Michael Jura for his numerous contributions to polluted white dwarf science and for inspiration. We thank the anonymous referee for fast responses and helpful comments. We also thank Siyi Xu, Dimitri Veras, and Boris Gänsike for useful discussions. S.N. acknowledges partial support from a Sloan Foundation Fellowship. B.Z. acknowledges support from a NASA grant to UCLA. Calculations for this project were performed on the UCLA cluster *Hoffman2*.

References

Barker, A. J., & Ogilvie, G. I. 2009, MNRAS, 395, 2268
Bonsor, A., & Veras, D. 2015, MNRAS, 454, 53
Debes, J. H., & Sigurdsson, S. 2002, ApJ, 572, 556
Dobbs-Dixon, I., Lin, D. N. C., & Mardling, R. A. 2004, ApJ, 610, 464
Duquennoy, A., & Mayor, M. 1991, A&A, 248, 485
Farihi, J. 2016, NewAR, 71, 9
Farihi, J., Koester, D., Zuckerman, B., et al. 2016, MNRAS, 463, 3186
Gentile Fusillo, N. P., Gänsicke, B. T., Farihi, J., et al. 2017, MNRAS, 468, 971
Gentile Fusillo, N. P., Gänsicke, B. T., & Greiss, S. 2015, MNRAS, 448, 2260
Goldreich, P., & Sari, R. 2009, ApJ, 691, 54
Grundy, W. M., Stansberry, J. A., Noll, K. S., et al. 2007, Icar, 191, 286
Hamers, A. S., & Portegies Zwart, S. F. 2016, MNRAS, 462, L84
Howard, A. W. 2013, Sci, 340, 572
Hurley, J. R., Pols, O. R., & Tout, C. A. 2000, MNRAS, 315, 543
Hut, P. 1980, A&A, 92, 167
Innanen, K. A., Zheng, J. Q., Mikkola, S., & Valtonen, M. J. 1997, AJ, 113, 1915
Jura, M. 2003, ApJL, 584, L91
Jura, M., Dufour, P., Xu, S., et al. 2015, ApJ, 799, 109
Jura, M., Muno, M. P., Farihi, J., & Zuckerman, B. 2009, ApJ, 699, 1473
Jura, M., & Xu, S. 2010, AJ, 140, 1129
Jura, M., & Xu, S. 2012, AJ, 143, 6
Jura, M., & Young, E. D. 2014, AREPS, 42, 45
Katz, B., Dong, S., & Malhotra, R. 2011, PhRvL, 107, 181101
Kepler, S. O., Pelisoli, I., Koester, D., et al. 2015, MNRAS, 446, 4078
Kepler, S. O., Pelisoli, I., Koester, D., et al. 2016, MNRAS, 455, 3413
Kiseleva, L. G., Eggleton, P. P., & Mikkola, S. 1998, MNRAS, 300, 292
Kleinman, S. J., Kepler, S. O., Koester, D., et al. 2013, ApJS, 204, 5
Koester, D., Gänsicke, B. T., & Farihi, J. 2014, A&A, 566, A34
Li, G., Naoz, S., Holman, M., & Loeb, A. 2014, ApJ, 791, 86
Lithwick, Y., & Naoz, S. 2011, ApJ, 742, 94
Malamud, U., & Perets, H. B. 2016, ApJ, 832, 160
Malamud, U., & Perets, H. B. 2017, ApJ, 842, 67
Marois, C., Macintosh, B., Barman, T., et al. 2008, Sci, 322, 1348
Melis, C., & Dufour, P. 2017, ApJ, 834, 1
Naoz, S. 2016, ARA&A, 54, 441
Naoz, S., Farr, W. M., Lithwick, Y., Rasio, F. A., & Teyssandier, J. 2013a, MNRAS, 431, 2155
Naoz, S., Fragos, T., Geller, A., Stephan, A. P., & Rasio, F. A. 2016, ApJL, 822, L24
Naoz, S., Kocsis, B., Loeb, A., & Yunes, N. 2013b, ApJ, 773, 187
Owen, J. E., & Wu, Y. 2013, ApJ, 775, 105
Paquette, C., Pelletier, C., Fontaine, G., & Michaud, G. 1986, ApJS, 61, 197
Petrovich, C., & Muñoz, D. J. 2017, ApJ, 834, 116
Raghavan, D., McAlister, H. A., Henry, T. J., et al. 2010, ApJS, 190, 1
Salpeter, E. E. 1955, ApJ, 121, 161
Shappee, B. J., & Thompson, T. A. 2013, ApJ, 766, 64
Stephan, A. P., Naoz, S., Ghez, A. M., et al. 2016, MNRAS, 460, 3494
Teyssandier, J., Naoz, S., Lizarraga, I., & Rasio, F. A. 2013, ApJ, 779, 166
Toonen, S., Hollands, M., Gaensicke, B. T., & Boekholt, T. 2017, A&A, 602, A16
Trujillo, C. A., Jewitt, D. C., & Luu, J. X. 2001, AJ, 122, 457
Valsecchi, F., Rasio, F. A., & Steffen, J. H. 2014, ApJL, 793, L3
Vanderburg, A., Johnson, J. A., Rappaport, S., et al. 2015, Natur, 526, 546
Veras, D. 2016, RSOS, 3, 150571
Veras, D., Carter, P. J., Leinhardt, Z. M., & Gänsicke, B. T. 2017a, MNRAS, 465, 1008
Veras, D., Georgakarakos, N., Dobbs-Dixon, I., & Gänsicke, B. T. 2017b, MNRAS, 465, 2053
Veras, D., Leinhardt, Z. M., Bonsor, A., & Gänsicke, B. T. 2014, MNRAS, 445, 2244
Veras, D., Leinhardt, Z. M., Eggl, S., & Gänsicke, B. T. 2015, MNRAS, 451, 3453
Veras, D., Mustill, A. J., Bonsor, A., & Wyatt, M. C. 2013, MNRAS, 431, 1686
Wegner, G. 1981, AJ, 86, 264
Wilson, D. J., Gänsicke, B. T., Koester, D., et al. 2015, MNRAS, 451, 3237
Xu, S., Jura, M., Dufour, P., & Zuckerman, B. 2016, ApJL, 816, L22
Xu, S., Zuckerman, B., Dufour, P., et al. 2017, ApJL, 836, L7
Zacharias, N., Finch, C. T., Girard, T. M., et al. 2012, AJ, 154, 44
Zuckerman, B. 2014, ApJL, 791, L27
Zuckerman, B., Koester, D., Dufour, P., et al. 2011, ApJ, 739, 101
Zuckerman, B., Koester, D., Melis, C., Hansen, B. M., & Jura, M. 2007, ApJ, 671, 872
Zuckerman, B., Koester, D., Reid, I. N., & Hünsch, M. 2003, ApJ, 596, 477
Zuckerman, B., Melis, C., Klein, B., Koester, D., & Jura, M. 2010, ApJ, 722, 725

CHAPTER 3

Binary Stars in the Galactic Center

The Galactic Center contains the SMBH Sagittarius A* with a mass of roughly 4×10^6 $M_\odot$, as well as millions of stars within the central parsec (Ghez et al. 2005; Gillessen et al. 2009). This dense and rich environment has provided an ideal testing ground for studying a variety of phenomena such as stellar cluster dynamics (e.g., Ghez et al. 2003; Alexander 2005; Ghez et al. 2005; Hopman and Alexander 2006; Alexander and Hopman 2009; Gillessen et al. 2009; Hopman 2009; Gillessen et al. 2012), general relativity (Hees et al. 2017; Chu et al. 2018; Do et al. 2019), the origin of hypervelocity stars (e.g., Hills 1988; Yu and Tremaine 2003; Ginsburg and Loeb 2007), X-ray sources suspected to be X-ray binaries (e.g., Muno et al. 2005; Cheng et al. 2018; Hailey et al. 2018; Zhu et al. 2018) or cataclysmic variables (e.g., Muno et al. 2006; Heinke et al. 2008; Muno et al. 2009), and, what the papers presented in this chapter focus on, the mergers of binary stars (e.g., Antonini et al. 2010, 2011; Prodan et al. 2015).

In 2012, a peculiar infrared-excess object, named G2, was discovered to orbit Sagittarius A* on a highly eccentric orbit, suspected to be a gas cloud poised to be tidally disrupted upon approaching periapsis (Gillessen et al. 2012). However, this object did indeed survive periapsis passage, supporting ideas that G2 and similar objects are indeed not gas clouds, but stellar merger products enshrouded by gas and dust (e.g., Antonini et al. 2010, 2011; Antonini and Perets 2012; Witzel et al. 2014; Prodan et al. 2015; Stephan et al. 2016; Witzel et al. 2017; Stephan et al. 2019). While the Galactic Center is a very dense environment, several binary stars have been confirmed to exist within it, supporting the idea that binary mergers can occur there (Ott et al. 1999; Martins et al. 2006; Pfuhl et al. 2014). Any stellar binary orbiting a SMBH will undergo the EKL mechanism, as they must form a hierarchical

triple system to be stable against the tidal forces of the SMBH.

Naturally, such stellar binaries will also undergo stellar evolution, influencing their dynamics. Therefore, the first study presented in this chapter, Stephan et al. (2016), was conducted to investigate the merger probability of such stellar binaries throughout all stellar evolutionary phases. The inclusion of tides and stellar evolution is particularly important as they can lead to orbital shrinking of the binary. This "hardens" the binary system against scattering events from other stars in the Galactic Center, increasing the effective survival and thus increasing the probability to merge. The second publication in this chapter, Stephan et al. (2019), studied the binary stellar evolution outcomes of such stellar mergers by applying the binary stellar evolution code `BSE` (Hurley et al. 2002), using the version improved by the COSMIC group (Breivik et al. 2019). This study predicts that many binary mergers can produce X-ray binaries, cataclysmic variables, gravitational wave sources, and that they can lead to supernovae and the formation of G2-like infrared-excess sources, explaining many observed features of the Galactic Center and galactic nuclei in general.

Monthly Notices of the ROYAL ASTRONOMICAL SOCIETY

MNRAS **460,** 3494–3504 (2016) doi:10.1093/mnras/stw1220
Advance Access publication 2016 May 20

Merging binaries in the Galactic Center: the eccentric Kozai–Lidov mechanism with stellar evolution

Alexander P. Stephan,[1]★ Smadar Naoz,[1]★ Andrea M. Ghez,[1] Gunther Witzel,[1] Breann N. Sitarski,[1] Tuan Do[1] and Bence Kocsis[2]

[1]*Department of Physics and Astronomy, University of California, Los Angeles, CA 90095, USA*
[2]*Institute of Physics, Eötvös University, Pázmány P. s. 1/A, Budapest 1117, Hungary*

Accepted 2016 May 15. Received 2016 May 3; in original form 2016 March 7

ABSTRACT

Most, if not all, stars in the field are born in binary configurations or higher multiplicity systems. In dense stellar environment such as the Galactic Center (GC), many stars are expected to be in binary configurations as well. These binaries form hierarchical triple-body systems, with the massive black hole (MBH) as the third, distant object. The stellar binaries are expected to undergo large-amplitude eccentricity and inclination oscillations via the so-called 'eccentric Kozai–Lidov' mechanism. These eccentricity excitations, combined with post-main-sequence stellar evolution, can drive the inner stellar binaries to merge. We study the mergers of stellar binaries in the inner 0.1 pc of the GC caused by gravitational perturbations due to the MBH. We run a large set of Monte Carlo simulations that include the secular evolution of the orbits, general relativistic precession, tides and post-main-sequence stellar evolution. We find that about 13 per cent of the initial binary population will have merged after a few Myr and about 29 per cent after a few Gyr. These expected merged systems represent a new class of objects at the GC, and we speculate that they are connected to G2-like objects and the young stellar population.

Key words: binaries: close – stars: evolution – stars: kinematics and dynamics – Galaxy: centre.

1 INTRODUCTION

The proximity of the Galactic Center (GC) provides an accessible laboratory for studying different physical processes in the presence of a massive black hole (MBH), many of which may also take place in many other galactic nuclei. Observations of the GC give an exquisite opportunity to test different theoretical arguments and physical processes that involve MBHs and dense environments. Binary populations within the central 1 pc play a significant role in numerous processes that take place at the GC, including the relaxation state of the GC (Alexander & Hopman 2009),[1] the stellar number density (e.g. Alexander & Pfuhl 2014; Prodan, Antonini & Perets 2015), the S-star cluster population (e.g. Antonini & Merritt 2013), as well as hypervelocity stars (e.g. Hills 1988; Yu & Tremaine 2003; Ginsburg & Loeb 2007; Perets 2009; Perets et al. 2009). Furthermore, compact object binaries in the GC are a potential source of gravitational wave emission (e.g. O'Leary, Kocsis & Loeb 2009; Antonini & Perets 2012).

Currently, there are three confirmed observed binaries in the inner ∼0.2 pc of the GC. The first confirmed binary, IRS 16SW, is an equal-mass binary ($m_{\rm primary} = m_{\rm secondary} = 50\ {\rm M}_{\odot}$) at a projected distance estimated as ∼0.05 pc from the MBH with a period of 19.5 d (Ott, Eckart & Genzel 1999; Martins et al. 2006). Recently, Pfuhl et al. (2014) discovered two additional binaries, an eclipsing Wolf–Rayet binary with a period of 2.3 d, and a long-period binary with an eccentricity of 0.3 and a period of 224 d. Both of these binaries are estimated to be at only ∼0.1 pc from the MBH. The long-period binary detection provides lower limits on the two-body relaxation time-scale, and an upper limit on the number density of the faint stars and the compact remnants (i.e. the dark cusp) that are expected to exist near the MBH (see Bahcall & Wolf 1977; Alexander & Hopman 2009; Alexander & Pfuhl 2014). The latter study is extremely interesting as it lays out the dynamical consequences of even a single detection of a long-period binary. This stresses the need for more observations and that combining them with the understanding of the dynamics will allow us to draw better conclusions and tighter constraints on the binary fraction. Recent observational endeavours were proven to be very promising in placing some

★ E-mail: alexpstephan@astro.ucla.edu (APS); snaoz@astro.ucla.edu (SN)
[1] If the GC is relaxed, a dense, mass-segregated cusp of stellar mass BHs is expected near the MBH.

limits on the binary fraction and the dynamical state of the GC. These suggest that the total massive binary fraction in the GC is comparable to the galactic binary fraction (e.g. Ott et al. 1999; Rafelski et al. 2007). Massive O-star binaries at the GC are estimated to be about 7 per cent of the total massive stellar population (Rafelski et al. 2007). These binaries (and those outside the central parsec) are mostly observed as eclipsing or ellipsoidal variable binaries (e.g. Ott et al. 1999; Rafelski et al. 2007). Lower mass binaries are currently not accessible by observations in the GC. Furthermore, the observed X-ray source overabundance in the central pc (Muno et al. 2005) suggests that compact binaries may reside there as well.

Gillessen et al. (2012) have recently reported the discovery of a gas cloud of about 3 $M_{\rm Earth}$, called G2, plunging towards the MBH, with a closest approach distance that brings it as close as 3100 times the event horizon (∼245 AU). This discovery generated many models to explain the origin of G2 (e.g. Burkert et al. 2012; Miralda-Escudé 2012; Morris, Meyer & Ghez 2012; Murray-Clay & Loeb 2012; Phifer et al. 2013; Guillochon et al. 2014). This object gives a rare opportunity to study the dynamics and tidal evolution of a source close to an MBH in real time. Follow-up observations have shown that G2 remained compact in the continuum and that its orbit is still consistent with a Keplerian orbit after periapsis passage (Meyer et al. 2014; Witzel et al. 2014; Valencia-S. et al. 2015). Thus, it was suggested that this object is actually a result of a merged stellar binary (Witzel et al. 2014; Sitarski, in preparation), a connection previously suggested by Prodan et al. (2015). Here we take their study further and couple post-main-sequence evolution to the dynamical evolution. The possibility of binary mergers due to perturbations by the MBH was first suggested, in the context of hypervelocity stars, by Ginsburg & Loeb (2007).

Stellar binaries in the GC form hierarchical triple-body systems, with the MBH as the third, distant object. Therefore, stellar binaries are expected to undergo large-amplitude eccentricity and inclination oscillations, i.e. the so-called 'eccentric Kozai–Lidov' (EKL) mechanism (see for review Naoz 2016). Eccentricity excitations in a binary, induced by the MBH, can cause the binary stars to merge (e.g. Antonini et al. 2010; Antonini, Lombardi & Merritt 2011). However, tidal forces between the binary companions tend to shrink and circularize their orbits, either preventing or severely delaying a merger. Here we take into account post-main-sequence stellar evolution and show that this, in combination with the EKL mechanism, can cause large fractions of merged systems. While the mass-loss during stellar evolution widens the orbit, the mass-loss can also re-trigger the EKL behaviour for similar-mass binaries, which will lead to large eccentricities (e.g. Shappee & Thompson 2013; Michaely & Perets 2014). In addition, as the star expands, it may undergo Roche lobe overflow, especially for binaries with tidally shrunken and circularized orbits (e.g. Naoz et al. 2016). Therefore, contact binaries and merger products can be formed after one of the binary companions has left the main sequence. Merging binaries solves many unanswered questions in the GC context. For example, merging binaries may form rejuvenated products that appear young, which could explain the unexpected population of young stars in the GC (Ghez et al. 2005) and it may change the initial mass function (IMF) of the GC stellar population, which could explain the observed top-heavy IMF in the GC (Lu et al. 2013).

The paper at first describes the numerical setup of our work (Section 2), after which it presents results and an analysis of the binary evolutions observed in our simulations (Section 3). This is followed by a discussion of our results in Section 4. Appendix A is attached to discuss the evaporation time-scale.

2 NUMERICAL SETUP

The numerical setup of the systems is chosen to be consistent with binaries in the field. The mass distribution of the primary stellar binary member is taken as a Salpeter function with $\alpha = 2.35$ with a minimum mass of 1 and a maximum of 150 $M_\odot$ (we denote this mass as m_1), while the mass ratio to the secondary mass (m_2) is taken from Duquennoy & Mayor (1991). This choice of numerical binary setup differs from Antonini & Perets (2012) and Prodan et al. (2015) as we do not have a large fraction of $m_1 = m_2$ systems. While some studies have suggested that stellar twin binaries are relatively common (see, for example, Pinsonneault & Stanek 2006; Kobulnicky & Fryer 2007), more recent works suggest that stellar twins do not form a relevant part of the binary population (Lucy 2006; Sana et al. 2012). Therefore, avoiding exact stellar twins is a more realistic choice for the mass distribution. Additionally, since the octupole level of approximation goes to zero for systems that have an exact symmetry (e.g. Naoz 2016), relaxing the symmetry allows the systems to undergo large-eccentricity excitations even for similar masses once the stars begin to evolve and lose mass (Shappee & Thompson 2013; Michaely & Perets 2014).

The mass of the MBH, $m_{\rm MBH}$, remains fixed at 4×10^6 $M_\odot$ (following Ghez et al. 2005; Gillessen et al. 2009) for all systems since we are mostly interested in the results for Sagittarius A*. The eccentricity distribution is taken as uniform from 0 to 1 for the stellar binary (inner) orbit (e_1), following Raghavan et al. (2010), while it is taken as thermal for the MBH (outer) orbit (e_2) (Jeans 1919). The mutual inclination between the inner and outer orbit is assumed to be uniformly distributed in cosine. The argument of periapsis is taken from a uniform distribution for both orbits, as is the angle of the stellar spin axis. The outer orbital period is distributed uniformly in log space, with an assumed minimum of ∼9 yr corresponding to a semi-major axis (a_2) of ∼700 AU (the closest known star to Sagittarius A*, SO-2, has an orbital period of ∼15 yr; Ghez et al. 2005) and an assumed maximum of ∼1500 yr or 0.1 pc, due to the conflicting time-scales for orbits larger than that, as seen in Fig. 1. The inner orbital semi-major axis (a_1) and period are taken from a lognormal distribution with a peak at ∼170 yr and the 1σ interval going from ∼0.9 to ∼35 000 yr (Duquennoy & Mayor 1991).

We require these randomly generated systems to satisfy dynamical stability so that we can separate the long-term secular effects. Similarly to Naoz & Fabrycky (2014), the first condition requires that the two stars are initially outside their binary companion star's Roche limit, otherwise the inner stars suffer a merger before the tertiary can act. The second condition requires that the system is hierarchical enough to allow usage of the EKL equations. This means that the systems have to fulfil the following criterion:

$$\epsilon = \frac{a_1}{a_2}\frac{e_2}{1-e_2^2} < 0.1, \quad (1)$$

where ϵ is a measure of the relative strengths of the octupole and quadrupole effects on the orbital dynamics (e.g. Naoz 2016).[2] Similar to the first condition, which requires that the inner binary members are not already crossing their partner stars' Roche limit, the

[2] Note that the precession of the outer orbit due to general relativity (Naoz et al. 2013b) or due to the precession from the spherical star cluster (i.e. Newtonian precession; Kocsis & Tremaine 2011) may have quantitative effects on a single system but will not change the overall statistics. We tested the effect of GR effects on the outer orbit and did not find any differences in our results.

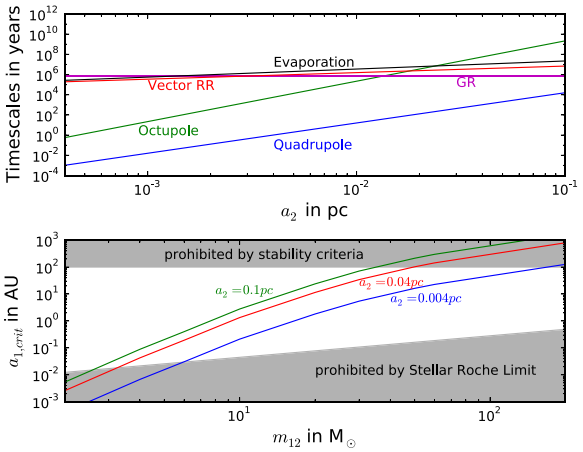

Figure 1. Time-scales of different physical effects and critical a_1 values for stellar evolution. Plotted in the top panel are the periapsis precession time-scales associated with the EKL mechanism (quadrupole in blue, octupole in green), general relativity (GR) in the inner binary (magenta), vector resonant relaxation (VRR, red), and the evaporation time-scale for an example binary of 2 $M_\odot$ total mass and $a_1 = 3$ AU as a function of a_2. Not shown is the outer orbit precession time-scale induced by GR by the MBH of $\sim 10^5$ yr, which is not of primary concern for our calculations. The scalar resonant relaxation time-scale is in general between 10^9 and 10^{11} yr and can dip down to 10^7 yr around $a_2 = 0.007$ AU due to the cancellation of the relativistic precession by Newtonian precession (see Kocsis & Tremaine 2011). We omit it here to avoid clutter. EKL oscillations can only occur if their associated time-scales are shorter than the other precession effects, since they counteract the buildup of large eccentricities. Note that the evaporation time-scale is comparable with the VRR time-scale, which allows us to ignore VRR for our calculations.[3] Plotted in the bottom panel are the critical maximum binary separations, a_1, allowed for stellar evolution to take place before the binaries evaporate. The grey areas denote a_1 values prohibited by the stellar Roche limits (bottom), or by the stability criteria of our initial conditions (top).

third criterion requires that the inner binary does not cross the MBH's Roche limit, in the form of

$$\frac{a_2}{a_1} > \left(\frac{3m_{\rm MBH}}{m_{\rm binary}}\right)^{1/3} \frac{1+e_1}{1-e_2}. \quad (2)$$

Even though we reject systems that violate equation (2) from the set of[3] initial conditions, some systems cross the MBH's Roche limit later during their evolution. We keep track of those and will analyse them separately.

After applying these stability tests, many of the original systems were rejected. Out of 7000 systems with the parameters mentioned above, we are left with 1570 systems. Note that the inner period initial conditions distribution following Duquennoy & Mayor (1991) is probably unrealistic for the condition for star formation in the GC. Specifically, it is unlikely that star formation episodes at the GC will lead to the formation of binaries with separations larger than 100 AU, as suggested by Duquennoy & Mayor (1991). Furthermore, the limited parameter space available for forming stable binary systems should also severely limit the possibility of forming triple or higher multiplicity stars in the GC, which we therefore ignore in our model.

[3] Numerically, this is very similar to the Mardling & Aarseth (2001) nominal triple stars stability criterion, as shown in Naoz et al. (2013b).

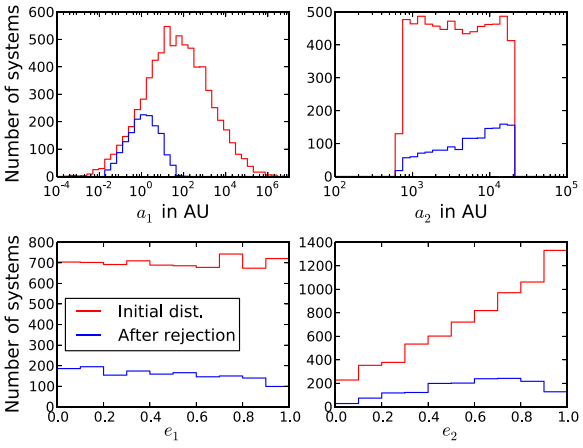

Figure 2. Parameter distributions before and after stability test. Shown are the distributions of a_1, a_2, e_1 and e_2 before and after the stability test. Note that the a_1 distribution remains lognormal after the stability test, and its peak is simply shifted to a smaller value. The new a_2 distribution has a small preference for larger a_2 values compared to the flat original distribution. The e_1 distribution remains flat, while the e_2 distribution preferentially suppresses large e_2 values of the originally thermal distribution. The inclination distribution (not shown) did not change at all.

The exact distribution for the inner binary period is unknown and thus we follow this recipe for initial conditions generation. We ensure the stability of the systems by our stability criteria. We thus caution the reader from interpreting the rejection method of our initial conditions as a physical process. The orbital parameter distributions before and after our rejection process are depicted in Fig. 2.

We solve the hierarchical triple secular equations up to the octupole level of approximation (as described in Naoz et al. 2013a; Naoz 2016), including general relativity (GR) effects for both the inner and outer orbit (Naoz et al. 2013b)[4] and static tides for both members of the stellar binary (following Hut 1980; Eggleton, Kiseleva & Hut 1998). See Naoz (2016) for the complete set of equations. We also include the effects of stellar evolution on stellar radii, masses and spins following the stellar evolution code SSE by Hurley, Pols & Tout (2000). The octupole level code with post-main-sequence effects was successfully tested in a previous study (Naoz et al. 2016). Our code, which couples the secular evolution with the physical processes mentioned above, allows us to go beyond the initial study of the dynamical evolution of binaries at the GC by Antonini & Perets (2012) and Prodan et al. (2015). Specifically, the post-main-sequence evolution adds significant contributions to merging the binaries.

We have two sets of Monte Carlo simulations adopting two different tidal efficiencies. One series of systems has efficient tides, which is achieved by using a constant viscous time of 1.5 yr (750 systems); the other set of systems has less efficient tides with a constant viscous time of 150 yr (1570 systems). The different assumptions for the viscous time cause variations in the formation likelihood of tight, circular binaries. The less efficient tides are probably more realistic (e.g. Hansen 2010), and we use a larger sample size for those runs in order to obtain better statistics. Unless

[4] We note that the GR precession of the outer orbit has an insignificant effect on the dynamical evolution and can be neglected.

explicitly stated otherwise, all results discussed in this work refer to the more realistic less efficient tide scenario.

Eccentricity excitations in the inner binary orbit will take place if the shortest time-scale associated with the EKL mechanism, i.e. the quadrupole time-scale, is shorter than the precession of the periapsis due to short-range forces. Such short-range forces come from GR and the precession of the nodes due to oblate objects from static tides or rotating objects (e.g. Naoz 2016). The octupole level of approximation assisted time-scale gives a sense of the time-scale required to pump the eccentricity up to extreme eccentricity spikes. In Fig. 1, we show the quadrupole, octupole and GR time-scales for a nominal example system (see Naoz 2016, for the relevant time-scales). This shows that the quadrupole time-scale is shorter than the GR time-scale for the considered values for a_2, thus allowing eccentricity and inclination oscillations to occur.

Binary mergers in dense stellar groups can be prevented through close encounters with other stars, which can change the orbital parameters of the binaries. The change depends to a large degree on whether the binary's orbital energy is larger or smaller than its centre-of-mass motion energy compared to other cluster stars, which are known as hard or soft binaries, respectively. Binaries in the GC are generally soft and are expected to become less bound through stellar encounters, until they disassociate or 'evaporate'. A derivation for the evaporation time-scale can be found in Binney & Tremaine (1987). For completeness, the derivation of the evaporation time-scale with the total mass of the system is presented in Appendix A. The evaporation time-scale for a nominal example system is also shown in Fig. 1. However, some binaries in the GC can be hard, especially if their orbital separation is reduced by tidal effects. Hard binaries can actually form even tighter, harder binaries through stellar interactions, and their evaporation time-scale becomes exponentially longer with their hardness (see, for example, Heggie 1975; Hut 1983; Hut & Bahcall 1983; Heggie, Hut & McMillan 1996). GC binaries need to be very tight in order to be hard, and a_1 needs to be of the order of $\sim$0.1 AU or less. At such separations, the tides of the binary companions become very strong. We therefore assume that such tight binaries survive evaporation effects for at least 10 Gyr, see Appendix A.

Mergers through EKL oscillations can only occur if the time-scale of quadrupole effects is shorter than the evaporation time-scale. However, post-main-sequence stellar evolution can also lead to mergers, which is likewise limited by the survival time of the binary. The bottom panel of Fig. 1 shows the maximum binary separation possible in order for post-main-sequence stellar evolution to occur before the binary evaporates.

Another important physical process that takes place in the GC is vector resonant relaxation (VRR). This process changes the direction of the outer orbit's angular momentum, but not its magnitude. Since efficient eccentricity excitations due to the EKL mechanism require large mutual inclinations between the inner and outer orbits,[5] VRR will change the inclination and will effectively refill the available phase space that allows large-eccentricity oscillations. Binaries that did not undergo substantial tidal effects nor merged can, due to the VRR process, change their inclination relative to the MBH such that they leave the favourable EKL regime. The associated time-scale is shown in Fig. 1 (e.g. Hopman & Alexander 2006; Kocsis & Tremaine 2011, 2015). As depicted in this example, the VRR time-scale is comparable to the evaporation time-scale for most parts of the parameter space, but becomes shorter than the evaporation time-scale beyond $\sim$0.1 pc. Thus, we neglect the VRR effects in our calculations, but limit them to the inner 0.1 pc of the GC. However, we note here that the VRR time-scale is in general too long to have an effect on EKL-induced mergers; see Section 3 for an explanation in light of the results of our calculations.

The integration time for each binary is determined by its evaporation time-scale (see Appendix A). If a binary became tightly locked, and thus decoupled from the gravitational perturbations of the MBH, we recalculate the evaporation time (we set the evaporation time to 10 Gyr for hard binaries) and continue the post-main-sequence evolution using the binary stellar evolution code BSE (Hurley, Tout & Pols 2002) until the binary either merged or evaporated. Our maximum evolution time is 10 Gyr.

3 RESULTS

During the EKL evolution, the inner orbit eccentricity is excited to extremely high values (e.g. Teyssandier et al. 2013; Li et al. 2014a,b) that can result in crossing of the Roche limit, which may drive the two stars into merging (e.g. Naoz & Fabrycky 2014). The Roche limit is defined by

$$a_{\mathrm{Roche},ij} = \frac{R_j}{\mu_{\mathrm{Roche},ji}}\,, \tag{3}$$

where R_j is the radius of the star at mass m_j and, following Eggleton (1983), $\mu_{\mathrm{Roche},ji}$ is a dimensionless number

$$\mu_{\mathrm{Roche},ji} = 0.49\frac{(m_j/m_i)^{2/3}}{0.6(m_j/m_i)^{2/3}+\ln(1+(m_j/m_i)^{1/3})}\,. \tag{4}$$

If the inner binary pericentre distance, $a_1(1-e_1)$, becomes smaller than either $a_{\mathrm{Roche},12}$ or $a_{\mathrm{Roche},21}$, we assume that one of the stars will overflow its Roche lobe. We stop the calculation here and identify this system as a merger candidate.

We categorize the outcomes of the binaries' evolution into three main cases.

(i) *Tidally locked binaries.* The tidal interactions of the binaries will in some cases lead to circularization and shrinking of binary orbits. The stars' spin periods and orbital period will in this case synchronize, tidally locking the binary. These tight, tidally locked binaries are an important class of objects, since the tightening of their orbits can significantly delay evaporation of the binaries. Since strong tidal evolution significantly slows down the computation, we stop the simulation if the orbit is sufficiently tight ($a_1 < 0.1$ AU), circularized ($e_1 < 10^{-5}$), and if the spin and orbital periods have synchronized to approximately reach the expected spin rate Ω (within a fractional difference of 10^{-5}) (e.g. Fabrycky, Johnson & Goodman 2007):

$$\Omega = 2\frac{2\pi/P_{\mathrm{in}}}{\cos\psi+\sec\psi}\,. \tag{5}$$

Here, P_{in} is the inner binary period and ψ is the orbital obliquity.

Tidally locked binaries are a transient phase with their duration determined by the main-sequence lifetime of the more massive star. If the post-main-sequence radial expansion occurs before the binary is somehow disrupted, the stars will merge (see below). We found that after 6 Myr of evolution, about 10 per cent of the systems became tidally locked (using the low-efficiency tides model; see the right-hand column of Fig. 3 as an example). The system undergoes large-eccentricity excitations while tidal interactions are

[5] If both the inner and the outer orbits are initially eccentric, further eccentricity excitations can take place in a nearly coplanar configurations (Li et al. 2014a).

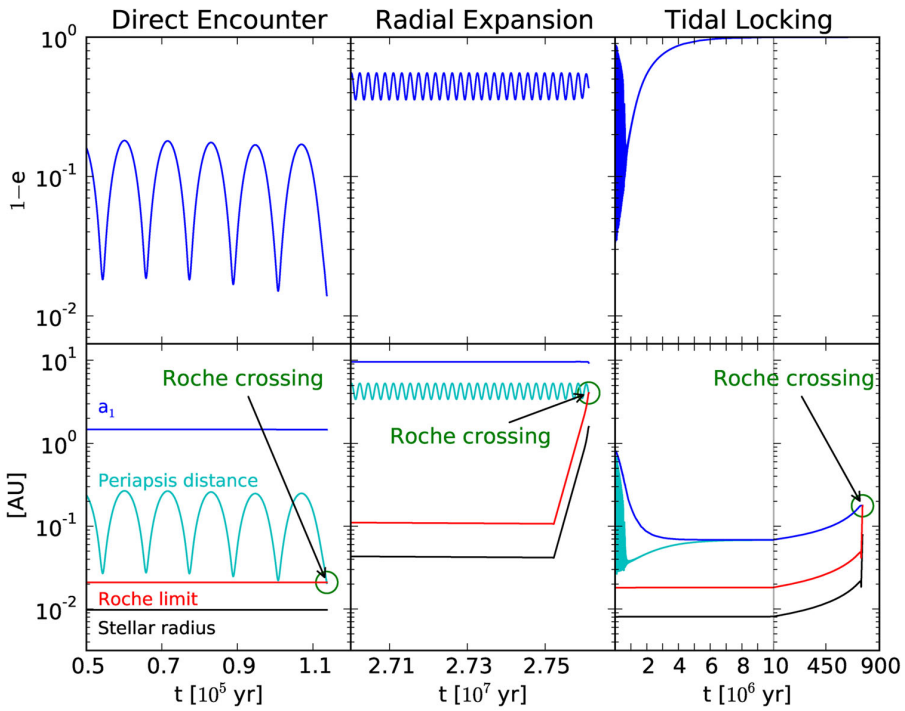

Figure 3. Example evolution for the three merger scenarios. The plot shows the evolution of eccentricity, semi-major axis, periapsis distance, Roche limit and stellar radius for three example systems that lead to mergers. The left column shows a direct merger caused by high orbital eccentricity due to EKL cycles, the centre column shows a radial merger caused by the rapid expansion of the larger stellar companion in the binary due to stellar evolution and the right column shows a tidal merger, a system that becomes tidally locked before it can evaporate and will survive long enough to merge due to radial expansion similar to the centre column's example system. Note that the systems in the centre and the right column are examples of regular contact binary mergers, while the left column's system could be an example of a direct collision or otherwise high-velocity merger with a much more complex binary evolution, which is beyond the scope of this work. After 6 Myr of evolution, we register mostly direct mergers and a few radial mergers; after 10 Gyr, 35 per cent of all mergers are direct mergers, 10 per cent are radial mergers and 55 per cent are tidal mergers.

slowly shrinking and circularizing the orbit. As discussed below, after post-main-sequence evolution, many of these tidally locked systems become merged binaries.

(ii) *Merged binaries and G2-like objects*. There are three channels for merging binaries. The first channel consists of Roche limit crossing at the periapsis via eccentricity excitations due to EKL dynamical evolution (depicted in the left column of Fig. 3), which we coin as 'direct mergers'.[6] The second channel consists of 'radial mergers' in wide binaries due to Roche lobe overflow during the post-main-sequence expansion of the more massive binary companions (see middle panels in Fig. 3). The final channel takes place in the post-main-sequence evolution of a tidally locked binary. This type of system has decoupled from the MBH gravitational perturbations and thus the subsequent evolution of the binary can be followed using BSE. We recalculate the evaporation time for this system and allow for stellar evolution to take place. As the more massive star evolves beyond the main sequence, its radius begins to expand and overflow its Roche lobe (see the left-hand panels in Fig. 3). We find, as expected, that most (about 95 per cent) of the tidally locked binaries end up as merged systems after 10 Gyr of evolution, while the remaining unmerged systems have just started expanding in radius as they are close to 1 $M_\odot$ in mass. We coin this merging channel as 'tidal mergers'.

Considering that the last star formation episode in the GC happened about 6 Myr ago, the merged binaries would still be in a morphed extended phase, which may be observable as G2-like objects (Witzel et al. 2014; Sitarski, in preparation). We find that at this time-scale nearly all merged systems would be direct mergers, with only a few radial mergers just occurring from the most massive stars. No tidal mergers would have occurred yet, as can be seen in Fig. 4. As mentioned before, binaries are registered as mergers if they crossed their Roche limit, and even direct mergers probably represent at most grazing encounters and not head-on collisions. The physical merging into a single star will occur after an extended merging process that may last for a few Myr (for circular orbits, as found using BSE). During the merging process, the two stars enter a dusty red phase (e.g. Tylenda et al. 2011a,b, 2013; Nicholls et al. 2013), which may be identified as an IR excess source (e.g. Witzel et al. 2014). Once the two stars have merged into one, the product will readjust to form a stable star of the order of a Kelvin–Helmholtz time-scale. This entire process gives enough time to observe a system that began merging within the last 6 Myr as a G2-like object today.

We postulate that all mergers will, in the short term, appear as G2-like IR excess sources, but after they have settled down the newly formed stars will look rejuvenated, younger than the other stars in their population, due to their now enlarged mass and previous slower

[6] This channel was noted already by Antonini et al. (2010), Antonini & Perets (2012) and Prodan et al. (2015), although their abundance of occurrences was smaller due to a larger abundance of twin stars.

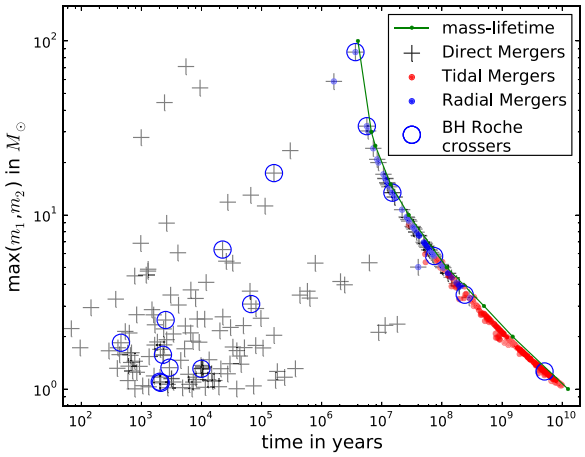

Figure 4. Time of mergers compared to main-sequence lifetimes. Plotted are the times that any particular merger happened versus the masses of the larger companion in the binary. The main-sequence lifetime for the range of 1–100 $M_\odot$ is plotted in green, which allows us to compare if a merger happened mostly due to EKL-induced large eccentricities or rather due to radial expansion of the more massive companion at the end of its main-sequence lifetime. Black crosses stand for mergers that were directly registered by our simulation, while red dots stand for those registered tidally locked systems that we expect to merge once inflation begins, based on the binaries' separation at tidal locking and expected radial size during inflation. Blue dots represent mergers of not tidally locked systems that were caused by the radial expansion of one of the binary companions due to stellar evolution. Blue circles indicate binaries registered as mergers that have crossed the MBH Roche limit during their evolution.

main-sequence evolution speed. If a star formation burst indeed took place about 6 Myr ago, then we expect that the G2-like objects are direct mergers still going through the merging process. However, our results also suggest a possible connection between the young stellar population and the merger products. The young stellar population in the GC consists of fairly massive stars and could be a sample of settled down mergers (e.g. Ghez et al. 2003). Specifically, the S-stars may be consistent with the late mergers in our simulations, which would indicate that a star formation period took place significantly earlier than 6 Myr ago, as these binary mergers would have needed time to settle down to their current state. Of course, it is possible that several star formation episodes have occurred, which would then allow G2-like objects to be formed from recent episodes, while older episode mergers would appear rejuvenated today. We find that after 10 Gyr of evolution the direct mergers constitute about 35 per cent of total merged population, while the radial mergers make up about 10 per cent and the tidal mergers about 55 per cent.

As an overview, merging binaries will either undergo direct mergers or mergers due to stellar evolution (either radial mergers or tidal mergers). This is depicted in Fig. 4, where the stellar evolution-induced mergers are mostly located close to the end of the stellar mass lifetime.

(iii) *Evaporated binaries*. Binary systems that never merged or tidally locked are assumed to evaporate after their evaporation time is reached and the simulation is halted. Stars that tidally locked, but did not evolve and merge before the end of their newly calculated evaporation time, are likewise assumed to evaporate. Furthermore, systems that, at any point in their evolution, crossed the MBH Roche limit due to changes of the inner binary eccentricity e_1 (see equation 2) are assumed to evaporate as well. Binaries that cross the MBH Roche limit will generally become unbound, while those in the double loss cone have a high chance of merging, as shown by Mandel & Levin (2015, the double loss cone is defined as the set of orbits around the MBH for which a binary is supposed to become unbound, while the individual binary companions are also supposed to be tidally disrupted). We have 104 of all 1570 calculated systems, among them 18 merging systems, that cross the single loss cone during their evolution. We therefore assume that those 18 systems evaporate instead of merge. This reduces the total number of merged system only insignificantly, of the order of 4 per cent of total mergers, or ∼1 per cent of all systems. None of our systems cross the double loss cone, since our initial conditions already rejected all systems that would bring the binary so close to the MBH. The systems also cannot evolve to cross the double loss cone later, since a_2 does not change.

As depicted in Fig. 5, the fraction of binary stars declines over time both due to merging and evaporating. Lu et al. (2013) found that the last star formation episode in the inner parts of the GC took place a few Myr ago (adopted here as 6 Myr ago). Considering this time-scale, about 70 per cent of the initial binary fraction is still expected to be present at the GC. Furthermore, we expect that about 13 per cent of the initial binary population has merged, and thus may be detectable as G2-like objects. Therefore, we refer below to all merged products after 6 Myr as G2-like candidates.

Interestingly, the different tidal assumptions are indistinguishable at the 6 Myr mark. Prior to that, the direct merger channel is the only operating channel. The efficiency of this channel is then reduced (see also Fig. 4), and the merger rate stalls. This leads to an apparent plateau in the fraction of mergers at this time-scale. A few tens of Myr later, the massive stars start to leave the main sequence and inflate in size. Thus, the merger rate increases again by allowing radial mergers to occur. As the tidal evolution equations are highly sensitive to the stellar radius (e.g. Naoz 2016), the more efficient tides tend to produce slightly more merged systems over long times by forming more tidally locked and circularized systems and enabling the tidal merger channel.

The binary population of the earliest star formation episode roughly 10 Gyr ago has been completely depleted and the binaries have either evaporated or have merged as depicted in Fig. 5. The binary merger rate at late times is dominated by the main-sequence lifetime of the more massive binary companion in the tidally locked binaries. Since these binaries are hard, we assumed a survival time of 10 Gyr, consistent with the estimated ionization rate (see Appendix A). After this time, basically all of the hard binaries have merged and all remaining soft binaries have evaporated, which leads to the second plateau in the merger rate. About 29 per cent of the initial binary population has merged after 10 Gyr. Thus, we expect that the old stars will harbour little to no binary systems. However, we expect that a significant fraction of this population will be the result of merged systems and may seem younger in comparison. A similar argument was raised for the blue straggler population (Perets & Fabrycky 2009; Naoz & Fabrycky 2014).

As expected from the EKL mechanism, merged binaries are preferentially found in systems with large mutual inclination (however, a large range is allowed), and with a stronger octupole contribution (estimated as ϵ), as seen in Fig. 6. The left-hand panel shows the distribution of all systems and the merged systems in inclination–epsilon space, while the right-hand panel shows the Gaussian kernel density estimate (KDE) of the merger distribution. The KDE can be understood as a smoothed 2D density distribution (a smoothed histogram of mergers per area in the plot's space), assuming an

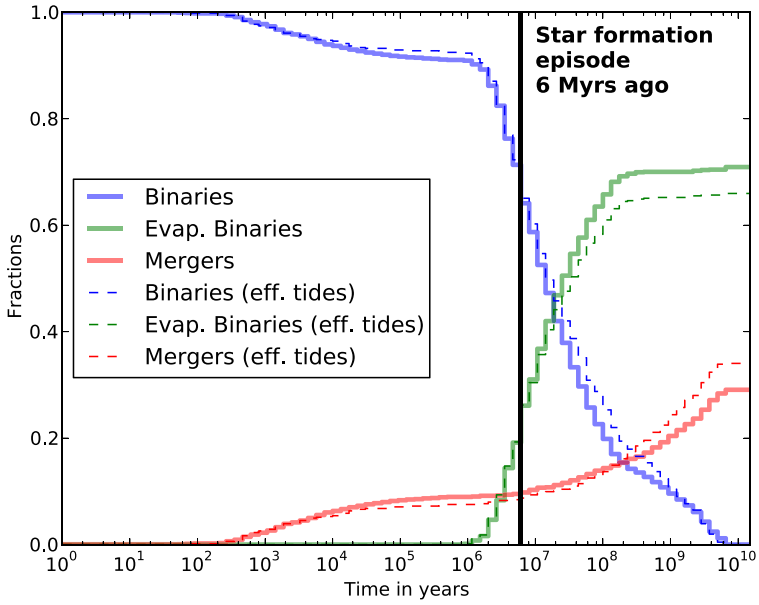

Figure 5. Binary, evaporated and merger fractions over time. Plotted are the fractions of binaries, evaporated binaries and merged binaries as a function of time. The solid, coloured lines show the results for the (normal) inefficient tide model, while the dashed lines show the results for the efficient tide model. Note that the only significant difference between those two models is in the long-term expected total fraction of mergers due to the larger probability for the formation of tidally locked systems. In the short to medium term, the results are virtually identical. The black vertical line marks the age of the young stellar population in the GC, determined to be 6 Myr by Lu et al. (2013). Note that the distributions of binaries and evaporated binaries of the two models begin to diverge only for stellar populations older than that, with fewer evaporated binaries in the efficient tide case. Thus, the tidal model is not of dominant importance in order to predict the fractions of mergers and binaries for the young stellar population. The different tidal strengths are mostly just influencing the formation of tidally locked systems, which can become merger products at later times.

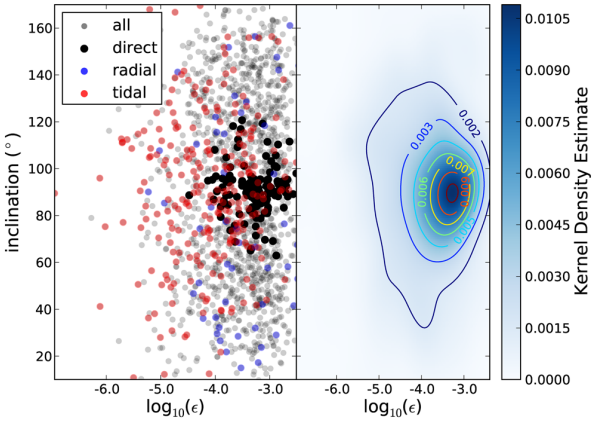

Figure 6. Merger distribution and Gaussian kernel density estimate (KDE) of the mergers as a function of inclination and epsilon. Plotted in the left-hand panel is the distribution of all systems (in grey) versus the distribution of mergers (direct in black, radial in blue, tidal in red), and plotted in the right-hand panel is the Gaussian KDE, or the smoothed density of all mergers in inclination–epsilon space, assuming an intrinsic Gaussian distribution. The colour bar shows the density, while the contours enclose certain density levels (see labels). While we do not expect the intrinsic distribution of mergers to be truly Gaussian, the KDE helps to highlight the strong concentration of mergers towards 90° inclination and high epsilon values due to direct mergers [for the definition of epsilon, see equation (1)].

underlying Gaussian distribution. It highlights the strong concentration of mergers at high epsilon values and towards 90° inclination.

We note that the binary inclination with respect to the MBH is sensitive to the VRR time-scale, which will alter the outer orbit angular momentum orientation. This cannot really decrease our merger rate as the direct mergers take place on much shorter time-scales than the VRR effects. Furthermore, tidally locked systems are decoupled from the tertiary and are thus insensitive to the outer orbit orientation. Finally, the radial mergers may be marginally effected; however, VRR will refill the EKL high inclination parameter space and can thus re-trigger eccentricity excitations.

The binary orbital configuration around the MBH (referred to here as the outer orbit) sets limits to the different outcomes of the inner orbit, and thus a promising observable is the outer orbit's period distribution. As shown in Fig. 6, the merger outcome is very sensitive to ϵ and thus to the eccentricity and the outer orbit separation a_2. We note that the outer orbit separation from the MBH, a_2, does not change during the evolution, as a consequence of the secular approximation. The outer orbit eccentricity does not change because the outer orbit carries most of the angular momentum in the system, and thus the changes on to e_2 are insignificant compared to the angular momentum variation of the inner orbit. The e_2 distribution of all merged systems is shown in Fig. 7. G2-like candidates, i.e. those binaries that merged in the last 6 Myr, are preferentially on eccentric orbits, with a long tail down to $e_2 \sim 0.1$. As time goes by, stellar evolution merger products become an important component of the overall merger population and allow for smaller values in the e_2 distribution. However, highly eccentric outer orbits are

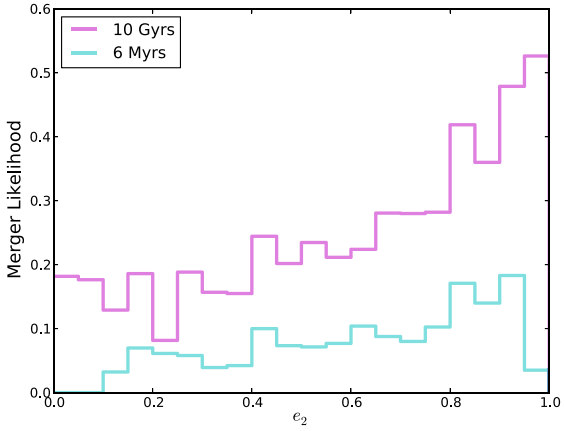

Figure 7. Merger likelihood as a function of eccentricity. Plotted are the fractions of merged systems as a function of the initial binary's orbital eccentricity around the MBH, shown after 6 Myr (cyan curve) and 10 Gyr (magenta curve). Note that the curves are normalized with the initial e_2 distribution after rejection (see Fig. 2), thus showing the merger fraction for a flat e_2 distribution. Both curves show a clear preference for higher eccentricities for mergers to form, which makes intuitively sense since larger eccentricities around the MBH induce stronger EKL interactions. At late times, however, low eccentricities can also yield a significant merger fraction. This can be explained with tidal effects and the evaporation time. These low-eccentricity systems had a higher long-term stability against evaporation and their weaker EKL oscillations allowed the systems to become tidally captured instead of directly merging.

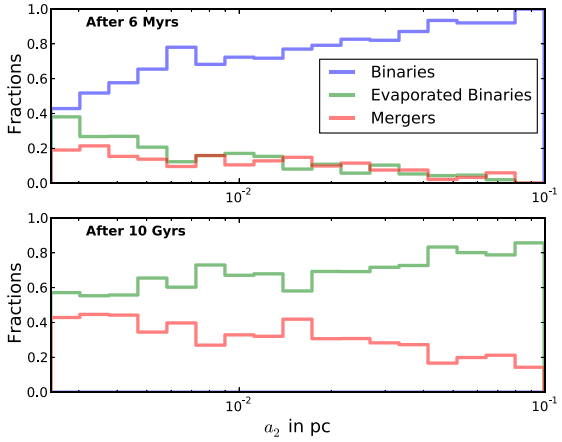

Figure 8. Binary, evaporated and merger fractions versus a_2. Plotted are the fraction of binaries, evaporated binaries and merged binaries as a function of a_2, the semi-major axis of the binary's orbit around the MBH. Shown are the distributions at two timesteps, 6 Myr (upper panel) and 10 Gyr (lower panel). Note that the distributions of mergers and evaporated binaries show a preference for smaller a_2 after 6 Myr and a lack of mergers at the largest a_2 values, but this preference is strongly reduced after 10 Gyr. This makes intuitively sense since the binaries with smaller a_2 values will undergo stronger EKL evolution; thus, they will merge faster and tidally lock faster, while they are also more likely to be evaporated due to a higher likelihood of scattering events. Binaries further away live longer, undergo weaker EKL oscillations and have more time to become tidally locked, which increases the merger fraction at large a_2 values once the binary leaves the main sequence. After 10 Gyr, all stars in our sample have been either evaporated or have undergone post-main-sequence stellar evolution, so there will be no binaries of the original population left after this time.

still preferred for forming mergers. This is due to the stronger EKL oscillations for eccentric outer orbits that enhance the formation of tidally locked systems.

Another potential observable is the separation of merger products and binaries from the MBH. Again, we expect a strong transition between the two time-scales considered throughout the paper. As can be seen in the top panel of Fig. 8, G2-like candidates have a long tail distribution with a preference to close separations. After 10 Gyr, the population of merger products is more uniformly distributed as a function of a_2, with a continued slight preference for smaller a_2 values (bottom panel).

Finally, we consider the validity of our secular approach in light of the extremely dense nature of the GC. The double averaging method applied here will break when the value of the inner orbit angular momentum goes to zero (i.e. extreme inner orbit eccentricity) on shorter time-scale than the inner orbital period (e.g. Ivanov, Polnarev & Saha 2005; Katz & Dong 2012; Antognini et al. 2014; Antonini, Murray & Mikkola 2014; Bode & Wegg 2014; Luo, Katz & Dong 2016). To test the validity of our method, we use the criterion described by Katz & Dong (2012) and Antonini et al. (2014, for the inner orbit), i.e.

$$\sqrt{1-e_1} \lesssim \frac{15/2}{\sqrt{2}}\pi\frac{m_{\rm MBH}}{m_{\rm binary}}\left[\frac{a_1}{a_2(1-e_2)}\right]^3. \quad (6)$$

If this criterion is fulfilled, the secular approach will underestimate the strength of the dynamical evolution; however, only about 10 per cent of merged system and 10 per cent of all unmerged systems enter this regime during their EKL evolution. In most cases, the expected consequences of violating the double averaging process, either for the inner or the outer orbit, are higher eccentricity excitations, which may also take place on slightly different time-scales. We conclude that we may be underestimating the rate of direct mergers and therefore also the total fraction of merged systems. The time-scales for these mergers are of the order of a few to tens of quadrupole time-scales, roughly 10^5 yr.

4 DISCUSSION

We have studied the secular evolution of binary stellar systems in the GC while considering the octupole level of approximation for the hierarchical three-body problem. We include GR, tidal effects and post-main-sequence stellar evolution. The latter includes mass-loss, inflation of stellar radii and magnetic braking for both stars. We predict a population of merged products that should exist in the GC.

We identify three distinct formation channels for merged systems. As a system evolves, the EKL mechanism can cause large-eccentricity excitations for the inner orbit. If the eccentricity excitation happens on a relatively short time-scale compared to the short-range forces such as tides or GR, the binary members may cross each other's Roche limits (see the left-hand panels of Fig. 3); we refer to this channel as direct mergers. On the other hand, during close pericentre passages when tides are important, the orbital energy is dissipated and the orbit circularizes while the separation shrinks. In this case, as the radius of the more massive star starts to expand as it exits the main sequence, it overflows its Roche lobe and the system merges (see the right-hand panels of Fig. 3). We refer to this channel as tidal mergers. Even binaries that neither undergo strong eccentricity excitations nor become tidally locked can become mergers due to radial expansion of the more massive binary member, if the periapsis distance is smaller than the

expanded star's new Roche limit (see the central panels of Fig. 3). We refer to this channel as radial mergers.

Direct mergers happen only early in the systems' evolution, up to the first few Myr after formation.[7] After roughly 6 Myr of evolution, 13 per cent of all our binaries will have merged as direct mergers (see Figs 4 and 5). The merger rate then stalls and the evolution of the remaining binaries can continue on one of three possible routes: (1) they can either evaporate without any further interesting interactions; (2) they can continue to undergo small-amplitude eccentricity and inclination oscillations for a significant amount of time; or (3) they can undergo strong tidal interactions which circularize and shrink their inner orbits. After a few Myr, as the massive stars start to expand in radius due post-main-sequence evolution, the merger rate begins to increase again as the surviving binaries become radial or tidal mergers. The total number of mergers increases over the next few Gyr until the fraction of available binaries goes to zero due to evaporation and mergers (see the plateau in Fig. 5 for times $>10^9$ yr). At this stage, the total merger fraction is around 29 per cent, 35 per cent of which are direct mergers from the first few Myr of evolution, 10 per cent of which are radial and 55 per cent are tidal mergers.

However, for these merger fractions, we assumed a minimum survival time of 10 Gyr for hard binaries, which gave many tidally locked binaries time to evolve past the main sequence and allowed them to merge during expansion. If we instead ignore the formation of hard binaries and continue to treat their evaporation time as we have for soft binaries, the total merger fraction is reduced to approximately 18 per cent since most tidally locked binaries would evaporate before they expand. See Appendix A for a justification of using the longer survival time, which yields more mergers.

If a star formation episode took place about 6 Myr ago, we suggest that the direct merger population are G2-like candidates. As the overall evolution of these merged products is still unclear, we can only speculate, based on observations of dusty binary mergers (e.g. Tylenda et al. 2011a,b, 2013; Nicholls et al. 2013) and the current state of common-envelope evolution theory (see for review Ivanova et al. 2013), that they will harbour extended gas and dust envelopes, which match G2 observations. Radial mergers would occur after $\sim$10 Myr until $\sim$200 Myr after star formation as the most massive stars begin to evolve past the main sequence and expand radially. This does not work for lower mass star binaries as these will evaporate before stellar evolution can occur. However, mergers can occur for smaller mass stars whose orbits have been tidally shrunken and circularized, extending their lifetime against evaporation. These tidal mergers begin to occur after a few tens of Myr until a few Gyr after star formation. There is considerable overlap in the occurrence times for radial and tidal mergers around the 100 Myr time mark, due to competing time-scales for the onset of stellar evolution and tidal circularization of the inner orbit for stellar masses between 3 and 10 $M_\odot$. Assuming that the earliest star formation episode occurred 10 Gyr ago, all of these old stellar binaries will have evaporated or merged by now. These merger products would have had time to cool down and relax and may look like young stars compared to the surrounding stars (e.g. Antonini et al. 2011, similar arguments were done for blue stragglers by Perets & Fabrycky 2009; Naoz & Fabrycky 2014).

Thus, we distinguish between the early merger population and the late population. These populations also show somewhat different orbital element distribution (see Figs 7 and 8). Early, direct mergers show a slight preference for small separations and high orbital eccentricities around the MBH, which is less profound for late (radial and tidal) mergers. This is consistent with the EKL mechanism for which closer eccentric binary orbit around the MBH may result in larger eccentricity excitations. However, for radial and tidal mergers, the dominating factor is the survival time of a system against evaporation, which is longer for larger semi-major axis values and smaller eccentricities.

We also find that the efficiency of tides has a negligible effect on the results. This is because the direct mergers are independent of the tides, and the radial and tidal mergers are more sensitive to the post-main-sequence radial expansion.

We conclude that there is a possible connection between the binary mergers described in this work and the formation of millisecond pulsars (MSPs). Macquart & Kanekar (2015) have recently pointed out that the GC could harbour a relative overabundance of MSPs, although they argued that this would be due to the dense nature of the GC stellar environment. Binary mergers, however, could naturally produce such rapidly spinning pulsars due to the need of conserving the binaries' orbital angular momentum.

We note that we do not speculate here on how the binaries arrived at their separations from the MBH. Instead, we pose a simpler question of what will be the resulting dynamical evolution of a binary at a given distance from the MBH. It is unclear if these binaries could have formed there as the gravitational and tidal forces should prevent the formation of stars so close to the MBH (see, for example, Allen & Sanders 1986; Morris 1993; Ghez et al. 2003; Alexander 2005; Genzel, Eisenhauer & Gillessen 2010). However, Levin & Beloborodov (2003) have claimed that *in situ* star formation close to the MBH would be possible in a dense gaseous disc (see Amaro-Seoane & Chen 2014; Chen & Amaro-Seoane 2014, for similar ideas). That disc could have existed around the MBH in the past, formed either through gradual accumulation of infalling gas or tidal disruption of an infalling molecular cloud. However, it has been suggested that the presence of such a gaseous disc could lead to efficient merging of binaries, see Bartos et al. (2016). If the binaries arrived at their location via two-body relaxation processes (see Antonini & Perets 2012), then the precession due to this process should also be taken into account.

The merger products formed through these mechanisms can undergo very interesting and potentially wildly differing further evolution. The direct merger scenario can lead to very violent mergers through collisions or grazing of the stars' outer envelope. Radial mergers will lead to Roche lobe overflow with a comparatively wide, moderately eccentric stellar orbit, while tidal mergers will lead to common-envelope evolution of circularly and tightly orbiting stars. All these mechanisms will lead to highly complex and interesting mass-transfer and post-main-sequence evolutions. Regardless of the details of the processes mentioned above, these merger products represent a new and interesting class of objects that should be present in the GC.

[7] Note that VRR is neglected in this calculation since direct mergers take place before VRR can have an effect. Furthermore, VRR acts to refill the high inclination parameter space that can lead to strong EKL evolution. By ignoring VRR effects, we are effectively underestimating the direct merger rate, which makes our results a conservative estimate.

ACKNOWLEDGEMENTS

APS and SN acknowledge the partial support from the Sloan foundation. We thank Avi Loeb for insightful discussions and we also thank Melvyn Davis, Tal Alexander and Fabio Antonini for useful

discussions that took place during the 2016 Aspen winter conference on Dynamics and Accretion at the Galactic Center. SN and APS thank Tassos Fragos and Aaron Geller for assistance in the initial stages of code development. We thank the reviewer, Joseph Antognini, for his helpful comments and suggestions for improving this paper. This work was supported in part by the National Science Foundation through grant AST-1412615 (awarded to AMG), as well as by the European Research Council under the European Union's Horizon 2020 Programme, ERC-2014-STG grant GalNUC 638435 (awarded to BK).

REFERENCES

Alexander T., 2005, Phys. Rep., 419, 65
Alexander T., Hopman C., 2009, ApJ, 697, 1861
Alexander T., Pfuhl O., 2014, ApJ, 780, 148
Allen D. A., Sanders R. H., 1986, Nature, 319, 191
Amaro-Seoane P., Chen X., 2014, ApJ, 781, L18
Antognini J. M., Shappee B. J., Thompson T. A., Amaro-Seoane P., 2014, MNRAS, 439, 1079
Antonini F., Merritt D., 2013, ApJ, 763, L10
Antonini F., Perets H. B., 2012, ApJ, 757, 27
Antonini F., Faber J., Gualandris A., Merritt D., 2010, ApJ, 713, 90
Antonini F., Lombardi J. C., Jr, Merritt D., 2011, ApJ, 731, 128
Antonini F., Murray N., Mikkola S., 2014, ApJ, 781, 45
Bahcall J. N., Wolf R. A., 1977, ApJ, 216, 883
Bartos I., Kocsis B., Haiman Z., Márka S., 2016, preprint (arXiv:1602.03831)
Binney J., Tremaine S., 1987, Galactic Dynamics. Princeton Univ. Press, Princeton, NJ
Bode J. N., Wegg C., 2014, MNRAS, 438, 573
Burkert A., Schartmann M., Alig C., Gillessen S., Genzel R., Fritz T. K., Eisenhauer F., 2012, ApJ, 750, 58
Chen X., Amaro-Seoane P., 2014, ApJ, 786, L14
Duquennoy A., Mayor M., 1991, A&A, 248, 485
Eggleton P. P., 1983, ApJ, 268, 368
Eggleton P. P., Kiseleva L. G., Hut P., 1998, ApJ, 499, 853
Fabrycky D. C., Johnson E. T., Goodman J., 2007, ApJ, 665, 754
Genzel R., Eisenhauer F., Gillessen S., 2010, Rev. Mod. Phys., 82, 3121
Ghez A. M., Becklin E., Duchjne G., Hornstein S., Morris M., Salim S., Tanner A., 2003, Astron. Nachr. Suppl., 324, 527
Ghez A. M., Salim S., Hornstein S. D., Tanner A., Lu J. R., Morris M., Becklin E. E., Duchêne G., 2005, ApJ, 620, 744
Gillessen S., Eisenhauer F., Trippe S., Alexander T., Genzel R., Martins F., Ott T., 2009, ApJ, 692, 1075
Gillessen S. et al., 2012, Nature, 481, 51
Ginsburg I., Loeb A., 2007, MNRAS, 376, 492
Guillochon J., Loeb A., MacLeod M., Ramirez-Ruiz E., 2014, ApJ, 786, L12
Hansen B. M. S., 2010, ApJ, 723, 285
Heggie D. C., 1975, MNRAS, 173, 729
Heggie D. C., Hut P., McMillan S. L. W., 1996, ApJ, 467, 359
Hills J. G., 1988, Nature, 331, 687
Hopman C., 2009, ApJ, 700, 1933
Hopman C., Alexander T., 2006, ApJ, 645, 1152
Hurley J. R., Pols O. R., Tout C. A., 2000, MNRAS, 315, 543
Hurley J. R., Tout C. A., Pols O. R., 2002, MNRAS, 329, 897
Hut P., 1980, A&A, 92, 167
Hut P., 1983, ApJ, 272, L29
Hut P., Bahcall J. N., 1983, ApJ, 268, 319
Ivanov P. B., Polnarev A. G., Saha P., 2005, MNRAS, 358, 1361
Ivanova N. et al., 2013, A&AR, 21, 59
Jeans J. H., 1919, MNRAS, 79, 408
Katz B., Dong S., 2012, preprint (arXiv:1211.4584)
Kobulnicky H. A., Fryer C. L., 2007, ApJ, 670, 747
Kocsis B., Tremaine S., 2011, MNRAS, 412, 187
Kocsis B., Tremaine S., 2015, MNRAS, 448, 3265
Levin Y., Beloborodov A. M., 2003, ApJ, 590, L33
Li G., Naoz S., Kocsis B., Loeb A., 2014a, ApJ, 785, 116
Li G., Naoz S., Holman M., Loeb A., 2014b, ApJ, 791, 86
Lu J. R., Do T., Ghez A. M., Morris M. R., Yelda S., Matthews K., 2013, ApJ, 764, 155
Lucy L. B., 2006, A&A, 457, 629
Luo L., Katz B., Dong S., 2016, MNRAS, 458, 3060
Macquart J.-P., Kanekar N., 2015, ApJ, 805, 172
Mandel I., Levin Y., 2015, ApJ, 805, L4
Mardling R. A., Aarseth S. J., 2001, MNRAS, 321, 398
Martins F. et al., 2006, ApJ, 649, L103
Meyer L. et al., 2014, in Sjouwerman L. O., Lang C. C., Ott J., eds, Proc. IAU Symp. 303, The Galactic Center: Feeding and Feedback in a Normal Galactic Nucleus. Cambridge Univ. Press, Cambridge, p. 264
Michaely E., Perets H. B., 2014, ApJ, 794, 122
Miralda-Escudé J., 2012, EPJ Web Conf., 39, 03003
Morris M., 1993, ApJ, 408, 496
Morris M. R., Meyer L., Ghez A. M., 2012, Res. Astron. Astrophys., 12, 995
Muno M. P., Lu J. R., Baganoff F. K., Brandt W. N., Garmire G. P., Ghez A. M., Hornstein S. D., Morris M. R., 2005, ApJ, 633, 228
Murray-Clay R. A., Loeb A., 2012, Nat. Commun., 3, 1049
Naoz S., 2016, preprint (arXiv:1601.07175)
Naoz S., Fabrycky D. C., 2014, ApJ, 793, 137
Naoz S., Farr W. M., Lithwick Y., Rasio F. A., Teyssandier J., 2013a, MNRAS, 431, 2155
Naoz S., Kocsis B., Loeb A., Yunes N., 2013b, ApJ, 773, 187
Naoz S., Fragos T., Geller A., Stephan A. P., Rasio F. A., 2016, ApJ, 822, L24
Nicholls C. P. et al., 2013, MNRAS, 431, L33
O'Leary R. M., Kocsis B., Loeb A., 2009, MNRAS, 395, 2127
Ott T., Eckart A., Genzel R., 1999, in Falcke H., Cotera A., Duschl W. J., Melia F., Rieke M. J., eds, ASP Conf. Ser. Vol. 186, The Central Parsecs of the Galaxy. Astron. Soc. Pac., San Francisco, p. 310
Perets H. B., 2009, ApJ, 698, 1330
Perets H. B., Fabrycky D. C., 2009, ApJ, 697, 1048
Perets H. B., Gualandris A., Kupi G., Merritt D., Alexander T., 2009, ApJ, 702, 884
Pfuhl O., Alexander T., Gillessen S., Martins F., Genzel R., Eisenhauer F., Fritz T. K., Ott T., 2014, ApJ, 782, 101
Phifer K. et al., 2013, ApJ, 773, L13
Pinsonneault M. H., Stanek K. Z., 2006, ApJ, 639, L67
Prodan S., Antonini F., Perets H. B., 2015, ApJ, 799, 118
Rafelski M., Ghez A. M., Hornstein S. D., Lu J. R., Morris M., 2007, ApJ, 659, 1241
Raghavan D. et al., 2010, ApJS, 190, 1
Sana H. et al., 2012, Science, 337, 444
Shappee B. J., Thompson T. A., 2013, ApJ, 766, 64
Teyssandier J., Naoz S., Lizarraga I., Rasio F. A., 2013, ApJ, 779, 166
Tylenda R. et al., 2011a, A&A, 528, A114
Tylenda R., Kamiński T., Schmidt M., Kurtev R., Tomov T., 2011b, A&A, 532, A138
Tylenda R. et al., 2013, A&A, 555, A16
Valencia-S. M. et al., 2015, ApJ, 800, 125
Witzel G. et al., 2014, ApJ, 796, L8
Yu Q., Tremaine S., 2003, ApJ, 599, 1129

APPENDIX A: BINARY EVAPORATION TIME-SCALE

We closely follow the work done by Binney & Tremaine (1987) for the evaporation time-scales of binaries at the GC, but allow different masses for the binary companions and interacting stars.

The dynamical behaviour of binaries in stellar groups and clusters can be generalized into two separate cases, i.e. soft and hard binaries. Given a binary with average orbital energy

$$\widetilde{E} = -\frac{Gm_1m_2}{2a_1} \tag{A1}$$

that travels through a cluster with velocity dispersion σ, the binary is soft if the energy of its centre-of-mass motion relative to the cluster is larger than $\widetilde{E}$, i.e.

$$\frac{2|\widetilde{E}|}{(m_1+m_2)\sigma^2} < 1. \tag{A2}$$

In general, soft binaries become softer through their interactions with other cluster stars until they evaporate, while hard binaries become harder until they merge or other forces become dominant (see, for example, Heggie 1975; Hut 1983; Hut & Bahcall 1983; Heggie et al. 1996). But, as has been pointed out by Hopman (2009), it is not obvious that this general rule holds true close to an MBH due to the more violent nature of the environment and the tidal influence of the MBH. However, binaries in the GC need to have extremely small inner orbital separations to qualify as hard binaries, of the order of $\sim$0.1 AU or less. At these separations, the stars will feel tidal forces from their binary companions which can help to stabilize the systems against external influences.

The softness condition is usually strongly satisfied by the GC. Assuming a velocity dispersion of $\sigma = 280\,\mathrm{km\,s^{-1}}\sqrt{0.1\,\mathrm{pc}/a_2}$ (Kocsis & Tremaine 2011), the ratio of the energies is small for nearly all systems under consideration (smaller than $\sim$0.2 even for two 100 $M_\odot$ binary companions on an $a_1 \sim 1$ AU orbit with an MBH semi-major axis of $a_2 \sim 0.1$ pc, assuming an average cluster star mass of 1 $M_\odot$). This means that the GC binaries will become wider over time through encounters with other stars in the cluster.

The widening or 'softening' of soft binaries works through close encounters of field or cluster stars with one of the binary companions. Since the velocity dispersion is high compared to the orbital velocity of the binary companions, such an encounter will have a much stronger influence on the companion closer to the passing third star than on the farther companion. The change of internal energy can be written as

$$\Delta\widetilde{E} = \frac{1}{2}\mu\Delta(V^2) = \mu(\Delta\boldsymbol{v}_1(\boldsymbol{v}_1 - \boldsymbol{v}_2) + \frac{1}{2}(\Delta\boldsymbol{v}_1)^2) \tag{A3}$$

with $\mu = \frac{m_1m_2}{m_1+m_2}$ and the $\boldsymbol{v}$ vectors describing the velocities of the binary companions. Following the derivation of Binney & Tremaine (1987), but allowing for different binary companion masses m_1 and m_2 and cluster star masses m_3, we derive an energy diffusion rate of

$$\langle D(\Delta\widetilde{E})\rangle = 16\sqrt{\frac{\pi}{3}}\frac{G^2\rho\ln\Lambda}{\sigma}\frac{m_1m_2m_3}{m_1+m_2} \tag{A4}$$

with a stellar mass density in the cluster of $\rho = 1.35 \times 10^6\,M_\odot\,\mathrm{pc}^{-3}(a_2/0.25\tilde{}\mathrm{pc})^{-1.3}$ (see Genzel et al. 2010), and $\ln\Lambda$ being the Coulomb logarithm with $\Lambda = 15$.

Combining equations (A1) and (A4), we can now find the expected lifetime of soft binaries in the GC, their *evaporation time*:

$$t_{\mathrm{EV}} = \frac{\sqrt{3}\sigma}{32\sqrt{\pi}G\rho a_1\ln\Lambda}\frac{m_1+m_2}{m_3}. \tag{A5}$$

This solution is equivalent to the result in Binney & Tremaine (1987) except for the last factor that includes the masses of the binary companions (m_1 and m_2) and of the average cluster star (m_3, assumed to be $\sim$1 $M_\odot$; see also Hopman 2009). This result immediately shows that massive binaries have a longer expected lifetime than binaries that are assumed to be comparable to the cluster stars. Considering the stellar IMF referred to in Section 2, the lifetime could therefore be longer by up to two orders of magnitude, a significant difference for our simulations as this allows stellar evolution to become relevant. Furthermore, reducing a_1 through tidal interactions will also increase the evaporation time, giving tidally evolved and locked systems more time to reach post-main-sequence evolution.

While the conditions of the GC strongly favour binaries to be soft, we do observe that some binaries can become hard over time due to tidal energy dissipation and shrinking of their inner orbits. If the radial separation becomes so small that a binary qualifies as a hard binary, we generally assume that the binary survives for at least 10 Gyr. As pointed out above, hard binaries will in general become harder through encounters with other stars, not softer. However, they can be ionized by single strong encounters, with an ionization probability per unit time of

$$B(\widetilde{E}) = \frac{8\sqrt{\pi}G^2m^3\rho\sigma}{3^{3/2}|\widetilde{E}|^2}\left(1+\frac{m\sigma^2}{5|\widetilde{E}|}\right)^{-1}\left[1+\exp\left(\frac{|\widetilde{E}|}{m\sigma^2}\right)\right]^{-1}. \tag{A6}$$

Equation (A6) is taken from Binney & Tremaine (1987) for an example of a binary with equal masses encountering another equal-mass star. This probability becomes very small (of the order of $\sim 10^{-10}$ per year or smaller) for the hard binaries in our sample, thus justifying our choice of a 10 Gyr survival time.

This paper has been typeset from a TEX/LATEX file prepared by the author.

The Astrophysical Journal, 878:58 (7pp), 2019 June 10 https://doi.org/10.3847/1538-4357/ab1e4d
© 2019. The American Astronomical Society. All rights reserved.

The Fate of Binaries in the Galactic Center: The Mundane and the Exotic

Alexander P. Stephan[1,2], Smadar Naoz[1,2], Andrea M. Ghez[1], Mark R. Morris[1], Anna Ciurlo[1], Tuan Do[1], Katelyn Breivik[3], Scott Coughlin[4,5], and Carl L. Rodriguez[6,7]
[1] Department of Physics and Astronomy, University of California, Los Angeles, Los Angeles, CA 90095, USA; alexpstephan@astro.ucla.edu
[2] Mani L. Bhaumik Institute for Theoretical Physics, University of California, Los Angeles, Los Angeles, CA 90095, USA
[3] Canadian Institute for Theoretical Astrophysics, University of Toronto, 60 St. George Street, ON M5S 3H8, Canada
[4] Physics and Astronomy, Cardiff University, Cardiff, CF10 2FH, UK
[5] Center for Interdisciplinary Exploration & Research in Astrophysics (CIERA), Northwestern University, Evanston, IL 60208, USA
[6] MIT-Kavli Institute for Astrophysics and Space Research, 77 Massachusetts Avenue, 37-664H, Cambridge, MA 02139, USA
Received 2019 February 28; revised 2019 April 17; accepted 2019 April 29; published 2019 June 13

Abstract

The Galactic center is dominated by the gravity of a super-massive black hole (SMBH), Sagittarius A*, and is suspected to contain a sizable population of binary stars. Such binaries form hierarchical triples with the SMBH, undergoing Eccentric Kozai–Lidov (EKL) evolution, which can lead to high-eccentricity excitations for the binary companions' mutual orbit. This effect can lead to stellar collisions or Roche-lobe crossings, as well as orbital shrinking due to tidal dissipation. In this work we investigate the dynamical and stellar evolution of such binary systems, especially with regards to the binaries' post-main-sequence evolution. We find that the majority of binaries (∼75%) is eventually separated into single stars, while the remaining binaries (∼25%) undergo phases of common-envelope evolution and/or stellar mergers. These objects can produce a number of different exotic outcomes, including rejuvenated stars, G2-like infrared-excess objects, stripped giant stars, Type Ia supernovae (SNe), cataclysmic variables, symbiotic binaries, or compact object binaries. We estimate that, within a sphere of 250 Mpc radius, about 7.5–15 SNe Ia per year should occur in galactic nuclei due to this mechanism, potentially detectable by the Zwicky Transient Facility and ASAS-SN. Likewise, we estimate that, within a sphere of 1 Gpc^3 volume, about 10–20 compact object binaries form per year that could become gravitational wave sources. Based on results of EKL-driven compact object binary mergers in galactic nuclei by Hoang et al., this compact object binary formation rate translates to about 15–30 events per year that are detectable by Advanced LIGO.

Key words: binaries: general – Galaxy: center – novae, cataclysmic variables – stars: black holes – stars: evolution – stars: kinematics and dynamics

1. Introduction

The Galactic center (GC) contains the closest known super-massive black hole (SMBH), Sagittarius A*, which dominates the gravitational dynamics of its environment due to its large mass of about $4 \times 10^6\,M_\odot$ (e.g., Ghez et al. 2005; Gillessen et al. 2009). Thus, the environment of the GC has served as a "laboratory" to test the nature of gravity, stellar cluster dynamics, and general relativity (GR) over the last decades (e.g., Ghez et al. 2003, 2005; Alexander 2005; Hopman & Alexander 2006; Gillessen et al. 2009, 2012; Hopman 2009; Alexander & Pfuhl 2014; Hees et al. 2017; Chu et al. 2018). The gravitational influence of the SMBH is suspected to cause a number of interesting astrophysical phenomena, such as hypervelocity stars (e.g., Ginsburg & Loeb 2007) and stellar binary mergers (e.g., Antonini et al. 2010, 2011; Prodan et al. 2015; Stephan et al. 2016). Furthermore, there appears to be a large number of X-ray sources associated with the GC, sometimes interpreted to indicate a large number of X-ray binaries, stellar-mass black hole–star binary pairs, where the black hole accretes material from its companion, emitting X-ray radiation (e.g., Muno et al. 2005; Cheng et al. 2018; Zhu et al. 2018). Muno et al. (2006, 2009) and Heinke et al. (2008), however, suggested that many of the observed GC X-ray sources are actually cataclysmic variables (CVs), consisting of white dwarf (WD)–main-sequence star binary pairs.

Any binary that orbits the GC's SMBH will feel gravitational perturbations on the binary's orbit by the SMBH. These perturbations can lead to chaotic orbital eccentricity and inclination excitations, the so-called Eccentric Kozai–Lidov (EKL) mechanism (see, for a review, Naoz 2016). This effect can cause binary stars in the GC to merge (e.g., Antonini et al. 2010, 2011; Antonini & Perets 2012; Witzel et al. 2014, 2017; Prodan et al. 2015; Stephan et al. 2016; Fragione 2019), which has been used to explain extended infrared-excess objects such as G2 (e.g., Gillessen et al. 2012). However, the exact nature of these merger-candidate events is not always the same. While some binary stars might just collide or have grazing encounters due to the induced large eccentricities, others might first undergo orbit shrinking and circularization due to tidal dissipation, and might not begin merging until the stars begin to expand due to stellar evolution (Stephan et al. 2016). The shrinking of the orbit can furthermore "harden" the orbit and make it long-term stable against scattering interactions with other stars in the GC (compare also with Trani et al. 2019), allowing the binary companions to remain coupled long enough for the stars to leave the main sequence and become red giants.

In this work, we investigate the possible outcomes of post-main-sequence binary star evolution in the GC, taking into consideration the effects of EKL, tides, GR, and interactions with the GC's stellar cluster. Most of these stars end their regular lives as WDs ($M_{*,\mathrm{ini}} \lesssim 8\,M_\odot$), as these constitute the bulk of the stellar population (e.g., Salpeter 1955), and which could serve as progenitors of Type Ia supernovae (SNe).

[7] Pappalardo Fellow.

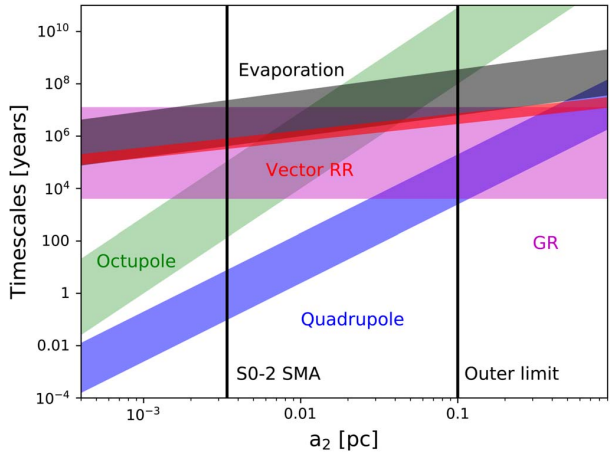

Figure 1. Timescales of physical effects in the GC. The figure shows the timescales for several physical effects acting on binaries in the GC as a function of outer orbital distance from the SMBH, such as GR (magenta), vector resonant relaxation (red), evaporation (dark gray), and the timescales for the quadrupole (blue) and octupole (green) levels of the EKL mechanism. The filled areas show the strengths of these effects for a range of possible binary parameters, ranging in combined binary mass from 2 to 10 $M_\odot$ and in binary semimajor axis from 1 to 10 au. The black lines show the inner and outer limits of semimajor axis (SMA) values around the SMBH used in this work, from ~700 au to 0.1 pc.

Furthermore, we also consider progenitors of stellar-mass black holes and neutron stars.

2. Numerical Setup

In Stephan et al. (2016), we executed a large Monte Carlo simulation of binary stars in the inner 0.1 pc around the GC's SMBH that explored the dynamical evolution of the binaries until they either merged, tidally locked, or separated. In this work, we expand on these earlier simulations and use the same system parameters for our new Monte Carlo runs: the primary stellar mass was chosen from a Salpeter distribution with $\alpha = 2.35$ (Salpeter 1955), with the masses limited between 1 and 150 $M_\odot$, the mass ratio to the secondary was taken from Duquennoy & Mayor (1991), and the mass of the SMBH was set to $4 \times 10^6 M_\odot$ (e.g., Ghez et al. 2005; Gillessen et al. 2009). The inner binary semimajor axis distribution was also taken from Duquennoy & Mayor (1991), while the outer binary semimajor axis was initially drawn uniformly between about 700 au and 0.1 pc. The inner limit corresponds approximately to the orbit of the star S0-2 (Ghez et al. 2005), while for most orbits beyond 0.1 pc the effects of vector resonant relaxation become nonnegligible (e.g., Hamers et al. 2018). This is also shown in Figure 1, where we show several important dynamical timescales for the GC. The inner binary orbit eccentricity was drawn uniformly between 0 and 1 (Raghavan et al. 2010), while the outer one was taken as thermal (Jeans 1919). The angle between the inner and outer angular momenta was drawn isotropically. These systems were then tested for orbital stability, requiring that

$$\epsilon = \frac{a_1}{a_2} \frac{e_2}{1 - e_2^2}, \quad (1)$$

where a_1 (a_2) is the inner (outer) orbit semimajor axis, and e_2 is the outer orbit eccentricity. Further analytic stability criteria had to be fulfilled, ensuring that the binaries do not cross the SMBH's tidal radius (see Naoz et al. 2016; Stephan et al. 2016, for a complete list of conditions). In total, we had 5203 stable systems, 1570 from Stephan et al. (2016) and 3633 additional ones, to provide better statistical significance. The distribution of semimajor axis and eccentricity values after application of the stability criteria for the new simulations are equivalent to the old ones shown by Stephan et al. (2016), Figure 2.

The systems were then evolved including effects from EKL, GR, tides (e.g., Naoz et al. 2016, for the complete set of equations), and stellar evolution, following the single-star stellar evolution code SSE by Hurley et al. (2000).[8] The time it takes on average for binaries to be separated by interactions with other stars in the GC, (called the "evaporation timescale") served as the time limit for our calculations. However, if tidal effects are able to shrink the inner orbital distance of a binary, its expected survival time increases, as it becomes more stable against such scattering events (for equations, see Binney & Tremaine 1987; Stephan et al. 2016). Scattering events can also lead to exchanges of stars in the binaries with other objects orbiting the GC (e.g., Trani et al. 2019); while this can have interesting implications for further secular binary evolution, the encounter and exchange rate for tidally shrunken binaries is rather low and does not substantially influence our results. Furthermore, short-period binaries do not feel strong EKL effects, as GR and tidal effects suppress the gravitational perturbations by the SMBH. This leads to the formation of a large population of long-lived short-period binaries, as described by Stephan et al. (2016) and in the present work.

High-eccentricity mergers induced by EKL occur very early in the binaries' lifetimes (as shown by Stephan et al. 2016). Radial mergers are caused by the radial expansion of one star in the binary and do not necessarily require EKL-induced eccentricity or tidal orbital shrinking (though either effect facilitates the occurrence of such mergers), and therefore occur somewhat later, when the most massive stars begin to evolve past the main-sequence. Tidal mergers are binaries that become short-period binaries due to the interplay of EKL-induced high eccentricities and tidal orbital shrinking, destined to merge during post-main-sequence stellar evolution due to stellar expansion, after hundreds of megayears or even several gigayears. Tidal mergers were the dominant merging mechanism described by Stephan et al. (2016), producing 56% of mergers, compared to 33% of mergers through EKL during the main-sequence, and 11% of mergers due to radial expansion of evolved, massive stars.

We use the merging binary systems from our simulations as the basis for this work. We take the orbital parameters of these binaries at the moment when they either crossed the Roche lobe or became tidally locked short-period binaries and determine their further binary star evolution using the binary stellar evolution code BSE (Hurley et al. 2002). In particular, we use the BSE version distributed with the COSMIC binary population synthesis suite.

Several updates have been made to the BSE version used in COSMIC. Metallicity-dependent wind prescriptions for high-mass stars have been implemented following Vink et al. (2001), Vink & de Koter (2005), and Belczynski et al. (2010). Prescriptions for compact object formation and natal kicks have

[8] It has been shown that stellar evolution can have significant effects on the dynamical evolution in many astrophysical settings involving the EKL mechanism (e.g., Shappee & Thompson 2013; Stephan et al. 2016, 2017, 2018; Petrovich & Muñoz 2017).

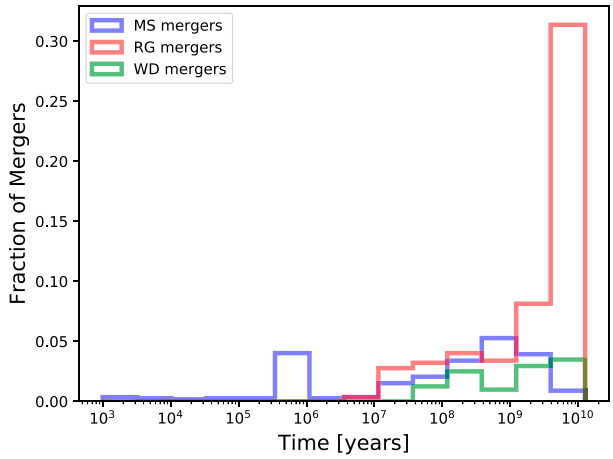

Figure 2. Types of mergers as a function of time. The plot shows a histogram of the times the main types of mergers occur. Mergers of two main-sequence stars are shown in blue, mergers involving at least one red giant star (and no WD or other compact object) are shown in red, and mergers involving at least one WD are shown in green. The peak of main-sequence binary mergers in the first megayear of evolution is due to EKL-driven high-eccentricity collisions, while the continued merging of RG and WD systems over several gigayears is due to tidally shrunken and circularized binaries. Mergers that involve at least one BH or NS constitute about 1% of the systems and are not depicted here to avoid clutter.

also been updated following Fryer & Kalogera (2001), Fryer et al. (2012), and, for electron-capture SNe for neutron stars, following Kiel et al. (2008). We used the default parameters for BSE except in the case of the updated prescriptions detailed above. In particular, we assume the "rapid" model from Fryer et al. (2012) for compact object formation and that natal kicks are drawn from a Maxwellian distribution with $\sigma = 265\,\mathrm{km\,s^{-1}}$ (Hobbs et al. 2005), with BH natal kicks being modified due to the amount of mass that falls back onto the proto-BH during formation. Finally, we note that our treatment for the common envelope follows the standard $\alpha\lambda$ formalism and default BSE values, with $\alpha = 1.0$ and λ determined by the stellar properties at the time just prior to the common envelope (Claeys et al. 2014).

BSE keeps track of the stars' evolutionary phases and, furthermore, indicates when and if binary stars merge and what type of object would be the outcome of such mergers. Double WD mergers would be candidates for SNe Ia, if their combined mass is large enough, while WD-red giant and WD-main-sequence mergers are candidates for symbiotic binaries (SBs) and CVs, as the WD would easily be able to accrete material from the companion star's envelope. Mergers involving helium stars, red giant stars, and main-sequence stars are probably candidates for G2-like objects, stars shrouded by a gaseous dust-rich cloud for a few megayears after merging had occurred (Witzel et al. 2014, 2017; Stephan et al. 2016). Helium stars themselves are examples of "stripped giants," which have been speculated to exist in the GC (Ghez et al. 2008).

We note that while we use BSE to perform the calculations for merger candidates' further stellar evolution, even for eccentric binaries, there are some limitations with this treatment (Sepinsky et al. 2007a, 2007b, 2010). However, BSE does include effects like SN kicks for neutron stars and provides results massively faster than full stellar hydrodynamic models. These are important advantages that allow us to advance this work.

3. Results and Discussion

Here we go into greater detail about the different types of outcomes and their implications for the binary population in the GC.

3.1. Dynamical Evolution Outcomes

We summarize the dynamical evolution outcomes before including binary evolution calculations below.

1. *Unbound Binaries:* 75% of the initial binary population is separated by interactions with other stars in the GC into single stars before the binary members can interact in a meaningful way. This unbinding (evaporation) of binaries begins after a few megayears of dynamical evolution and is mostly finished after a few hundred megayears (∼25% of binaries have separated after about 6 Myr). After that point, any binary that has not separated has either merged or has a tidally shrunken orbit that is long-term stable against separation.
2. *EKL Mergers:* 10% of binaries merge due to high eccentricities induced by EKL-oscillations. The binaries merge early, within the first few megayears of their dynamical evolution.
3. *Radial Mergers:* 2% of binaries merge simply due to radial expansion of one of their members during the red giant phase. These systems generally include very massive stars that evolve rapidly, within the first few megayears of evolution.
4. *Tidally Locked:* 13% of binaries have tightened and circularized their orbits due to the interplay of EKL and tides to such a degree that they are long-term stable against separation. These systems must reach this tidally locked state within only a few megayears after formation to escape evaporation. Their subsequent fate then depends on the stellar masses and orbital separation.

3.2. Binary Evolution Outcomes

The different outcomes of binary evolution are essential to understand the census of binaries in galactic nuclei. The outcomes were determined using BSE, as applied to EKL and radial mergers as well as the tidally locked binaries described above. We refer to these systems as "merger candidates." BSE evolves these systems while keeping track of common-envelope phases, Roche lobe overflow phases, mergers, kicks, and possible separation. Sometimes this will result in the formation of very tight compact object binaries instead of true mergers (e.g., Taam & Ricker 2010), though, it can usually be expected that such systems merge eventually either through gravitational wave emission or further gravitational perturbations by the SMBH. In general, the results can be divided into three groups, based on the evolutionary state of the stars when they merge:[9]

1. *Main-sequence or Red Giant Mergers:* 85.4% of merger candidates eventually merge as some combination of main-sequence, red giant, and/or helium (stripped giant) stars. We extrapolate from current observations of binary

[9] Merged stars undergo a much more violent evolution, where it can be expected that a lot of material is ejected and forms an extended envelope. Thus, while the Kelvin–Helmholtz timescale of a new star is on the order of a few 10^5 years, an extended envelope may still be engulfing it.

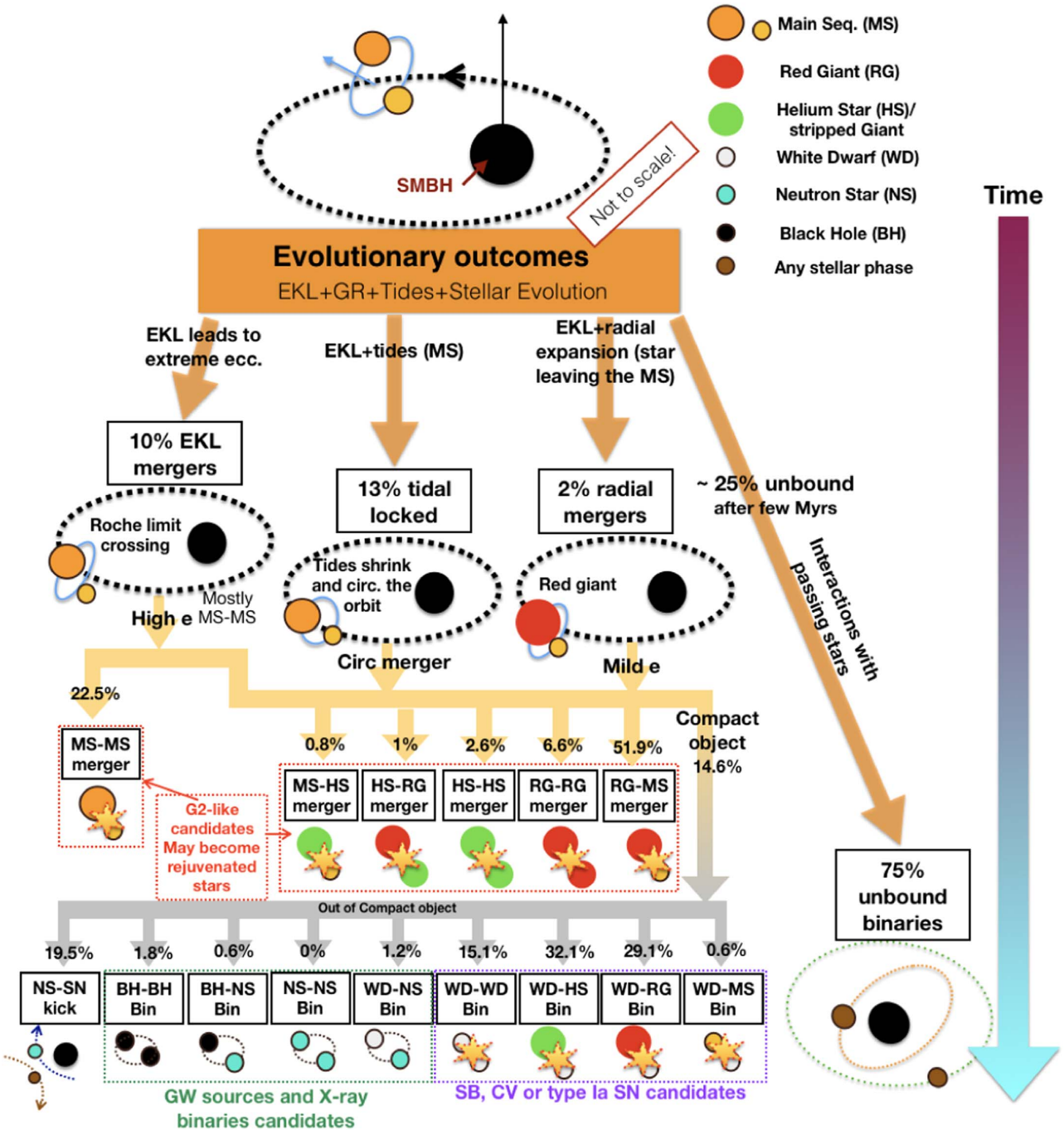

Figure 3. Flowchart of binary evolution outcomes. The diagram shows the outcomes of binary evolution in the inner 0.1 pc of the GC. Dynamical effects such as scattering with other stars separate 75% of all binaries into independent singles before they can interact with each other. 10% of binaries will collide or have grazing encounters due to EKL-induced high eccentricities. 2% will merge simply due to radial expansion of one of the binary members due to stellar evolution. 13% of binaries will tidally shrink their orbits and become decoupled from gravitational perturbations by the SMBH. We determined the further evolution of these binary pairs and their evolutionary phases during merging using BSE. The different possible outcomes are shown in the figure. Generally, the most likely combinations for merging binaries are pairs of main-sequence stars, main-sequence and red giant stars, pairs of red giant stars, and white dwarfs with evolved stellar companions. There is also a sizable population of binaries that were separated due to neutron star kicks, producing single neutron stars orbiting the SMBH, as well as a small population of binaries containing black holes or neutron stars that can become gravitational wave sources and might have been X-ray sources at some point, marked by the green box (see Bortolas et al. 2017; Hoang et al. 2018). Mergers involving white dwarfs are candidates for SBs, CVs, and SNe Ia (purple box), while mergers involving red giants, stripped giants, or main-sequence stars are candidates for G2-like objects or progenitors of rejuvenated stars (red boxes; e.g., Witzel et al. 2014, 2017; Stephan et al. 2016).

star mergers (e.g., Tylenda et al. 2011a, 2011b, 2013; Nicholls et al. 2013; Kamiński et al. 2018) that the forming objects will be shrouded by extended gas and dust clouds for an extended period of time. These mergers are therefore candidates for explaining the sizable population of observed G2-like objects (A. Ciurlo et al. 2019, in preparation). We show the occurrence rate of these mergers, split into mergers only involving main-sequence stars and mergers involving red giants, as the blue and red, respectively, histograms in Figure 2. Note that main-sequence star-only mergers tend to occur early, especially due to EKL-driven high-eccentricity mergers.

The resulting merger product may appear as a rejuvenated star, as it is now a more massive star that has burned less fuel than equally massive stars that evolved as singles. Such stars are also known as blue stragglers in open clusters (e.g., Perets & Fabrycky 2009; Geller et al. 2011; Naoz & Fabrycky 2014). The difference in measured age versus the actual age of the star could be substantial, but is highly dependent on the types of stars and their evolutionary state at the moment of merging, as well as the details of the merging process. According to the results given by BSE, the new star could appear younger by several gigayears, or just a few megayears, depending on the exact circumstances. Exploring the exact stellar evolution processes that determine the degree of rejuvenation, however, goes beyond the scope of this work. Regarding mergers involving red giants and helium stars, previous studies suggest that the resulting products can be carbon stars or even R Coronae Borealis (R CrB) variables (e.g., Iben et al. 1996; Izzard et al. 2007; Zhang & Jeffery 2013).

We note here that a small fraction of binaries can produce Type Ia-like SNe during their red giant evolution. These are mostly similar-mass stellar pairs on very short orbits ($\sim$1 day). When these binaries evolve into red giants, they form helium cores that can eventually collide as the stars enter common-envelope evolution and coalesce into a single object. As they collide, some of these helium cores are able to ignite and explode the stars without leaving a remnant behind. While this is very similar to an SN Ia, the cores' combined mass is generally very low ($\lesssim 0.5\,M_{\odot}$), probably producing somewhat less energy than a typical SN Ia ($\sim 10^{50}$–10^{51} erg; for a review of types of SNe and their luminosities, see Kasliwal 2012); such events might therefore be more difficult to identify and characterize correctly when occurring in the crowded environment of galactic nuclei. However, the combination of tidal effects and EKL with an SMBH serves to strongly enhance the formation of such short-period binaries. According to BSE, about 1% of the entire GC stellar binary population lead to such low-energy SNe.

2. *White Dwarf Binaries:* 11.2% of merger-candidate systems evolve to contain a WD star with either a WD, stripped giant, red giant, or main-sequence star companion. Such systems (i.e., WD–WD or WD–MS) are candidates for SNe Ia, given enough mass or enough collision energy. BSE evolution concluded that 15.4% of these systems would result in SNe Ia (which is 0.4% of the entire GC stellar binary population). Binaries and higher-multiplicity systems containing WDs outside of the GC have been investigated in previous studies as potential sources for WD collisions and SNe Ia, including due to EKL effects (e.g., Katz & Dong 2012; Toonen et al. 2017). The occurrence rate over time of these mergers is shown in green in Figure 2.

Given our results for SNe Ia, we can estimate the occurrence rate of such SNe in the galactic neighborhood. The GC contains on the order of $10^7\,M_{\odot}$ of stars and stellar remnants within a radius of about one parsec from the SMBH (e.g., Genzel et al. 2003; Schödel et al. 2003). Given an age of the Galaxy of about 10 Gyr, the star formation rate is approximately $10^3\,M_{\odot}\,\mathrm{Myr}^{-1}$. Assuming a Salpeter Initial Mass Function (IMF), and an average star mass of 1 $M_{\odot}$, the SN Ia likelihood is 0.4% and the SN Ia rate is $4 \times 10^{-6}\,\mathrm{yr}^{-1}$ for our GC.[10] Based on the observation statistics of the ASAS-SN collaboration (e.g., Holoien et al. 2019), we assume an effective observation radius of 250 Mpc (up to redshift 0.06), or an effectively observable sphere of 0.065 Gpc^3. Assuming a galaxy density of 0.02 Galaxies/Mpc^3 (Conselice et al. 2005), there are about 1.3×10^6 galaxies within this sphere. If we assume that half (or all) of these galaxies have central massive BHs and nuclear star clusters similar to ours, the expected rate of SNe Ia within this observable sphere would be about $2.5\,\mathrm{yr}^{-1}$ (or $5\,\mathrm{yr}^{-1}$), on average. If we also include Type Ia-like SNe from colliding helium cores (see red giant mergers), the rate is approximately tripled, to a maximum of $7.5\,\mathrm{yr}^{-1}$ (or $15\,\mathrm{yr}^{-1}$), on average; unfortunately, due to their low energy, these explosions might be more challenging to observe. However, the Zwicky Transient Facility (ZTF) should be capable of observing even these fainter supernovae, at even greater distances (Bellm et al. 2019).

Furthermore, binary pairs of WDs and main-sequence or red giant stars are also candidates for CVs or SBs, respectively, as the WDs will be accreting material from their companions for some part of their evolution. These objects, as well as some WD pairs, could remain as tight binaries for extended periods of time before merging (e.g., Taam & Ricker 2010). The large population of observed X-ray sources in the GC might be explained by these WD harboring binaries (see also Zhu et al. 2018). As the binary pairs eventually merge, some of them are candidates for carbon stars or, in some cases, R CrB variables (e.g., Iben et al. 1996; Izzard et al. 2007; Zhang & Jeffery 2013).

3. *Black holes and Neutron stars:* 3.4% of merger candidates will eventually evolve to contain a stellar-mass black hole or a neutron star, many of which could have been high-mass X-ray binaries before the secondary became a compact object; however, most of these pairs will separate due to SN kicks when the neutron stars form (see also Bortolas et al. 2017; Lu & Naoz 2019). Lu & Naoz (2019) showed that this can also bring NSs onto eccentric orbits close enough to the SMBH to merge via gravitational wave emissions, which should be detectable by LISA. Nevertheless, a small number of binary black holes and black hole–neutron star binaries will survive ($\sim$0.1% of the entire GC binary population) and can

[10] This is a conservative estimate, as the GC's actual IMF is top-heavy (Lu et al. 2013). We would expect this to lead to a higher rate than the one calculated here.

serve as gravitational wave sources in the GC (e.g., Hoang et al. 2018). The formation rate of such binaries would be about $10^{-6}\,\mathrm{yr}^{-1}$ for our GC (see calculations above for SNe Ia, assuming again a Salpeter IMF and an average star mass of $1\,M_{\odot}$). Within a sphere of 1 Gpc^3 volume, with 0.02 Galaxies/Mpc^3, and half (up to all) of galaxies containing an MBH and nuclear star cluster, the total expected formation rate of compact object binaries is about $10\text{–}20\,\mathrm{yr}^{-1}$. Assuming a merger efficiency of these compact object binaries due to further EKL effects of about 10%, as was shown by Hoang et al. (2018), this formation rate translates to about 1–2 gravitational wave signals producing inspirals per year per Gpc^3. Given Advanced LIGO's detection range of up to 1.5 Gpc (Abbott et al. 2018), this implies a rate of about 15–30 detectable events per year, with 7 to 15 (2 to 5) being BH–BH (BH–NS) mergers. Other merger scenarios for BH binaries in galactic nuclei exist (e.g., Bartos et al. 2017; Stone et al. 2017); however, future observations by LISA should be able to distinguish between them (Hoang et al. 2019).

There will also be a small number of neutron stars with WD companions, which can evolve into ultracompact X-ray binaries (e.g., Bobrick et al. 2017). Some of these systems will also have been low-mass X-ray binary (LMXB) or transient X-ray source (Zhu et al. 2018) candidates before the secondaries became WDs, potentially explaining part of the observed GC population of X-ray sources (e.g., Hailey et al. 2018; for examples of LMXB formation models, see Naoz et al. 2016; Generozov et al. 2018).

The dynamical and evolutionary outcomes of our simulations listed above are summarized in Figure 3.

4. Conclusions

We have followed the dynamical evolution of binary stars in the vicinity of an SMBH following a burst of star formation, including the effects of stellar evolution, tides, and GR. In the first few megayears, about 25% of binaries became unbound due to scattering interactions with passing stars, while 10% merged due to EKL-induced high eccentricities, 2% crossed their companion's Roche lobe due to stellar expansion, and 13% became tightly bound binaries due to tidal dissipation. Over the next few gigayears, the fraction of unbound binaries rose to 75%, becoming part of the rather mundane population of GC single stars, while the merged and tightly bound binaries evolved into a number of more exotic outcomes. These outcomes include G2-like objects shrouded by gas and dust for an extended period of time, white dwarfs with main-sequence and red giant star companions forming CVs and SBs, some SNe Ia from WD–WD pairs, as well as Type Ia-like events from the collision of red giant helium cores. Furthermore, some compact object binaries form that could be detected as gravitational wave sources. The results are summarized in Figure 3.

These results, of course, can be extended to more continuous or episodic star formation histories, leading to the continuous formation of such binary merger products. If this is the case, we estimate that SN Ia detecting surveys such as ASAS-SN and ZTF would see about 7.5–15 SN Ia, on average, per year from the processes described in this work, out to redshift 0.06. Furthermore, this study suggests that compact object binaries can form at a rate of about $10\text{–}20\,\mathrm{yr}^{-1}\,\mathrm{Gpc}^{-3}$, which should yield about 15–30 gravitational wave inspiral events per year detectable by Advanced LIGO, with 7 to 15 (2 to 5) being BH–BH (BH–NS) mergers.

S.N. thanks the KECK Foundation for its partial support of the NStarOrbits Project. S.N. acknowledges the partial support of NASA grant No. 80NSSC19K0321 and also thanks Howard and Astrid Preston for their generous support. S.N. and A.P.S. also acknowledge partial support from the NSF through grant No. AST-1739160. Calculations for this project were performed on the UCLA cluster *Hoffman2*. We thank Vicky Kalogera for facilitating the involvement of `COSMIC` team members in this work and for useful discussions in updating the `BSE` version used in `COSMIC`. We thank the anonymous reviewer for suggestions to improve this paper.

ORCID iDs

Alexander P. Stephan https://orcid.org/0000-0001-8220-0548
Smadar Naoz https://orcid.org/0000-0002-9802-9279
Andrea M. Ghez https://orcid.org/0000-0003-3230-5055
Mark R. Morris https://orcid.org/0000-0002-6753-2066
Katelyn Breivik https://orcid.org/0000-0001-5228-6598
Carl L. Rodriguez https://orcid.org/0000-0003-4175-8881

References

Abbott, B. P., Abbott, R., Abbott, T. D., et al. 2018, LRR, 21, 3
Alexander, T. 2005, PhR, 419, 65
Alexander, T., & Pfuhl, O. 2014, ApJ, 780, 148
Antonini, F., Faber, J., Gualandris, A., & Merritt, D. 2010, ApJ, 713, 90
Antonini, F., Lombardi, J. C., Jr., & Merritt, D. 2011, ApJ, 731, 128
Antonini, F., & Perets, H. B. 2012, ApJ, 757, 27
Bartos, I., Kocsis, B., Haiman, Z., & Márka, S. 2017, ApJ, 835, 165
Belczynski, K., Bulik, T., Fryer, C. L., et al. 2010, ApJ, 714, 1217
Bellm, E. C., Kulkarni, S. R., Graham, M. J., et al. 2019, PASP, 131, 018002
Binney, J., & Tremaine, S. 1987, Galactic Dynamics (Princeton, NJ: Princeton Univ. Press)
Bobrick, A., Davies, M. B., & Church, R. P. 2017, MNRAS, 467, 3556
Bortolas, E., Mapelli, M., & Spera, M. 2017, MNRAS, 469, 1510
Cheng, Z., Li, Z., Xu, X., & Li, X. 2018, ApJ, 858, 33
Chu, D. S., Do, T., Hees, A., et al. 2018, ApJ, 854, 12
Claeys, J. S. W., Pols, O. R., Izzard, R. G., Vink, J., & Verbunt, F. W. M. 2014, A&A, 563, A83
Conselice, C. J., Blackburne, J. A., & Papovich, C. 2005, ApJ, 620, 564
Duquennoy, A., & Mayor, M. 1991, A&A, 248, 485
Fragione, G. 2019, arXiv:1903.03117
Fryer, C. L., Belczynski, K., Wiktorowicz, G., et al. 2012, ApJ, 749, 91
Fryer, C. L., & Kalogera, V. 2001, ApJ, 554, 548
Geller, A. M., Hurley, J. R., & Mathieu, R. D. 2011, BAAS, 43, 327.02
Generozov, A., Stone, N. C., Metzger, B. D., & Ostriker, J. P. 2018, MNRAS, 478, 4030
Genzel, R., Schödel, R., Ott, T., et al. 2003, ApJ, 594, 812
Ghez, A. M., Becklin, E., Duchjne, G., et al. 2003, ANS, 324, 527
Ghez, A. M., Salim, S., Hornstein, S. D., et al. 2005, ApJ, 620, 744
Ghez, A. M., Salim, S., Weinberg, N. N., et al. 2008, ApJ, 689, 1044
Gillessen, S., Eisenhauer, F., Trippe, S., et al. 2009, ApJ, 692, 1075
Gillessen, S., Genzel, R., Fritz, T. K., et al. 2012, Natur, 481, 51
Ginsburg, I., & Loeb, A. 2007, MNRAS, 376, 492
Hailey, C. J., Mori, K., Bauer, F. E., et al. 2018, Natur, 556, 70
Hamers, A. S., Bar-Or, B., Petrovich, C., & Antonini, F. 2018, ApJ, 865, 2
Hees, A., Do, T., Ghez, A. M., et al. 2017, PhRvL, 118, 211101
Heinke, C. O., Ruiter, A. J., Muno, M. P., & Belczynski, K. 2008, in AIP Conf. Ser. 1010, A Population Explosion: The Nature & Evolution of X-ray Binaries in Diverse Environments, ed. R. M. Bandyopadhyay et al. (Melville, NY: AIP), 136
Hoang, B.-M., Naoz, S., Kocsis, B., Farr, W., & McIver, J. 2019, ApJ, 875, 31

Hoang, B.-M., Naoz, S., Kocsis, B., Rasio, F. A., & Dosopoulou, F. 2018, ApJ, 856, 140
Hobbs, G., Lorimer, D. R., Lyne, A. G., & Kramer, M. 2005, MNRAS, 360, 974
Holoien, T. W.-S., Brown, J. S., Vallely, P. J., et al. 2019, MNRAS, 484, 1899
Hopman, C. 2009, ApJ, 700, 1933
Hopman, C., & Alexander, T. 2006, ApJ, 645, 1152
Hurley, J. R., Pols, O. R., & Tout, C. A. 2000, MNRAS, 315, 543
Hurley, J. R., Tout, C. A., & Pols, O. R. 2002, MNRAS, 329, 897
Iben, I., Jr., Tutukov, A. V., & Yungelson, L. R. 1996, ApJ, 456, 750
Izzard, R. G., Jeffery, C. S., & Lattanzio, J. 2007, A&A, 470, 661
Jeans, J. H. 1919, MNRAS, 79, 408
Kamiński, T., Steffen, W., Tylenda, R., et al. 2018, A&A, 617, A129
Kasliwal, M. M. 2012, PASA, 29, 482
Katz, B., & Dong, S. 2012, arXiv:1211.4584
Kiel, P. D., Hurley, J. R., Bailes, M., & Murray, J. R. 2008, MNRAS, 388, 393
Lu, C. X., & Naoz, S. 2019, MNRAS, 484, 1506
Lu, J. R., Do, T., Ghez, A. M., et al. 2013, ApJ, 764, 155
Muno, M. P., Bauer, F. E., Baganoff, F. K., et al. 2009, ApJS, 181, 110
Muno, M. P., Bauer, F. E., Bandyopadhyay, R. M., & Wang, Q. D. 2006, ApJS, 165, 173
Muno, M. P., Lu, J. R., Baganoff, F. K., et al. 2005, ApJ, 633, 228
Naoz, S. 2016, ARA&A, 54, 441
Naoz, S., & Fabrycky, D. C. 2014, ApJ, 793, 137
Naoz, S., Fragos, T., Geller, A., Stephan, A. P., & Rasio, F. A. 2016, ApJL, 822, L24
Nicholls, C. P., Melis, C., Soszyński, I., et al. 2013, MNRAS, 431, L33
Perets, H. B., & Fabrycky, D. C. 2009, ApJ, 697, 1048
Petrovich, C., & Muñoz, D. J. 2017, ApJ, 834, 116
Prodan, S., Antonini, F., & Perets, H. B. 2015, ApJ, 799, 118
Raghavan, D., McAlister, H. A., Henry, T. J., et al. 2010, ApJS, 190, 1
Salpeter, E. E. 1955, ApJ, 121, 161
Schödel, R., Ott, T., Genzel, R., et al. 2003, ApJ, 596, 1015
Sepinsky, J. F., Willems, B., & Kalogera, V. 2007a, ApJ, 660, 1624
Sepinsky, J. F., Willems, B., Kalogera, V., & Rasio, F. A. 2007b, ApJ, 667, 1170
Sepinsky, J. F., Willems, B., Kalogera, V., & Rasio, F. A. 2010, ApJ, 724, 546
Shappee, B. J., & Thompson, T. A. 2013, ApJ, 766, 64
Stephan, A. P., Naoz, S., & Gaudi, B. S. 2018, AJ, 156, 128
Stephan, A. P., Naoz, S., Ghez, A. M., et al. 2016, MNRAS, 460, 3494
Stephan, A. P., Naoz, S., & Zuckerman, B. 2017, ApJL, 844, L16
Stone, N. C., Metzger, B. D., & Haiman, Z. 2017, MNRAS, 464, 946
Taam, R. E., & Ricker, P. M. 2010, NewAR, 54, 65
Toonen, S., Hollands, M., Gaensicke, B. T., & Boekholt, T. 2017, A&A, 602, 16
Trani, A. A., Fujii, M. S., & Spera, M. 2019, ApJ, 875, 42
Tylenda, R., Hajduk, M., Kamiński, T., et al. 2011a, A&A, 528, A114
Tylenda, R., Kamiński, T., Schmidt, M., Kurtev, R., & Tomov, T. 2011b, A&A, 532, A138
Tylenda, R., Kamiński, T., Udalski, A., et al. 2013, A&A, 555, A16
Vink, J. S., & de Koter, A. 2005, A&A, 442, 587
Vink, J. S., de Koter, A., & Lamers, H. J. G. L. M. 2001, A&A, 369, 574
Witzel, G., Ghez, A. M., Morris, M. R., et al. 2014, ApJL, 796, L8
Witzel, G., Sitarski, B. N., Ghez, A. M., et al. 2017, ApJ, 847, 80
Zhang, X., & Jeffery, C. S. 2013, MNRAS, 430, 2113
Zhu, Z., Li, Z., & Morris, M. R. 2018, ApJS, 235, 26

CHAPTER 4

Conclusions

The studies presented in this dissertation have investigated how the interplay of the EKL mechanism, tidal forces, general relativity, and stellar evolution shape the long-term dynamical evolution of hierarchical triple systems. Additionally, these studies have also explored what types of astrophysical phenomena can be caused by some of the dynamical evolution outcomes, such as stellar mergers and planetary engulfment. Regardless of each specific outcome, the results have shown that stellar evolution must be included for a complete understanding of hierarchical triple dynamics, as it can often fundamentally alter the dynamical behavior of a given system.

In the context of exoplanets (Chapter 2), the inclusion of stellar evolution in the hierarchical triple dynamics has allowed to make several predictions, some of which have already been confirmed by observations. Stephan et al. (2018) predicted that giant planets can evolve into Temporary Hot Jupiters around evolving post-main sequence stars. These planets would persist as normal giant planets far from their host star for most of their lifetime, where they are generally not observable due to their long orbital periods and small transit likelihoods. As their host stars evolve and expand, however, the interplay of tides and EKL allow such planets to be driven closer to the star, enhancing chances to observe them.

Since its launch, TESS has discovered several planets that confirm the Temporary Hot Jupiter prediction (e.g., Huber et al. 2019; Wang et al. 2019). Such planets will be important targets for future studies investigating exoplanet system architecture, formation, and evolution. Furthermore, these Temporary Hot Jupiters will eventually be engulfed by their stars, leading to interactions with their stellar envelopes, which was investigated in Stephan

et al. (2020). This study predicted a whole array of phenomena, including phases of X-ray and UV excess radiation, stellar chemical enrichment, stellar spin increases, or stellar mass ejections. Several observed objects can be explained by these results, such as non-spherical planetary nebulae (e.g., Soker 1998; Livio and Soker 2002), collimated gas ejection from the carbon star V Hydrae (e.g., Sahai et al. 2016; Salas et al. 2019, . The latter publication followed the methodology presented in this dissertation), or abnormally fast spinning stars (e.g., Mamajek and Hillenbrand 2008; Qureshi et al. 2018).

Lastly, concerning stellar chemical enrichment of stars by planetary material, Stephan et al. (2017) predicted that white dwarf pollution by volatile-rich comets or gas giants can be caused through enhanced EKL oscillations due to stellar mass loss. This result perfectly explains the nitrogen pollution observed by Xu et al. (2017), and our prediction for giant planets polluting white dwarfs was confirmed by recent discoveries (Gänsicke et al. 2019). Stephan et al. (2020) similarly predicted that stellar atmospheres can be chemically polluted by engulfed planets, which can explain observed lithium enrichment in some red giants (e.g., Alexander 1967; Brown et al. 1989; Montalbán and Rebolo 2002; Aguilera-Gómez et al. 2016), as well as stellar binaries with unequal metallicities (e.g., Oh et al. 2018).

Concerning binary stars orbiting SMBHs (Chapter 3), Stephan et al. (2016) predicted that the interplay of EKL, tides, and stellar evolution drives a large fraction of these binaries to merge. Such mergers were suspected to produce G2-like objects, and our study predicted that there should be a whole population of such objects, with a variety of orbital orientations and trajectories around Sagittarius A*. This prediction was in contrast to some claims that G2 ought to be a gas cloud, potentially part of a gas stream (e.g., Gillessen et al. 2012). However, observations of a total of six G2-like objects with a wide variety of orbital parameters and orientations, appear to confirm our prediction (Ciurlo et al. 2020).

Apart from G2-like objects, Stephan et al. (2019) also studied other binary evolution outcomes that might occur in galactic nuclei. This study showed that galactic nuclei can be hosts to a wide variety of astrophysical objects, such as X-ray binaries, cataclysmic variables, or symbiotic binaries, which can explain observed X-ray sources (e.g., Muno et al.

2005, 2006; Heinke et al. 2008; Cheng et al. 2018). Compact object binaries can also be formed, which can lead to gravitational wave events as observed by LIGO (e.g., Hoang et al. 2018) or which might be observable by the Laser Interferomete Space Antenna (LISA) (e.g., Hoang et al. 2019). Our study also predicts the existence of a population of white dwarf binaries that might produce Type Ia supernovae, which have yet to be observed in galactic nuclei. However, it might be difficult to localize a supernova in such crowded and bright environments. These white dwarf binaries should produce a background gravitational wave signal that LISA might observe.

Finally, it is evident that the interplay of EKL and stellar evolution has a major impact on the long-term evolution of many hierarchical triple systems. For many such systems, the hierarchical triple configuration is just a transient state, with the two inner bodies eventually merging or colliding. These mergers, collisions, and close encounters are responsible for many of the astrophysical phenomena we observe today, including Hot Jupiters, white dwarf pollution, gravitational wave events, or stellar mergers, and the studies presented in this dissertation have contributed to our understanding of them.

Looking ahead, I plan to continue my study of the interplay of stellar evolution and hierarchical triple dynamics, but I also intend to expand the application of the methods I have developed in the course of this dissertation. While hierarchical triples can describe a large number of real astrophysical systems, they are limited to only three bodies. In a recent study I collaborated in, Denham et al. (2019), the secular dynamics of a four-body system were investigated. The system consisted of a central star, two close-in, low-eccentricity, and nearly co-planar planets, and a distant, inclined fourth body. In such a configuration, the outer body causes EKL precession on the inner two planets, while the planets themselves exchange angular momentum via Laplace-Lagrange secular interactions. This particular study investigated the stability limits for this type of configuration, without including stellar evolution or tidal effects. In the future, I intend to include those effects into similar multi-planet models, and to expand these models to larger numbers of planets. These models will be able to investigate the long-term dynamical evolution of most known exoplanet systems.

Bibliography

(1) Abbott, B. P. et al. (2016). Observation of Gravitational Waves from a Binary Black Hole Merger. *Phys. Rev. Lett. 116*, 061102.

(2) Abramovici, A. et al. (1992). LIGO: The Laser Interferometer Gravitational-Wave Observatory. *Science 256*, 325–333.

(3) Aguilera-Gómez, C., Chanamé, J., Pinsonneault, M. H. and Carlberg, J. K. (2016). On Lithium-rich Red Giants. I. Engulfment of Substellar Companions. *ApJ 829*, 127.

(4) Alexander, J. B. (1967). A possible source of lithium in the atmospheres of some red giants. *The Observatory 87*, 238–240.

(5) Alexander, T. (2005). Stellar processes near the massive black hole in the Galactic center [review article]. *Phys. Rep. 419*, 65–142.

(6) Alexander, T. and Hopman, C. (2009). Strong Mass Segregation Around a Massive Black Hole. *ApJ 697*, 1861–1869.

(7) Anderson, K. R., Storch, N. I. and Lai, D. (2016). Formation and stellar spin-orbit misalignment of hot Jupiters from Lidov-Kozai oscillations in stellar binaries. *MNRAS 456*, 3671–3701.

(8) Antonini, F., Faber, J., Gualandris, A. and Merritt, D. (2010). Tidal Breakup of Binary Stars at the Galactic Center and Its Consequences. *ApJ 713*, 90–104.

(9) Antonini, F., Lombardi, J. C., Jr. and Merritt, D. (2011). Tidal Breakup of Binary Stars at the Galactic Center. II. Hydrodynamic Simulations. *ApJ 731*, 128.

(10) Antonini, F. and Perets, H. B. (2012). Secular Evolution of Compact Binaries near Massive Black Holes: Gravitational Wave Sources and Other Exotica. *ApJ 757*, 27.

(11) Barnes, J. W., van Eyken, J. C., Jackson, B. K., Ciardi, D. R. and Fortney, J. J. (2013). Measurement of Spin-orbit Misalignment and Nodal Precession for the Planet around Pre-main-sequence Star PTFO 8-8695 from Gravity Darkening. *ApJ 774*, 53.

(12) Bowler, B. P. et al. (2010). Retired A Stars and Their Companions. III. Comparing the Mass-Period Distributions of Planets Around A-Type Stars and Sun-Like Stars. *ApJ 709*, 396–410.

(13) Breivik, K. et al. (2019). COSMIC Variance in Binary Population Synthesis. *arXiv e-prints*, arXiv:1911.00903.

(14) Brown, J. A., Sneden, C., Lambert, D. L. and Dutchover, J., Edward (1989). A Search for Lithium-rich Giant Stars. *ApJS 71*, 293.

(15) Charpinet, S. et al. (2011). A compact system of small planets around a former red-giant star. *Nature 480*, 496–499.

(16) Cheng, Z., Li, Z., Xu, X. and Li, X. (2018). A Chandra Survey of Milky Way Globular Clusters. I. Emissivity and Abundance of Weak X-Ray Sources. *ApJ 858*, 33.

(17) Chu, D. S. et al. (2018). Investigating the Binarity of S0-2: Implications for Its Origins and Robustness as a Probe of the Laws of Gravity around a Supermassive Black Hole. *ApJ 854*, 12.

(18) Ciurlo, A. et al. (2020). A population of dust-enshrouded objects orbiting the Galactic black hole. *Nature 577*, 337–340.

(19) Denham, P., Naoz, S., Hoang, B.-M., Stephan, A. P. and Farr, W. M. (2019). Hidden planetary friends: on the stability of two-planet systems in the presence of a distant, inclined companion. *MNRAS 482*, 4146–4154.

(20) Do, T. et al. (2019). Relativistic redshift of the star S0-2 orbiting the Galactic Center supermassive black hole. *Science 365*, 664–668.

(21) Dobbs-Dixon, I., Lin, D. N. C. and Mardling, R. A. (2004). Spin-Orbit Evolution of Short-Period Planets. *ApJ 610*, 464–476.

(22) Duquennoy, A. and Mayor, M. (1991). Multiplicity among solar-type stars in the solar neighbourhood. II - Distribution of the orbital elements in an unbiased sample. *A&A 248*, 485–524.

(23) Eggleton, P. P., Kiseleva, L. G. and Hut, P. (1998). The Equilibrium Tide Model for Tidal Friction. *ApJ 499*, 853–870.

(24) Einstein, A. (1916). Die Grundlage der allgemeinen Relativitätstheorie. *Annalen der Physik 354*, 769–822.

(25) Fabrycky, D. and Tremaine, S. (2007). Shrinking Binary and Planetary Orbits by Kozai Cycles with Tidal Friction. *ApJ 669*, 1298–1315.

(26) Ford, E. B., Kozinsky, B. and Rasio, F. A. (2000). Secular Evolution of Hierarchical Triple Star Systems. *ApJ 535*, 385–401.

(27) Frewen, S. F. N. and Hansen, B. M. S. (2014). Eccentric planets and stellar evolution as a cause of polluted white dwarfs. *MNRAS 439*, 2442–2458.

(28) Frewen, S. F. N. and Hansen, B. M. S. (2016). The effect of stellar evolution on migrating warm jupiters. *MNRAS 455*, 1538–1552.

(29) Gänsicke, B. T., Schreiber, M. R., Toloza, O., Fusillo, N. P. G., Koester, D. and Manser, C. J. (2019). Accretion of a giant planet onto a white dwarf star. *Nature 576*, 61–64.

(30) Gettel, S., Wolszczan, A., Niedzielski, A., Nowak, G., Adamów, M., Zieliński, P. and Maciejewski, G. (2012). Substellar-mass Companions to the K-giants HD 240237, BD +48 738, and HD 96127. *ApJ 745*, 28.

(31) Ghez, A. M., Becklin, E., Duchjne, G., Hornstein, S., Morris, M., Salim, S. and Tanner, A. (2003). Full Three Dimensional Orbits For Multiple Stars on Close Approaches to the Central Supermassive Black Hole. *Astronomische Nachrichten Supplement 324*, 527–533.

(32) Ghez, A. M., Salim, S., Hornstein, S. D., Tanner, A., Lu, J. R., Morris, M., Becklin, E. E. and Duchêne, G. (2005). Stellar Orbits around the Galactic Center Black Hole. *ApJ 620*, 744–757.

(33) Gillessen, S., Eisenhauer, F., Trippe, S., Alexander, T., Genzel, R., Martins, F. and Ott, T. (2009). Monitoring Stellar Orbits Around the Massive Black Hole in the Galactic Center. *ApJ 692*, 1075–1109.

(34) Gillessen, S. et al. (2012). A gas cloud on its way towards the supermassive black hole at the Galactic Centre. *Nature 481*, 51–54.

(35) Ginsburg, I. and Loeb, A. (2007). Hypervelocity collisions of binary stars at the Galactic Centre. *MNRAS 376*, 492–496.

(36) Hailey, C. J., Mori, K., Bauer, F. E., Berkowitz, M. E., Hong, J. and Hord, B. J. (2018). A density cusp of quiescent X-ray binaries in the central parsec of the Galaxy. *Nature 556*, 70–73.

(37) Harrington, R. S. (1969). The Stellar Three-Body Problem. *Celestial Mechanics 1*, 200–209.

(38) Hees, A. et al. (2017). Testing General Relativity with Stellar Orbits around the Supermassive Black Hole in Our Galactic Center. *Phys. Rev. Lett. 118*, 211101.

(39) Heinke, C. O., Ruiter, A. J., Muno, M. P. and Belczynski, K. In *A Population Explosion: The Nature & Evolution of X-ray Binaries in Diverse Environments*, ed. by Bandyopadhyay, R. M., Wachter, S., Gelino, D. and Gelino, C. R., 2008; Vol. 1010, pp 136–142.

(40) Hills, J. G. (1988). Hyper-velocity and tidal stars from binaries disrupted by a massive Galactic black hole. *Nature 331*, 687–689.

(41) Hoang, B.-M., Naoz, S., Kocsis, B., Rasio, F. A. and Dosopoulou, F. (2018). Black Hole Mergers in Galactic Nuclei Induced by the Eccentric Kozai-Lidov Effect. *ApJ 856*, 140.

(42) Hoang, B.-M., Naoz, S., Kocsis, B., Farr, W. M. and McIver, J. (2019). Detecting Supermassive Black Hole-induced Binary Eccentricity Oscillations with LISA. *ApJ 875*, L31.

(43) Hopman, C. (2009). Binary Dynamics Near a Massive Black Hole. *ApJ 700*, 1933–1951.

(44) Hopman, C. and Alexander, T. (2006). Resonant Relaxation near a Massive Black Hole: The Stellar Distribution and Gravitational Wave Sources. *ApJ 645*, 1152–1163.

(45) Howard, A. W. et al. (2012). Planet Occurrence within 0.25 AU of Solar-type Stars from Kepler. *ApJS 201*, 15.

(46) Huber, D. et al. (2019). A Hot Saturn Orbiting an Oscillating Late Subgiant Discovered by TESS. *AJ 157*, 245.

(47) Hurley, J. R., Pols, O. R. and Tout, C. A. (2000). Comprehensive analytic formulae for stellar evolution as a function of mass and metallicity. *MNRAS 315*, 543–569.

(48) Hurley, J. R., Tout, C. A. and Pols, O. R. (2002). Evolution of binary stars and the effect of tides on binary populations. *MNRAS 329*, 897–928.

(49) Hut, P. (1980). Stability of tidal equilibrium. *A&A 92*, 167–170.

(50) Ivanova, N. et al. (2013). Common envelope evolution: where we stand and how we can move forward. *A&A Rev. 21*, 59.

(51) Izzard, R. G., Jeffery, C. S. and Lattanzio, J. (2007). Origin of the early-type R stars: a binary-merger solution to a century-old problem? *A&A 470*, 661–673.

(52) Johnson, J. A., Fischer, D. A., Marcy, G. W., Wright, J. T., Driscoll, P., Butler, R. P., Hekker, S., Reffert, S. and Vogt, S. S. (2007). Retired A Stars and Their Companions: Exoplanets Orbiting Three Intermediate-Mass Subgiants. *ApJ 665*, 785–793.

(53) Johnson, J. A., Marcy, G. W., Fischer, D. A., Wright, J. T., Reffert, S., Kregenow, J. M., Williams, P. K. G. and Peek, K. M. G. (2008). Retired A Stars and Their Companions. II. Jovian Planets Orbiting κ CrB and HD 167042. *ApJ 675*, 784–789.

(54) Johnson, J. A. et al. (2011). Retired A Stars and Their Companions. VII. 18 New Jovian Planets. *ApJS 197*, 26.

(55) Katz, B., Dong, S. and Malhotra, R. (2011). Long-Term Cycling of Kozai-Lidov Cycles: Extreme Eccentricities and Inclinations Excited by a Distant Eccentric Perturber. *Phys. Rev. Lett. 107* 181101, 181101.

(56) Kiel, P. D., Hurley, J. R., Bailes, M. and Murray, J. R. (2008). Populating the Galaxy with pulsars - I. Stellar and binary evolution. *MNRAS 388*, 393–415.

(57) Kiseleva, L. G., Eggleton, P. P. and Mikkola, S. (1998). Tidal friction in triple stars. *MNRAS 300*, 292–302.

(58) Kobulnicky, H. A. and Fryer, C. L. (2007). A New Look at the Binary Characteristics of Massive Stars. *ApJ 670*, 747–765.

(59) Kozai, Y. (1962). Secular perturbations of asteroids with high inclination and eccentricity. *AJ 67*, 591–598.

(60) Li, G., Naoz, S., Holman, M. and Loeb, A. (2014). Chaos in the Test Particle Eccentric Kozai-Lidov Mechanism. *ApJ 791*, 86.

(61) Li, G., Naoz, S., Kocsis, B. and Loeb, A. (2014). Eccentricity Growth and Orbit Flip in Near-coplanar Hierarchical Three-body Systems. *ApJ 785*, 116.

(62) Lidov, M. L. (1962). The evolution of orbits of artificial satellites of planets under the action of gravitational perturbations of external bodies. *Planet. Space Sci. 9*, 719–759.

(63) Lithwick, Y. and Naoz, S. (2011). The Eccentric Kozai Mechanism for a Test Particle. *ApJ 742*, 94.

(64) Livio, M. and Soker, N. (2002). The Effects of Planets and Brown Dwarfs on Stellar Rotation and Mass Loss. *ApJ 571*, L161–L164.

(65) Lu, C. X. and Naoz, S. (2019). Supernovae kicks in hierarchical triple systems. *MNRAS 484*, 1506–1525.

(66) Magorrian, J. et al. (1998). The Demography of Massive Dark Objects in Galaxy Centers. *AJ 115*, 2285–2305.

(67) Mamajek, E. E. and Hillenbrand, L. A. (2008). Improved Age Estimation for Solar-Type Dwarfs Using Activity-Rotation Diagnostics. *ApJ 687*, 1264–1293.

(68) Martins, F., Trippe, S., Paumard, T., Ott, T., Genzel, R., Rauw, G., Eisenhauer, F., Gillessen, S., Maness, H. and Abuter, R. (2006). GCIRS 16SW: A Massive Eclipsing Binary in the Galactic Center. *ApJ 649*, L103–L106.

(69) Montalbán, J. and Rebolo, R. (2002). Planet accretion and the abundances of lithium isotopes. *A&A 386*, 1039–1043.

(70) Muno, M. P., Bauer, F. E., Bandyopadhyay, R. M. and Wang, Q. D. (2006). A Chandra Catalog of X-Ray Sources in the Central 150 pc of the Galaxy. *ApJS 165*, 173–187.

(71) Muno, M. P., Lu, J. R., Baganoff, F. K., Brandt, W. N., Garmire, G. P., Ghez, A. M., Hornstein, S. D. and Morris, M. R. (2005). A Remarkable Low-Mass X-Ray Binary within 0.1 Parsecs of the Galactic Center. *ApJ 633*, 228–239.

(72) Muno, M. P. et al. (2009). A Catalog of X-Ray Point Sources from Two Megaseconds of Chandra Observations of the Galactic Center. *ApJS 181*, 110–128.

(73) Naoz, S. (2016). The Eccentric Kozai-Lidov Effect and Its Applications. *ARA&A 54*, 441–489.

(74) Naoz, S. and Fabrycky, D. C. (2014). Mergers and Obliquities in Stellar Triples. *ApJ 793*, 137.

(75) Naoz, S., Farr, W. M., Lithwick, Y., Rasio, F. A. and Teyssandier, J. (2011). Hot Jupiters from secular planet–planet interactions. *Nature 473*, 187–189.

(76) Naoz, S., Farr, W. M., Lithwick, Y., Rasio, F. A. and Teyssandier, J. (2013). Secular dynamics in hierarchical three-body systems. *MNRAS 431*, 2155–2171.

(77) Naoz, S., Farr, W. M. and Rasio, F. A. (2012). On the Formation of Hot Jupiters in Stellar Binaries. *ApJ 754*, L36.

(78) Naoz, S., Kocsis, B., Loeb, A. and Yunes, N. (2013). Resonant Post-Newtonian Eccentricity Excitation in Hierarchical Three-body Systems. *ApJ 773*, 187.

(79) Nicholls, C. P. et al. (2013). The dusty aftermath of the V1309 Sco binary merger. *MNRAS 431*, L33–L37.

(80) Niedzielski, A., Villaver, E., Nowak, G., Adamów, M., Maciejewski, G., Kowalik, K., Wolszczan, A., Deka-Szymankiewicz, B. and Adamczyk, M. (2016). Tracking Advanced Planetary Systems (TAPAS) with HARPS-N. IV. TYC 3667-1280-1: The most massive red giant star hosting a warm Jupiter. *A&A 589*, L1.

(81) Niedzielski, A., Wolszczan, A., Nowak, G., Adamów, M., Kowalik, K., Maciejewski, G., Deka-Szymankiewicz, B. and Adamczyk, M. (2015). Three Red Giants With Substellar-Mass Companions. *ApJ 803*, 1.

(82) Nowak, G., Niedzielski, A., Wolszczan, A., Adamów, M. and Maciejewski, G. (2013). BD+15 2940 and HD 233604: Two Giants with Planets Close to the Engulfment Zone. *ApJ 770*, 53.

(83) Oh, S., Price-Whelan, A. M., Brewer, J. M., Hogg, D. W., Spergel, D. N. and Myles, J. (2018). Kronos and Krios: Evidence for Accretion of a Massive, Rocky Planetary System in a Comoving Pair of Solar-type Stars. *ApJ 854* 138, 138.

(84) Ott, T., Eckart, A. and Genzel, R. In *The Central Parsecs of the Galaxy*, ed. by Falcke, H., Cotera, A., Duschl, W. J., Melia, F. and Rieke, M. J., 1999; Vol. 186, p 310.

(85) Petrovich, C. and Muñoz, D. J. (2017). Planetary Engulfment as a Trigger for White Dwarf Pollution. *ApJ 834*, 116.

(86) Pfuhl, O., Alexander, T., Gillessen, S., Martins, F., Genzel, R., Eisenhauer, F., Fritz, T. K. and Ott, T. (2014). Massive Binaries in the Vicinity of Sgr A*. *ApJ 782*, 101.

(87) Pinsonneault, M. H. and Stanek, K. Z. (2006). Binaries Like to Be Twins: Implications for Doubly Degenerate Binaries, the Type Ia Supernova Rate, and Other Interacting Binaries. *ApJ 639*, L67–L70.

(88) Prodan, S., Antonini, F. and Perets, H. B. (2015). Secular Evolution of Binaries near Massive Black Holes: Formation of Compact Binaries, Merger/Collision Products and G2-like Objects. *ApJ 799*, 118.

(89) Qureshi, A., Naoz, S. and Shkolnik, E. L. (2018). Signature of Planetary Mergers on Stellar Spins. *ApJ 864*, 65.

(90) Raghavan, D., McAlister, H. A., Henry, T. J., Latham, D. W., Marcy, G. W., Mason, B. D., Gies, D. R., White, R. J. and ten Brummelaar, T. A. (2010). A Survey of Stellar Families: Multiplicity of Solar-type Stars. *ApJS 190*, 1–42.

(91) Reffert, S., Bergmann, C., Quirrenbach, A., Trifonov, T. and Künstler, A. (2015). Precise radial velocities of giant stars. VII. Occurrence rate of giant extrasolar planets as a function of mass and metallicity. *A&A 574*, A116.

(92) Sahai, R., Scibelli, S. and Morris, M. R. (2016). High-speed Bullet Ejections during the AGB-to-Planetary Nebula Transition: HST Observations of the Carbon Star, V Hydrae. *ApJ 827*, 92.

(93) Salas, J. M., Naoz, S., Morris, M. R. and Stephan, A. P. (2019). Unseen companions of V Hya inferred from periodic ejections. *MNRAS 487*, 3029–3036.

(94) Sana, H., de Mink, S. E., de Koter, A., Langer, N., Evans, C. J., Gieles, M., Gosset, E., Izzard, R. G., Le Bouquin, J.-B. and Schneider, F. R. N. (2012). Binary Interaction Dominates the Evolution of Massive Stars. *Science 337*, 444.

(95) Shappee, B. J. and Thompson, T. A. (2013). The Mass-loss-induced Eccentric Kozai Mechanism: A New Channel for the Production of Close Compact Object-Stellar Binaries. *ApJ 766*, 64.

(96) Soker, N. (1998). Can Planets Influence the Horizontal Branch Morphology? *AJ 116*, 1308–1313.

(97) Spiegel, D. S. and Madhusudhan, N. (2012). Jupiter will Become a Hot Jupiter: Consequences of Post-main-sequence Stellar Evolution on Gas Giant Planets. *ApJ 756*, 132.

(98) Stephan, A. P., Naoz, S. and Gaudi, B. S. (2018). A-type Stars, the Destroyers of Worlds: The Lives and Deaths of Jupiters in Evolving Stellar Binaries. *AJ 156*, 128.

(99) Stephan, A. P., Naoz, S., Ghez, A. M., Witzel, G., Sitarski, B. N., Do, T. and Kocsis, B. (2016). Merging binaries in the Galactic Center: the eccentric Kozai-Lidov mechanism with stellar evolution. *MNRAS 460*, 3494–3504.

(100) Stephan, A. P., Naoz, S. and Zuckerman, B. (2017). Throwing Icebergs at White Dwarfs. *ApJ 844*, L16.

(101) Stephan, A. P., Naoz, S., Gaudi, B. S. and Salas, J. M. (2020). Eating Planets for Lunch and Dinner: Signatures of Planet Consumption by Evolving Stars. *ApJ 889*, 45.

(102) Stephan, A. P., Naoz, S., Ghez, A. M., Morris, M. R., Ciurlo, A., Do, T., Breivik, K., Coughlin, S. and Rodriguez, C. L. (2019). The Fate of Binaries in the Galactic Center: The Mundane and the Exotic. *ApJ 878*, 58.

(103) Thompson, T. A. (2011). Accelerating Compact Object Mergers in Triple Systems with the Kozai Resonance: A Mechanism for "Prompt" Type Ia Supernovae, Gamma-Ray Bursts, and Other Exotica. *ApJ 741*, 82.

(104) Tylenda, R. et al. (2011). V1309 Scorpii: merger of a contact binary. *A&A 528*, A114.

(105) Vanderburg, A. et al. (2015). A disintegrating minor planet transiting a white dwarf. *Nature 526*, 546–549.

(106) Veras, D. and Tout, C. A. (2012). The great escape - II. Exoplanet ejection from dying multiple-star systems. *MNRAS 422*, 1648–1664.

(107) Wang, S. et al. (2019). HD 202772A b: A Transiting Hot Jupiter around a Bright, Mildly Evolved Star in a Visual Binary Discovered by TESS. *AJ 157*, 51.

(108) Witzel, G. et al. (2014). Detection of Galactic Center Source G2 at 3.8 μm during Periapse Passage. *ApJ 796*, L8.

(109) Witzel, G. et al. (2017). The Post-periapsis Evolution of Galactic Center Source G1: The Second Case of a Resolved Tidal Interaction with a Supermassive Black Hole. *ApJ 847*, 80.

(110) Wolszczan, A. and Frail, D. A. (1992). A planetary system around the millisecond pulsar PSR1257 + 12. *Nature 355*, 145–147.

(111) Wu, Y. and Lithwick, Y. (2011). Secular Chaos and the Production of Hot Jupiters. *ApJ 735*, 109.

(112) Wu, Y., Murray, N. W. and Ramsahai, J. M. (2007). Hot Jupiters in Binary Star Systems. *ApJ 670*, 820–825.

(113) Xu, S., Zuckerman, B., Dufour, P., Young, E. D., Klein, B. and Jura, M. (2017). The Chemical Composition of an Extrasolar Kuiper-Belt-Object. *ApJ 836*, L7.

(114) Yu, Q. and Tremaine, S. (2003). Ejection of Hypervelocity Stars by the (Binary) Black Hole in the Galactic Center. *ApJ 599*, 1129–1138.

(115) Zhu, Z., Li, Z. and Morris, M. R. (2018). An Ultradeep Chandra Catalog of X-Ray Point Sources in the Galactic Center Star Cluster. *ApJS 235*, 26.